UNIVERSIDAD POLITÉNICA DE MADRID

ESCUELA TÉCNICA SUPERIOR DE INGENIERÍA AGRÓNOMICA
ALIMENTARIA Y DE BIOSISTEMAS

Vegetation dynamic patterns of arid rangelands: a multifractal approach

Tesis doctoral

Por

Ernesto Sanz Sancho

Licenciado en Biología

Febrero, 2023

Departamento de Matemática Aplicada

Escuela Técnica Superior de Ingeniería Agrónomica Alimentaria y de Biosistemas

Universidad Politécnica de Madrid

Tesis Doctoral

Vegetation dynamic patterns of arid rangelands: a multifractal approach

Por

Ernesto Sanz Sancho

Licenciado en Biología

Directora:

Ana María Tarquis Alfonso

Dra. Ingeniera Agrónoma

Madrid, Febrero 2023

A mi familia y mis amig@s (mi segunda familia elegida)

“The value of biodiversity is that it makes our ecosystems more resilient, which is a prerequisite for stable societies; its wanton destruction is akin to setting fire to our lifeboat”

Johan Rockström

“Be ferociously optimistic and radically pragmatic, it is our only option”

Layla Martínez

AGRADECIMIENTOS

Especial agradecimiento a mi directora de tesis doctoral: Dra. Ana M. Tarquis Alfonso, quien me ha apoyado y guiado a lo largo de todo este proyecto. Sin ella esta tesis no sería lo que es. Muchas gracias por hacer que nuestras reuniones fueran constructivas, llenas de aprendizaje y risas, una combinación verdaderamente maravillosa.

Gracias al Centro de Estudios e Investigaciones para la Gestión de Riesgos Agrarios y Medioambientales (CEIGRAM). A todo el personal administrativo, técnico e investigador. Desde los que estuvieron unos pocos meses, pero compartimos cafés y ánimos, a los que estuvieron desde el comienzo al final. Con especial mención a Andrea, Andrés, David, Hamid, Jesús, José Luis, Luz, María, María Dolores, Miriam y Xiao. Gracias por la complicidad, entendimiento y cariño. Incluso cuando no podíamos ni acercarnos o tocarnos, hasta que volvieron los abrazos y sonrisas sin mascarillas.

Agradezco a la Comunidad de Madrid, la Unión Europea y a la Entidad Estatal de Seguros Agrarios del Ministerio de Agricultura por su apoyo financiero y proporción de datos necesarios para la realización de esta investigación.

Y finalmente agradezco de todo corazón a toda mi familia y amigos por su amor, aunque a veces hablase de cosas raras, sin explicar todo bien o suficiente... Y por sus ánimos y diversión sin los cuales ni esta tesis ni la mayoría de proyectos personales y laborales podría haberlos llevado a cabo y terminado.

RESUMEN

Los pastos son ecosistemas complejos con dinámicas espaciales y temporales no lineales. Sin embargo, sus dinámicas temporales se han empezado solo a investigar más recientemente y todavía no se conocen completamente. Los pastos cubren un 30-40% de la superficie terrestre de la Tierra, y su degradación, causada por el incremento del mal uso de estos ecosistemas, es una preocupación a nivel global, afectando al 73% de los pastos terrestres. La teledetección y métodos de monitoreo con satélites son comúnmente usados para el estudio en ecología y agricultura. Entre los diferentes índices satélites, el Índice de Vegetación de Diferencia Normalizada (NDVI, por sus siglas en inglés) es uno de los más usados como índice de vegetación por ecólogos. El NDVI muestra una buena correlación con la biomasa de diferentes tipos de vegetaciones climas áridos y semiáridos. Las anomalías del NDVI (NDVIa y Z_{NDVI}) son otros índices que han demostrado su utilidad para la identificación de sequías y estrés hídrico en vegetación, por ello tiene gran potencial para el estudio de ecosistemas áridos y semiáridos.

Dado el incremento de la longitud de las series temporales disponibles a través de la teledetección, en la actualidad se están utilizando y desarrollando herramientas relacionadas con la complejidad para el estudio de las relaciones temporales entre series de teledetección y sus interacciones con otros parámetros físicos como la temperatura y la precipitación, dos de los variables climáticas más influyentes en el crecimiento de la vegetación. Los fractales son una herramienta bien establecidas en los estudios de complejidad. Esta herramienta permite describir las relaciones escalares que se encuentran en la naturaleza y estas se pueden, a su vez relacionarse y ser entendidas en términos de principios físicos y biológicos. Por ejemplo, la persistencia de una serie temporal (la probabilidad de que la serie mantenga o no su tendencia actual) puede ser relacionada con el

manejo de vegetación, como el pastoreo o tratamientos forestales, así como con diferentes tipos de vegetaciones.

El objetivo principal es el mejor entendimiento de las relaciones entre diferentes variables físicas en pastos áridos como un sistema complejo, dinámico y agrícola; así como el estudio de la naturaleza fractal de sus series temporales de índices de vegetación. Para ello se ha dividido en cuatro objetivos específicos. El primer objetivo es analizar la respuesta temporal del NDVI frente a la temperatura y la precipitación en las áreas seleccionadas. Análisis de correlación y regresión fueron utilizadas en diferentes fases o momentos del año, ajustando los límites de esas fases a cambios fenológicos década área. Los resultados de esta investigación muestran que la relación entre el NDVI con las variables meteorológicas cambiaba dependiendo de las fases seleccionadas. Ya que los cambios en dinámicas de la vegetación no siempre coinciden con los cambios de las estaciones, diferentes fases temporales específicas a cada región deben ser propuestas y optimizadas para estudiar las respuestas temporales del NDVI.

El segundo objetivo se centra en el estudio de la relación entre el índice de contenido hídrico del suelo y el NDVI, y analizar si es factible utilizar la serie de anomalía de ambos índices para proponer un índice de alarma de sequía. Para ello, se calculó las anomalías y se analizó la probabilidad de coincidencia de anomalías negativas teniendo en cuenta el posible retraso entre las dos series de anomalías. Los resultados muestran que, para ciertos periodos del año, el índice de anomalía del contenido hídrico del suelo tiene una alta probabilidad de predecir con antelación las anomalías negativas del NDVI.

El tercer objetivo es analizar la estructura de memoria de las series temporales de vegetación áridas de las áreas seleccionadas, así como comparar diferentes métodos para su estudio. La estructura de memoria está relacionada con la persistencia de la serie y nos permite entender mejor los cambios de tendencia de la serie. Adicionalmente se ha estudiado la multifractalidad de las áreas de

estudio. Se analizaron tres métodos fractales y multifractales (rango reescalado, función de estructura generalizado y análisis multifractal de fluctuación sin tendencia). Estos resultados muestran la importancia de eliminar la tendencia de las series temporales (cuando está presente) para el estudio multifractal.

Por último, el cuarto objetivo es estudiar si es factible agrupar áreas de pastos áridos con diferentes tipos de vegetación usando los patrones anuales y la persistencia de sus series de vegetación. Se han comparado dos métodos para calcular el exponente de Hurst (rango reescalado y análisis de fluctuación sin tendencia) y dos métodos de agrupamiento (K-means y random forest no supervisado). Los resultados muestran que el uso del índice de Hurst usando análisis de fluctuación sin tendencia y el random forest no supervisado mejoró la clasificación de zonas de pastos. Estos pastos presentan un gran rango de persistencia, especialmente visible en las zonas arbustivas con diferentes estados de la sucesión de vegetación (desde arbustos rodeados de zonas herbáceas a arbustos con árboles dispersos). El uso de la persistencia permitió mejorar el análisis de agrupamiento y esta debería ser tenida en cuenta cuando se trabaja y estudia zonas de pastos.

Esta tesis ha demostrado el potencial del análisis multifractal para ayudar a caracterizar tipos de pastos áridos y sus tendencias temporales para mejorar nuestro entendimiento sobre la complejidad de los pastos. Especialmente la persistencia o antipersistencia de las series temporales de vegetación junto con el estudio de otras variables físicas, como el contenido hídrico del suelo, puede mejorar la gestión de pastos y se recomienda tenerlas en consideración como métricas de complejidad temporal.

SUMMARY

Rangelands are complex ecosystems with non-linear dynamics in space and time, however, their temporal dynamics have only recently started to be studied and they are not fully understood. Rangelands comprise 30-40% of the Earth´s landmass and their degradation caused by increasing misuse remains a global concern, affecting 73 % of all rangelands. Remote sensing and satellite monitoring methods are commonly used to study ecology and agriculture. Among different satellite indices, the Normalized Difference Vegetation Index (NDVI) is the most widely used vegetation index by rangeland ecologists. The NDVI reveals a good correlation with the biomass of different vegetation types in arid and semi-arid areas. NDVI anomalies (NDVIa and Z_{NDVI}) are other indexes proven useful for identifying drought and water stress on vegetation; therefore, it is suited to study arid and semi-arid ecosystems

Given the increasing lengths of temporal series from remote sensing, complexity tools are being used and developed to study the temporal relationships among remote sensing series and their interaction with other physical parameters such as temperature and precipitation. Fractals are a well-established tool to measure mathematical properties of both temporally and spatially complex systems such as rangelands. Fractals can describe scaling relationships that are found in nature. For example, the persistence of time series (the probability of the series continuing or not its current trend).

This work has the main goal of further understanding the relationships among different physical variables in arid rangelands as a complex agricultural dynamical system, and the fractal nature of vegetation index time series. And it is divided into four main specific objectives.

The first objective was to reveal the temporal response of NDVI to temperature and precipitation in our target areas. Correlation and regression analysis were studied at different phases throughout the year adjusting the limits of these

phases to phenological changes to the vegetation of each area. Finally, the areas were compared using the aridity index. The results revealed that the relationship between NDVI and meteorological variables shifted when the phases of the year changed. The vegetation dynamics in arid areas do not always match the seasons and specific phases should be delimited and optimized to study the NDVI temporal responses.

The second goal was to study the relationship between the soil water content index and the NDVI and assess the feasibility of their anomaly series as a drought warning index. In this section, we calculated their anomaly and study the probability of coincidence of their negative anomalies with lags between anomaly indexes. The results show that for particular periods of the year, the anomaly of the water content index has a strong probability to inform in advance where the negative anomaly of NDVI is going to decrease.

The third goal is to analyse the memory structure of arid vegetation time series, comparing different methods. The memory structure is related to the persistence of a series. Additionally, we studied the multifractality of the target areas. For this section, we analyse three fractal or multifractal methods and compared their results (rescale range, generalized structure function and multifractal detrended fluctuation analysis). These results show the relevance of detrending the time series when the series presents an increasing or decreasing trend to analyse their multifractal character.

Finally, the fourth objective is to study the feasibility of clustering rangeland areas with different vegetation types based on the annual patterns and the persistence of their vegetation series. We compared two methods to calculate the persistence using the Hurst exponent (rescale range and detrended fluctuation analysis) and two different methods of unsupervised classification or clustering (K-means and Unsupervised Random Forest). The results showed the use of the Hurst exponent from detrended fluctuation analyses in unsupervised random

forest improved the clustering of rangeland areas. The rangelands presented a large diversity of persistence, especially reflected as a continuum for shrublands (with different types of vegetation mixes: sometimes associated mainly with grasses and sometimes with trees, in different proportions). Persistence improved the clustering analysis and it should be taken into consideration when working with rangeland.

In summary, this thesis has shown the potential of multifractal analysis to help characterize arid rangeland types and time trends to further understand the insights into rangelands' complexity. Especially the persistence character of rangeland vegetation time series with the study of meteorological and other physical attributes, such as water soil content, could aid in rangeland management and it is recommended to be taken under consideration as temporal complexity metrics.

LIST OF CONTENTS

LIST OF MAIN ABBREVIATIONS

AI	Aridity Index
DFA	Detrended Fluctuation Analysis
GSF	Generalized Structure Function
H2	Hurst Exponent from detrended fluctuation analysis
HI	Hurst Exponent from Rescale range method
LR	Low Resolution
MF-DFA	Multifractal Detrended Fluctuation Analysis
MR	Medium Resolution
NDVI	Normalized Difference Vegetation Index
NDVIa	Anomaly of Normalized Difference Vegetation Index
OPTRAM	OPtical TRApezoid Model
R/S	Rescale Range Method
URF	Unsupervised Random Forest
VCI	Vegetation Condition Index
W	Water, Moisture Soil Content
WCI	Water Condition Index
Z_{NDVI}	Z-score of Normalized Difference Vegetation Index
Z_{VCI}	Z-score of Vegetation Condition Index
Z_{WCI}	Z-score of Water Condition Index
ΔH	Change in Hurst exponent in multifractal analysis. H(max)-H(min).

LIST OF FIGURES

LIST OF TABLES

1. INTRODUCTION

1.1. Rangelands

Rangelands were described in 1923 as grazing lands that do not favour farmlands due to their climatic conditions (Sampson, 1923). However, the rangeland concept and its management have shifted throughout the decades, as the conceptual models used to understand these types of habitats have changed. In 1917, the succession theory (theory describing the process of change in species structure over time) was included and heavily influenced rangeland management. In 1975, Heady expanded the definition of rangeland management to "optimize returns from rangelands in those combinations most desired and suitable to society" (Heady et al., 1975). These differences in approaches of rangeland management were related to the two models that were used up to this moment, steady-state management was the first use linked to succession theory and equilibrium ecology. Whereas ecosystem management, based on non-equilibrium ecology and state and transition models was developed in the 1970s and widely adopted in the 1990s, increasing the functions of rangelands. A more recent management called the resilience-based was applied to provide more effective manners to manage this type of natural resource. This resilience theory represents equilibrial and non-equilibrial dynamics co-occurring at different levels, such as equilibrium vegetations at multiple states. This management model was developed based on resilience ecology and the inclusion of social sciences as part of rangeland sciences to study social-ecological systems (Briske, 2017).

Rangelands are currently defined as ecosystems supporting native or naturalized vegetation characterized as grasslands, shrub-steppe, shrublands, savannas, and deserts that are managed as adaptive social-ecological systems to provide multiple ecosystem services to benefit human well-being (Briske, 2017). They represent almost 33% of ice-free land globally. The vast majority of rangelands

are drylands (dry sub-humid, semi-arid, arid and hyper-arid lands), although some rangelands exist in the tundra and high elevation and latitude grasslands. This biome is associated with low available soil water due to low precipitation and high evapotranspiration. Rangelands provide great ecosystem values including biodiversity, carbon sequestration and cultural values. They often provide habitats for human settlements (Ellis and Ramankutty, 2008; Zerga, 2015).

Scarce precipitation and variable temperatures lead to high spatial and temporal heterogeneity. The ability of rangelands to regulate and provide water is strongly dependent on 1) water infiltration in the soil, 2) how this is accumulated in the root zone or as groundwater and 3) how this is absorbed by the plants or lost through evapotranspiration (Briske, 2017; Vetter, 2005). Vegetation, soil properties and water redistribution present non-linear patterns conforming to a heavily interconnected landscape, where each component can trigger cascading feedback that may heavily change these landscapes (Saco et al., 2018).

As socio-ecological systems in addition to biogeophysical components, social actors must be studied to fully understand rangeland dynamics. Limited resource availability makes these lands highly vulnerable to ecological and social disruption. Unfortunately, these habitats suffer severe degradation causing the disappearance of 5–10 million hectares of agricultural land every year (Ellis and Ramankutty, 2008; Zerga, 2015). Rangelands are spatially and temporally heterogeneous making their management a complex process that requires bridging the gap between theory and reality. For this purpose, parallel development of novel model productions and statistical analyses of complex spatiotemporal data to link ecological and social phenomena to their underlying mechanism are essential.

1.1.1. Rangelands as a complex system

Ecosystems are complex dynamical systems composed of different communities driven by various processes operating at different spatial and temporal scales. This means they are more than the sum of their parts, as the system is providing emergent properties (properties that appear from the group and you could not find in the individuals), and the response of the system to a different event may shift spatially and temporally (Cornell and Karlson, 1997; Muller, 2000; Ricklefs and Schluter, 1993). Among these emergent properties, ecosystems show a self-organising capacity, which is a non-linear dynamic process that leads to an increase in complexity based on cooperative interactions of the parts (Jorgensen and Fath, 2014; Muller, 2000; Naeem and Li, 1997; Tilman et al., 2001, 1996; Wolf and Holvoet, 2004). Self-organization can make the ecosystem more robust and resilient (Holling, 1973; Ludwig et al., 2001; Zhao et al., 2019). Therefore, non-linear techniques can be used to understand plant community spatio-temporal dynamics (Rand, 1994; Stone and Ezrati, 1996; Watt, 1947). The mathematical properties of both temporally and spatially complex systems are often fractal (Mandelbrot, 1983).

Rangelands are ecosystems coupled with a social system, making them complex adaptive systems (complex systems that present a dynamic network of interaction). These systems include not only biophysical dynamics, such as prey and predator dynamics but also social aspects such as selling or restocking livestock (Gross et al., 2006). To support their management new, quantitative models are needed at different spatial scales (Lempert, 2002; Levin, 1998). Complex problems can arise when considering different temporal and/or spatial scales. For example, managing rangeland productivity in the short term while avoiding long-term decline, with spatial heterogeneity due to woody plant encroachment (Eldridge et al., 2011; Janssen et al., 2000).

Many of the mechanisms involved in rangelands are clear, such as thermodynamics, biological inheritance or natural selection. But it is far from clear how these fundamental processes, interact and give rise to ecological systems. Despite being recognized for decades or centuries, their explanations remain elusive in terms of physical or biological principles. One restricted class of ecological phenomena can be characterized mathematically: scaling relationships that are self-similar or fractal-like over a range of spatial and temporal scales (Brown et al., 2002). Power laws describe emergent patterns of nature that can be understood in terms of basic physical and biological principles (Brown et al., 2002; Feder, 2013; Mandelbrot, 1983).

Research is often seen as a tool for solving management problems. However, linkages between applied and theoretical science can be weak. Research efforts should be focused on testable ecological theory to provide a framework for understanding root causes for complex system dynamics and foster incremental learning (Boyd and Svejcar, 2009). In this context, geospatial data is one of the key aspects to approaching ecological and general resilience to prioritize management action and develop appropriate strategies for the present and future (Chambers et al., 2019). Effective management requires the understanding of an ecosystem´s responses to stressors, disturbances and management actions at different levels (spatially and temporally) (Boyd and Svejcar, 2009).

1.1.2. Arid and semiarid rangelands

Arid areas have primary productivity limited by water. They receive 100-300 mm of mean annual precipitation. Semiarid areas receive a higher amount of precipitation 300-800 mm of mean annual precipitation. In addition to low precipitations, these tend to be erratic. Furthermore, high temperatures and low precipitations tend to co-occur during the summer months (Sjoholm et al., 1989). As a result of these conditions productivity per area is typically low and highly

variable from year to year, especially in arid rangelands (Fern et al., 2018; Vetter, 2005).

Arid and semiarid rangelands have progressively lost productivity and biodiversity over the past century (Breman and de Wit, 1983; Dean and Macdonald, 1994; Downing, 1978; Friedel et al., 1990; le Houerou, 2012; Milton et al., 1994; Schlesinger et al., 1990; Talbot, 1961; West, 1993). This was attributed to the overuse of rangelands by domestic herbivores, as arid and semiarid rangeland appear to be more sensitive to domestic livestock than mesic rangelands (Mack and Thompson, 1982; Milton et al., 1994). However, a debate regarding this criticism of grazing management was lately raised around the 1990s, and a new rangeland ecology was proposed. This new debate opposed the previous vision that stressed the importance of biotic feedback between herbivores and their resource. On the other hand, the new rangeland ecology related to non-equilibrium rangelands sees the abiotic conditions as the primary drivers of vegetation considering the spatial heterogeneity and climatic variability of semi-arid and arid rangelands. It is now widely accepted that equilibrium and non-equilibrium dynamics can be found in rangelands (Briske, 2017; Briske et al., 2003; Vetter, 2005).

Management under incomplete or not applicable ecological models can lead to altering rangeland dynamics and should be carefully thought in policy-making and management, especially in arid rangelands. Overgrazing leads to vegetation changes such as the replacement of palatable grasses by less palatable plants, the replacement of perennials by annuals, reduced basal cover, possible soil erosion, etc. These changes can be reversible when caught on time but they can also be irreversible after trespassing a threshold. Differences are found between arid and semiarid rangelands compared to mesic rangelands. In arid and semi-arid areas where rainfall coefficients of variability are over 30%, vegetation cover, composition and productivity are determined by rainfall, while grazing intensity

had a negligible, therefore non-equilibrium dynamics predominate in arid and semiarid rangelands. This makes rangeland's condition difficult to monitor and degradation assessment should be carefully considered to study grazing pressures. Especially in arid years, grazing pressures can lead to irreversible changes in rangeland dynamics (Milton et al., 1994; Pickup et al., 1998; Vetter, 2005).

1.2. Vegetation indices

The tailored monitoring of vegetation to inform sustainable management of these areas is a key aspect of stopping its degradation (Ellis and Ramankutty, 2008; Pickup et al., 1998; Zerga, 2015). Remote sensing and satellite monitoring methods are commonly used to study ecology and agriculture (Curran et al., 1992; Fern et al., 2018; Henebry, 1993; Wabnitz et al., 2008). New tools and metrics use complexity to understand and predict natural systems' behaviour and improve monitoring and management programs. In the past decades, advances suggest that complex-systems science can develop predicting frameworks with metrics that explain spatiotemporal dynamics' underlying causes (Guichard and Gouhier, 2014).

Vegetation mapping is typically static. However, vegetation is highly dynamic and understanding when changes happened helps improve management. For this reason, time series through remote sensing can provide a look into the past to aid our future. Studying vegetation cover has been widely recognised as one of the best indicators to determine land conditions (Bastin et al., 1999; Booth and Tueller, 2003; Wallace et al., 2006). Several vegetation indices have been used more commonly to assess rangeland's condition and productivity (Table 1.1) (Escribano Rodríguez et al., 2014; Jafari et al., 2007; Richardson and Everitt, 1992). Each index has its advantages and disadvantages and among these the

normalized difference vegetation index (NDVI) is by far the most commonly used by rangeland ecologists (Yagci et al., 2014).

Table 1.1. Eight of the most common vegetation indices used in rangelands and ecology.

Indices	**Source**	**Formula**
Ratio VI	Birth & McVey (1968)	$RVI = \frac{\mathrm{NIR}}{\mathrm{RED}}$
Green Ratio VI	Richardson & Everitt (1992)	$GRVI = \frac{\mathrm{NIR}}{\mathrm{GREEN}}$
Normalized Difference VI	Rouse et al. (1973)	$NDVI = \frac{\mathrm{NIR} - \mathrm{RED}}{\mathrm{NIR} + \mathrm{RED}}$
Soil Adjusted VI	Huete (1988)	$SAVI = \frac{\mathrm{NIR} - \mathrm{RED}}{\mathrm{NIR} + \mathrm{RED} + 0.5}\ (1.5)$
Modified Soil Adjusted VI	Qi et al. (1994)	$MSAVI = \frac{\mathrm{NIR} - \mathrm{RED}}{\mathrm{NIR} + \mathrm{RED} + \mathrm{L_M}}\ (1 + \mathrm{L_M})$
Transformed Soil Adjusted VI	Baret & Guyot (1991)	$\mathrm{TSAVI} = \frac{\mathrm{a(NIR} - \mathrm{aRED} - \mathrm{b)}}{\mathrm{RED} + \mathrm{aNIR} - \mathrm{ab}}$
Perpendicular VI	Kauth et al. (1979)	$\mathrm{PVI} = \frac{\mathrm{NIR} - \mathrm{aRED} - \mathrm{b}}{\sqrt{1 + a2}}$
Enhanced VI	Liu & Huete (2019)	$\mathrm{EVI} = \frac{\mathrm{g(NIR} - \mathrm{RED)}}{\mathrm{NIR} + \mathrm{C1} \times \mathrm{RED} - \mathrm{C2} \times \mathrm{B} + \mathrm{L}}$

NDVI has shown robust results to identify damaged vegetation, and therefore it is especially suited to analyse the status of semiarid and arid areas (Amri et al., 2011). On the other hand, arid and semiarid rangelands have highly variable rainfall, productivity, and vegetation cover. These are greatly affected by seasonal history. The lack of vegetation and the presence of background soil signifies a problem in remote sensing as it affects vegetation indices (Wallace et al., 2006). Therefore, depending on the goal of the study, such as differentiating soil from biomass or differentiating the presence of perennial or annual plants, soil-adjusted VI or other indices may be better suited. The selection of best fit should be made on a case basis, especially in the most extreme areas (Almeida-Ñauñay et al., 2021; Fern et al., 2018). Nevertheless, NDVI has been proven well

suited to assess general cover monitoring, regardless of soil or vegetation variations (Al-Bakri and Suleiman, 2004; Klisch and Atzberger, 2016; Peters et al., 2002; Ünal et al., 2014; Wallace et al., 2006; Yagci et al., 2014).

1.3. NDVI relationship to meteorological variables

Temperature and precipitation are mostly studied as drivers of NDVI (Al-Bakri and Suleiman, 2004; Ghebrezgabher et al., 2020; Hao et al., 2012; Ichii et al., 2002; Joiner et al., 2018; Liu et al., 2013; Martiny et al., 2006; Wang et al., 2003; Yue et al., 2007). However, the interactions among them and with other factors are still not fully comprehended (Piedallu et al., 2019). Temperature effects on NDVI are significant when water is available in the ecosystem; in these circumstances, precipitation plays a minor role. However, this relationship grows more assertive in arid regions, where water availability seems to be one of the main drivers of NDVI (Birtwistle et al., 2016; Vicente-Serrano et al., 2013; Zhang et al., 2018). Furthermore, some authors (Piao et al., 2014) suggest studying additional climatic factors further to understand thermal and hydric stress effects on NDVI patterns. Other climatic variables that have been reviewed are soil moisture, evapotranspiration, and land cover (Joiner et al., 2018; Wang et al., 2003; Yue et al., 2007). The relationships of NDVI with these climatic variables differ by season and vegetation type and biome. Another factor that makes it more difficult to disentangle the interactions is the effect of human activities on both NDVI and the ecosystem itself, especially when it comes to overexploitation such as overgrazing or water overuse (Zewdie et al., 2017). Therefore, it is essential to deeply understand NDVI and meteorological variables' relationship, especially accounting for the differences in this relationship between seasons and across types of land management. This is particularly relevant for agrometeorological indices, often used in rangelands (Dhakar et al., 2013).

NDVI and its relationship with meteorological variables have reported different results depending on the analyzed spatial scale (Peng et al., 2017; Stefanov and Netzband, 2005; Tarnavsky et al., 2008). Additionally, human activities negatively correlated with NDVI at a medium spatial resolution while it exerted a positive correlation at a lower resolution. Therefore, considering different spatial scales to identify the causes of NDVI patterns remains a challenging task (Peng et al., 2017).

The Aridity Index (AI) represents water availability, and different expressions have been developed (Nastos et al., 2013). United Nations Environment Programme developed a modified and widely accepted ratio of annual precipitation to the annual potential evapotranspiration (Maestre et al., 2012; Middleton and Thomas, 1992). This index has been used to quantify droughts and estimates possible changes in climate regimes (Bannayan et al., 2010; Sepehr et al., 2007), manage afforestation and reforestation projects, and prioritize and assess future conservation efforts in rangelands (Girvetz et al., 2012; Zheng and Zhu, 2017). It has also been previously compared to vegetation indices such as NDVI (Costantini et al., 2009; Nyamtseren et al., 2018; Scordo et al., 2009).

1.3.1. Temporal response to temperature and precipitation

Variations in temperature and precipitation strongly influence NDVI, however, these interactions change over time. Precipitation's link to NDVI will be much higher when water is not readily available in the ground, such as after a dry period, or when the temperature is not the limiting factor by stopping growth or evaporating water (cold and hot temperatures, respectively). Several researchers have seen differences among seasons (Braswell et al., 1997; Cui and Shi, 2010; Gang and Congbin, 2000; Wang et al., 2003), however, the interaction among NDVI and temperature and precipitation also changed based on space. For

example, NDVI can positively or negatively be related to temperature (Cao et al., 2011; Li & Shi, 2000; Zhao et al., 2011).

As these relationships change based on ecological zone, arid areas are shown to have precipitation as the most influencing variable in NDVI, as these rangelands are characterized by a ratio of mean annual precipitation and evapotranspiration between 0.02 and 0.5 for semiarid rangelands and 0.05 to 0.2 for arid rangelands (UNEP, 1992). This situation leads to an enhanced risk of land degradation caused by climate change. More intense rainfall events with no change in the total annual precipitation and temperatures are likely to intensify water stress and soil erosion (Fay et al., 2003; Hughes, 2003; Tietjen and Jeltsch, 2007).

1.3.2. Relationship of NDVI and water soil content

Precipitation and temperature directly influence water balance, causing changes in soil moisture regime which, in turn, influences plant growth. Thus, soil moisture is widely recognized as a key parameter that links precipitation, temperature, evapotranspiration and NDVI, though temperature also affects plant phenology and growth directly. Farrar et al. (1994) studied NDVI, rainfall and model-calculated soil moisture in Botswana. Their results showed that while the correlation between NDVI and precipitation is highest for a multi-month average, NDVI is controlled by soil moisture in the concurrent month. Other research focused more on grassland and woodlands showed the link between NDVI and water soil content with different lags (Adegoke & Carleton, 2002; Liu & Kogan, 1996).

When studying water soil content, it must be noted the difference between surface soil layers and root zone soil. Even though, a strong correlation has been shown between these layers (Albergel et al., 2008; Babaeian et al., 2018; Hirschi et al., 2014; Sadeghi et al., 2017). Different responses of NDVI to water soil content are found among vegetation and especially between humid and arid or semiarid

areas. This is due to the disparities among these areas in root zone soils and surface soil layers (Adegoke and Carleton, 2002; Liu and Kogan, 1996; Wang et al., 2007). NDVI has been shown to have strong links with root zone soil moisture and surface soil moisture in grassland and shrubland in semi-arid regions (Guan et al., 2020; Schnur et al., 2010; Wang et al., 2007)

1.4. Drought types. Warning indices.

Droughts are often considered into four major types: meteorological, agricultural, hydrological and socioeconomic. Meteorological drought results from a reduction of precipitation. Agricultural drought when plants do not have enough available water to meet their requirements, therefore this type of drought varies based on the type of vegetation. Since this is vegetation specific some soil water deficit may affect differently dissimilar vegetation and there tends to be a lag between soil water deficit and how this is reflected in the vegetation with shorter or wider periods. Hydrological droughts are when the water moving through the ground is significantly reduced; and finally, socioeconomic drought is when a drought affects the supply of goods and services of a community. These types of droughts are sequential in time and increasing complexity in their impacts and conflicts (Allaby, 2014; American Meteorological Society, 2004, 1997; Wilhite and Buchanan-Smith, 2005).

Remote sensing observation can be used to monitor drought-related variables and assess their effects and impacts from an ecosystem perspective. Precipitation has been studied with several indices (Kim et al., 2009; Mahmoudi et al., 2019), such as the Standardized Precipitation Index (SPI; McKee et al., 1993), Effective Drought Index (EDI; Byun and Wilhite, 1999), or Percent Normal Precipitation Index (PNPI; Willeke et al., 1994). To estimate soil moisture several indices were also developed (AghaKouchak et al., 2015; Wang and Qu, 2009) such as the Standardized Soil Moisture Index (SSI; Hao and AghaKouchak, 2013), the soil

moisture percentile (SMP; Sheffield et al., 2004; Wang and Qu, 2009), and OPTRAM (OPtical TRapezoid Model; Babaeian et al., 2018; Sadeghi et al., 2017). And most common vegetation indices to assess vegetation status have already been explained in a previous section.

As the drought types are sequential, an alarm index can be developed before more damage is caused. Drought indicators represent different stages of the hydrological cycle such as precipitation or soil moisture and later impacts can be perceived in vegetation water stress. How each stage behaves depends on the particular vegetation or ecosystem. Droughts cannot be avoided but their impacts can be reduced, by preparing for them. Different combined indicators present indices with warning thresholds (Hao and AghaKouchak, 2013; Sepulcre-Canto et al., 2012; Shofiyati et al., 2021; Skees et al., 2001; Wilhite, 2006). Early warning indices can provide a drought probability that can be used as a management tool. A proactive approach can then be taken in drought risk management using different sets of risk reduction instruments at different levels such as farm or government levels. These instruments include insurance, irrigation schemes or budget releases. Despite presenting different challenges early warning systems have already been used in the past (Canedo Rosso et al., 2018; Desai et al., 2015)

1.5. Multifractal analysis in vegetation dynamics

As mentioned before fractal or multifractal (a generalization of the scaling process of fractals) can be used to describe and understand vegetation. Fractal was coined in 1977 and simply put it is a geometry that repeats itself at different scales, spatially or over time. Or otherwise stated, it has self-similarity through power law relation (Mandelbrot, 1977). The more fractal a figure or series is the more complex it is as it changes more when the scale changes. In fractal geometry, fractal dimension can be used to measure it, providing a statistical index of

complexity based on fractal patterns. Fractal time series show power law properties related to the concepts of memory and persistence. Hurst exponent is widely used in fractal time series as it measures the long-term memory of time series (Hurst, 1951). Hurst exponent characterizes the roughness of the profile as will be further discussed in section 4.4 of materials and methods.

Among fractals, we can find monofractals, such as the Brownian motion or white noise, and multifractals, very common in nature. Monofractal only bear one scaling factor, therefore they can be described by one fractal characteristic such as fractal dimension or Hurst exponent. On the other hand, multifractals possess at least two scaling factors and cannot be described by a single exponent and a continuous spectrum of exponents is required. Fractals have often been used in ecology and agronomy (Anderson et al., 1997; Frontier, 1987; Halley et al., 2004; Mandelbrot, 1983). However, only recently fractals have been used in vegetation time series as satellite series of larger resolutions have provided large enough time series, and this discipline keeps currently changing as new resolutions and methods come to light.

Most papers studying vegetation series have focused on monofractal techniques calculating the Hurst index (HI), a persistence test, usually estimated by the Rescaled Range (R/S) method (Liu et al., 2017, 2018; Wang et al., 2005). Li et al. (Li et al., 2017) began to calculate the HI using the Detrended Fluctuation Analysis (DFA) as it is a more robust method to detect the scaling behaviour in time series as it can be used in non-stationary series. Many of these works focus on studying how different HI values are related to different vegetation dynamics and can lead to a further understanding of the interaction between their different components (Liang et al., 2015).

Besides HI, several multifractal analyses are giving a more in-depth comparison of the time series. For example, Generalised Structure Function (GSF) (Frisch, U. and Parisi, 1985), and Multifractal Detrended Fluctuation Analysis (MF-DFA)

(Kantelhardt et al., 2002), focus on measuring variations of the moments of the absolute difference of their values at different scales. GSF has been used to study vegetation (Lovejoy et al., 2008) and other geophysical data (Lovejoy et al., 2001). More recently, MF-DFA has been used to study the long-term ecosystem dynamics at a large scale (Baranowski et al., 2015; Hou et al., 2018; Igbawua et al., 2019; Mali, 2015) and compare the dynamics of affected and unaffected areas by fire (Ba et al., 2020). MF-DFA allows studying multiscaling on vegetation and detecting whether it is related to long-term correlations or a broad probability density function. Studying the difference in multiscaling between different areas can further support our understanding of vegetation dynamics and its interaction with other components (Katul et al., 2001). Interpretations of monofractal and multifractal analyses of landscapes have been used to inform policymakers. Different studies have been conducted to predict vegetation dynamics (Miao et al., 2015; Tong et al., 2018), while others have developed tools to evaluate current management practices (Igbawua et al., 2019; Kalisa et al., 2021; Wang et al., 2020; Zhou et al., 2020).

1.6. GENERAL AND SPECIFIC GOALS

Rangelands are complex adaptive systems, where in the past different management options have resulted in the degradation of the ecosystem due to a lack of understanding of their ecological relationships and interactions. The vegetation and meteorological time series have been demonstrated to have fractal properties as part of this complexity. The mathematical properties of their fractal nature can be used for research and management, as has been suggested by Igbawua et al. (2019) and Kalisa et al. (2021).

The main goal of this thesis is to further understand the relationships among different variables (vegetation indices, temperature, precipitation and water soil content index) in arid rangelands as a complex agricultural dynamical system, and the fractal nature of vegetation indices time series.

The main goal was divided into four main questions as written below:

1. Which is the temporal response of NDVI to temperature and precipitation in arid areas and how does it change through the year?
2. How does the soil water content index time series relate to the vegetation index throughout the year? Can we use the water content index as a warning index before vegetation damage?
3. How is the memory structure of vegetation time series, do different methods provide distinct results?
4. Is it feasible to use annual patterns and persistence to cluster rangelands with different vegetation types?

The thesis structure has been established to address these goals and their specific chapters are stated below:

- Chapter 3: Temporal response of NDVI to temperature and precipitation in arid rangelands

- The results obtained in the article: (Sanz et al., 2021a)

- Chapter 4: Soil water content and vegetation. The temporal relationship between Z_{WCI} and Z_{VCI}
  - Part of an ongoing research (to expand target areas).
- Chapter 5: multifractal character of NDVI and NDVIa
  - The results obtained in the article: (Sanz et al., 2021b)
- Chapter 6: clustering arid rangelands based on NDVI annual patterns and their persistence
  - The results obtained in the article: (Sanz et al., 2022)

1.7. RELATED PUBLICATIONS

This research was partially financed by the Autonomous Community of Madrid under Garantía Juvenil project, Boosting Agricultural Insurance based on Earth Observation data–BEACON project under agreement No. 821964, funded under H2020_EU, DT-SPACE-01-EO-2018-2020 and Entidad de seguros agrarios (ENESA). The study was developed in the centre of studies and research for agricultural and environmental risk management (CEIGRAM). This thesis has motivated three scientific publications. Moreover, we have participated in various international congresses which are all listed below organized by date:

- Sanz E., Saa-Requejo, A., Diaz-Ambrona, C., Ruiz-Ramos, M., & Tarquis, A. (2020). Multifractal Analyses on Normalized Difference Vegetation Index Series on Pastures (No. 4585). EasyChair.
- Sanz, E.; Saa-Requejo, A.; Díaz-Ambrona, C.H.; Ruiz-Ramos, M.; Rodríguez, A.; Iglesias, E.; Esteve, P.; Soriano, B.; Tarquis, A.M. (2021a). Normalized Difference Vegetation Index Temporal Responses to Temperature and Precipitation in Arid Rangelands. Remote Sensing, 13(5), 840. https://doi.org/10.3390/rs13050840
- Sanz, E.; Saa-Requejo, A.; Díaz-Ambrona, C.H.; Ruiz-Ramos, M.; Rodríguez, A.; Iglesias, E.; Esteve, P.; Soriano, B.; Tarquis, A.M. (2021b). Generalized Structure Functions and Multifractal Detrended Fluctuation Analysis Applied to Vegetation Index Time Series: An Arid Rangeland Study. Entropy, 23(5), 576. https://doi.org/10.3390/e23050576
- Sanz Sancho, E., Saa-Requejo, A., Diaz-Ambrona, C. G., Ruiz-Ramos, M., & Tarquis, A. M. (2021). Multifractal analysis of spatial heterogeneity in Spanish arid rangelands. In EGU General Assembly Conference Abstracts (pp. EGU21-2698). https://doi.org/10.5194/egusphere-egu21-2698

- Sanz, E., Almeida-Ñauñay, A., Ambrona, C. G. D., Saa-Requejo, A., Ruiz-Ramos, M., Rodríguez, A., & Tarquis, A. M. (2021). Spatial rangeland variability: using summary statistics and multifractal analysis to classify and monitor rangelands (No. ISMC2021-48). Copernicus Meetings. https://doi.org/10.5194/ismc2021-48

- Sanz Sancho, E., Almeida-Ñauñay, A., Díaz-Ambrona, C. G., Saa-Requejo, A., Ruiz-Ramos, M., Rodríguez, A., and Tarquis, A. M.: Clustering arid rangeland pixels using NDVI series and fractal analysis to classify land uses. Case in Southeastern Spain., EGU General Assembly 2022, Vienna, Austria, 23–27 May 2022, EGU22-287, https://doi.org/10.5194/egusphere-egu22-287, 2022.

- Sanz, E., Sotoca, J. J. M., Saa-Requejo, A., Díaz-Ambrona, C. H., Ruiz-Ramos, M., Rodríguez, A., & Tarquis, A. M. (2022). Clustering Arid Rangelands Based on NDVI Annual Patterns and Their Persistence. Remote Sensing, 14(19), 4949. https://doi.org/10.3390/rs14194949

2. MATERIALS AND METHODS

2.1. Temporal response of NDVI to temperature and precipitation

2.1.1. NDVI and Meteorological Data Collection

MOD09A1.006 and MOD09Q1.006 MODIS products were collected from AppEEARS (Team, 2020), downloading the RED (band 1) and NIR (band 2) values for the target areas. These products differ in spatial resolution: MOD09A1.006 has a 250 m spatial resolution (Medium Resolution, MR) and MOD09Q1.006 has a 500 m spatial resolution (Low Resolution, LR). Both of them have an 8-day temporal resolution from the beginning of 2000 to 2019, a total of 20 years of data. R was used to calculate the NDVI for each pixel, using the following formula:

$$NDVI = 100 \times \frac{\text{NIR}-\text{RED}}{\text{NIR} + \text{RED}} \qquad (1)$$

Both spatial resolutions were used to study the temporal response of NDVI to temperature and precipitation and compared. However, only the MR was used for the rest of the thesis: (relationship of vegetation condition index (VCI) and water condition index (WCI) anomalies, the scaling properties of vegetation indices and clustering rangelands). However, to study the relationship of VCI and WCI anomalies and clustering rangelands the temporal resolution was transformed to 10 days and the series started on 2002 to 2019, to match the time series used in Spanish indexed agricultural insurance as the selection of the pixels was provided by them.

The NDVI values were then checked for quality. If the data were not categorized as ideal quality, in the quality band from AppEEARS, this data was deleted; less than 0.01 % were deleted for all areas. The gaps were filled using running averages with a gap interval of seven dates. Then, the time series were smoothed using the Savitzky-Golay method (Savitzky and Golay, 1964), with a window size of 9 selected based on the best-fitted outputs.

Two different types of anomalies were calculated: the NDVI anomaly (NDVIa) following Anyamba and Tucker (2012):

$$NDVIa = \mathrm{NDVI} - \mu_{\mathrm{NDVI}} \qquad (2)$$

Where μ_{NDVI} is the average of all samples in all available years measured on the same calendar date.

The NDVI anomaly (Z_{NDVI}) was calculated by applying a z-score by date (Klisch and Atzberger, 2016):

$$Z_{\mathrm{NDVI}} = \frac{\mathrm{NDVI} - \mu_{\mathrm{NDVI}}}{\sigma_{\mathrm{NDVI}}} \qquad (3)$$

where we used μ_{NDVI} with the same definition and σ_{NDVI}, which corresponds to the standard deviation of all samples in all available years measured on the same calendar date.

The seasonal variation is removed in both anomaly types. Additionally, in Z-score when dividing by the standard deviation, if a trend was present in the time series, this one was removed. Each anomaly is used for different purposes. Z_{NDVI} was used to study the temporal responses of NDVI to temperature, precipitation and water soil content (WCI and VCI anomalies. On the other hand, the NDVIa was used to study the scaling properties and clustering rangelands. This last anomaly was used to remove fewer characteristic from the original series for the multifractal analyses.

Daily meteorological data from the closest meteorological stations (Appendix 1) were also used (Ministerio de Agricultura, 2020; SIAM, 2020). Average temperature and accumulated precipitation were calculated every eight days to match the NDVI dates. To examine the variation of NDVI during the year, boxplots of NDVI and meteorological variables were plotted.

Different phases were defined based on the NDVI pattern during the year as this region presents harshness and aridity. These phases (i) were based on the trend

of NDVI values: increasing, decreasing, or constant. A Chow test (Chow, 1960) of NDVI and time was used to confirm whether NDVI phases presented structural differences at the selected breaking points.

2.1.2. Correlations of NDVI with Meteorological Variables

The NDVI data were based on eight-day compound images. The image was selected based on criteria such as clouds and solar zenith. To match this temporal resolution the daily meteorological data were transformed as follows. The temperature data was the average for every eight days. Precipitations were accumulated every eight days. For exploring the existence of temporal patterns, we focused on correlations without and with lags:

Pearson's correlation coefficient of the NDVI values with Temperature (Temp) and Precipitation (Pp) at different phases (i) is:

$$\rho_{NDVI,Temp,i} = \frac{cov(\langle NDVI_i(t)\rangle, \langle Temp_i(t)\rangle)}{\sigma_{\langle NDVI_i(t)\rangle}\sigma_{\langle Temp_i(t)\rangle}} \quad (4)$$

$$\rho_{NDVI,Pp,i} = \frac{cov(\langle NDVI_i(t)\rangle, \langle Pp_i(t)\rangle)}{\sigma_{\langle NDVI_i(t)\rangle}\sigma_{\langle Pp_i(t)\rangle}} \quad (5)$$

where $\langle V_i(t)\rangle$ is the average of the 18 years of the variable V ($NDVI, Temp\ or\ Pp$) at time t belonging to phase i; $\sigma_{\langle V_i(t)\rangle}$ is the standard deviation of the $\langle V_i(t)\rangle$.

Pearson's correlation coefficient of the NDVI series belonging to phase i, through the 18 years (j), with each of the climatic variables ($Temp$ and Pp) at different time lags (s) is:

$$\rho_{NDVI,Temp,i}(s) = \frac{cov\big(NDVI_i(j,t), Temp(j,t-s)\big)}{\sigma_{NDVI_i(j,t)}\sigma_{Temp(j,t-s)}} \quad (6)$$

$$\rho_{NDVI,Pp,i}(s) = \frac{cov\big(NDVI_i(j,t), Pp(j,t-s)\big)}{\sigma_{NDVI_i(j,t)}\sigma_{Pp(j,t-s)}} \quad (7)$$

where $NDVI_i(j,t)$ are the $NDVI$ values at year j and time t that belong to phase i. The $Temp(j,t-s)$ are the temperature values at year j and delayed s times the lag time, which is eight days. Analogously, $Pp(j,t-s)$ can be defined.

2.1.3. Aridity Index and NDVI

The aridity index was calculated following (Middleton and Thomas, 1992), but instead of accumulating annually, we used the phases described by the NDVI patterns:

$$AI_i = \frac{P_i}{\mathrm{ETo_i}} \qquad (8)$$

where P_i is the summation of the accumulated precipitation of each phase for each year and was analogously done for the accumulated potential evapotranspiration ($\mathrm{ETo_i}$,Jensen et al., 1990) . Then, the average NDVI value for each phase was calculated. The aridity index and the average NDVI for each phase were plotted, in a cumulative plot, where each value was added to the sum of the previous values, starting at the first value of the time series. A linear regression was calculated to compare the four areas. A high slope would indicate an efficient use of its water resources.

2.2. Soil water content and its relationship with the vegetation condition index

2.2.1. Estimation of vegetation and soil indices

NDVI with 10 days temporal resolution and 250 m spatial resolution was used to calculate another vegetation index especially used for drought detection, the Vegetation Condition Index (VCI, (Kogan, 1995). This index was calculated following equation 9 where NDVI is each value for each time series and $\mathrm{NDVI_{min}}$ and $\mathrm{NDVI_{max}}$ are respectively, their multiyear minimum and maximum for every ten days:

$$VCI = \frac{\mathrm{NDVI} - NDVI_{min}}{NDVI_{max} - NDVI_{min}} \qquad (9)$$

The dynamics of the VCI were analysed and compared to the surface soil moisture index. To estimate surface soil moisture, we used the OPtimized TRapezoid Model (OPTRAM, (Sadeghi et al., 2017)). This model requires the Shortwave Transformed Reflectance (STR) and the NDVI. To calculate the STR we downloaded shortwave infrared reflectance from band 7 (2105-2155 nm) from MOD09A1.006 product from AppEEARS (Team, 2020). This product has a 500 m spatial resolution, lower than the one used for the vegetation indices, but a higher spatial resolution was not available for this reflectance band. This band´s temporal resolution is 8 days. STR was calculated using equation 10, where R_{SWIR} was band 7.

$$STR = \frac{(1-R_{SWIR})^2}{2R_{SWIR}} \qquad (10)$$

Firstly, we converted the 8 days-time series to 10 days period series like the NDVI and VCI. For every month that had 4 values of this time series, every two values were averaged to obtain 3 values instead of 4. When a month had 3 values, its values remained untouched. Secondly, to match spatially the STR and NDVI, every NDVI pixel was given an STR value based on their centroid proximity. This was made for every pixel in all its time series. After building a dataset of time series and pixels. We proceeded to calculate the trapezoidal space NDVI-STR. We divided the pixels into two areas based on their land use differences. Therefore, the soil moisture estimator was calculated separately for the north and south parts, where the pixels were cereal croplands and pasture, respectively. To calculate W, the moisture estimator, four parameters are calculated for each STR-NDVI space i_d and s_d are the intercept and the slope of the dry (upper) edge and i_w and s_w are the intercept and the slope of the wet (lower) edge (Figure 2.1). Using these parameters, NDVI and STR, the W is calculated using equation 11. After this calculation, all values higher than 1 were replaced by 1, producing a 0-1 range for this index.

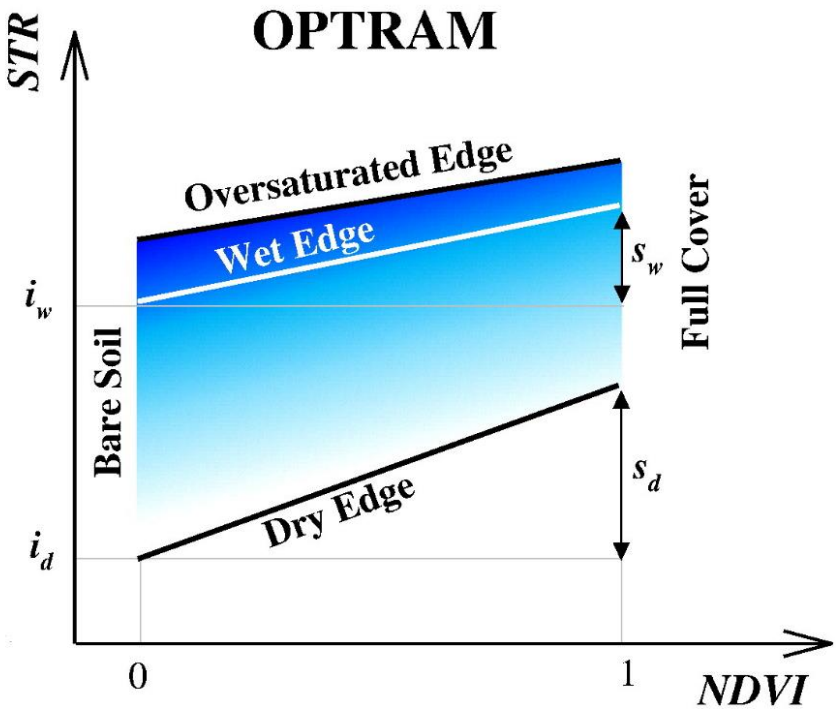

Figure 2.1. Sketch illustrating parameters of the OPTRAM model used in equation 12 to estimate parameters.

$$W = \frac{i_d + s_d NDVI - STR}{i_d - i_w + (s_d - s_w) NDVI} \qquad (11)$$

Given that ultimately, we wanted to compare the anomaly of VCI (Z_{VCI}) with the anomaly of soil moisture we took an additional step in calculating the Water Condition Index (WCI), submitting the W to the same transformation that NDVI had undergone to calculate VCI. Therefore, we calculated the WCI using equation 12, where W is each value of the time series and W_{min} and W_{max} are respectively, their multiyear minimum and maximum for every 10 days.

$$WCI = \frac{W - W_{min}}{W_{max} - W_{min}} \qquad (12)$$

2.2.2. Probabilities of anomalies for WCI and VCI

For both WCI and VCI anomalies were calculated using a Z-score as in equation 13, where μ is the yearly average and σ is the yearly standard deviation for each date of the year.

$$Z_{WCI} = \frac{\mathrm{WCI} - \mu_{\mathrm{WCI}}}{\sigma_{\mathrm{WCI}}} \qquad (13)$$

For these anomalies, the probabilities of passing different thresholds were calculated for each 10-day period throughout the time series. Three thresholds (-0.5, -0.7, and -1) were selected following the thresholds used for Standard Precipitation Index (SPI, McKee et al., 1993) and Standard Precipitation Evaporation Index (SPEI, Vicente-Serrano et al., 2010), indices commonly used for drought monitoring (Almeida-Ñauñay et al., 2022; Pei et al., 2020). These levels were established based on previous research for drought identification using the multi-thresholds run theory proposed by He et al. (2016) (Ma et al., 2022). Firstly, we calculated the probability of having a negative anomaly given the time series, for easier understanding this will be called base probability. Secondly, the conditional probability going through each level of the anomaly of Z_{VCI} given an anomaly of Z_{WCI} below -0.3. The conditional probability (understood as frequentist probability or relative frequency) was calculated using equations 14A and 14B, for Z_{VCI} and Z_{WCI}, for data from the same time period and taking a lead or positive lags of Z_{VCI} regarding Z_{WCI}.

$$P(A|B) = \frac{\mathrm{P(A \cap B)}}{\mathrm{P(B)}} \qquad (14A)$$

$$\mathrm{P(A \cap B)} = P(A|B) \times \mathrm{P(B)} \qquad (14B)$$

Where the probability of A under the condition of B equals the probability of A and B occurring together divided by the probability of B.

2.3. Scaling properties of vegetation time series

2.3.1. Hurst index

To analyse the persistence of NDVI in each area, HI (Hurst, 1951) was calculated using the package "pracma" (version 1.9.9, Borchers and Borchers, 2019) in R Software. We used the corrected Hurst index. This index splits the time series into subseries, with τ indicating the subseries number. It normalises the subseries

by subtracting the average for each subseries of the time series. Secondly, it calculates the cumulative series range (R(τ)) for each subseries. This range is divided by the standard deviation (S(τ)) of each subseries. The Hurst exponent (H) is then calculated using equation 15:

$$\frac{R(\tau)}{S(\tau)} = c\tau^{H} \qquad (15)$$

Where c as a constant of proportionalities, related to the log-log plot from R(τ)/ S(τ) and the size of the subseries as it is exemplified for three subseries in Figure 2.2. From the slope of the log-log plot, the H can be calculated.

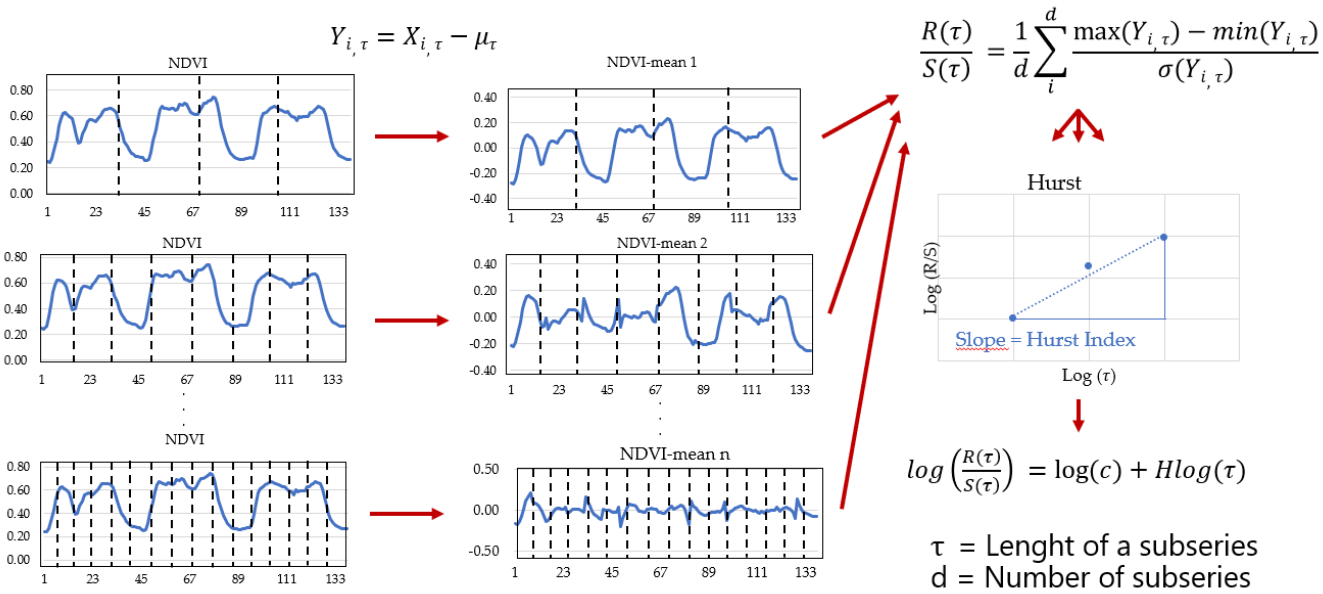

Figure 2.2: Exemplification for three subseries size (d) of how the Hurst Index using the rescale range method is calculated. Where R(τ)/ S(τ) is the assembled average of the range divided by the standard deviation.

2.3.2. Generalised Structure Function

GSF is used to characterise the scaling behaviour of non-overlapping fluctuation at different scale increments. For non-stationary processes, GSF of order q is defined as the qth moment of initial values x(i) increments, similar to a generalized variogram. The equation is:

$$M_q(\tau) \equiv \langle |x(i+\tau) - x(i)|^q \rangle \qquad (16)$$

Where i denotes the ith data point and ⟨ ⟩ represents the ensemble average, and τ is the lag time (i.e. i ± τ representing the$(i \pm \tau)^{th}$ data point). GSF are generalised correlation functions. It is particularly evident from eq (16) for q=2, giving the variogram, which is frequently used in geostatistics. In general, q may be any real number, either positive or negative. However, there are divergence problems inherent to the negative order exponent so computations are best restricted to positive real numbers. We will use positive q up to 4 in this work to reduce increasing errors related to higher-order statistical moments (Davis et al., 1994). If the process x(i) is scale-invariant and self-similar or self-affine over some range of time lags $\tau_{min} \leq \tau \leq \tau_{max}$ then the qth –order structure function is expected to scale as:

$$Mq(\tau) \equiv C_q \tau^{\zeta(q)} \approx \tau^{\zeta(q)} \qquad (17)$$

Where C_q can be a function of τ, which varies more slowly than any power of τ and (q) is the exponent of the structure-function. ζ(q) has been calculated as a log-log plot of $Mq(\tau)$ and τ/τ_{max} , where ζ(q) would be the slope for each q. ζ(q) is a monotonically non-decreasing function of q if x(i) has absolute bounds (Frisch and Kolmogorov, 1995; Marshak et al., 1994). *ζ(q)* is calculated for the time scales where the fluctuation functions increase linearly, with lags starting at eight days (time between NDVI collections).

The behaviour described by Equations (16) and (17) is called "multiscaling" because each statistical moment scales with a different exponent. Therefore, a hierarchy of exponents can be defined using (q) as shown in Equation (18) and simplified to be an example in Figure 2.3. Where H(q) is the generalised Hurst exponent (Davis et al., 1994) and is used to calculate ΔH as H(0.25)-H(4).

$$H(q) = \frac{\zeta(q)}{q} \qquad (18)$$

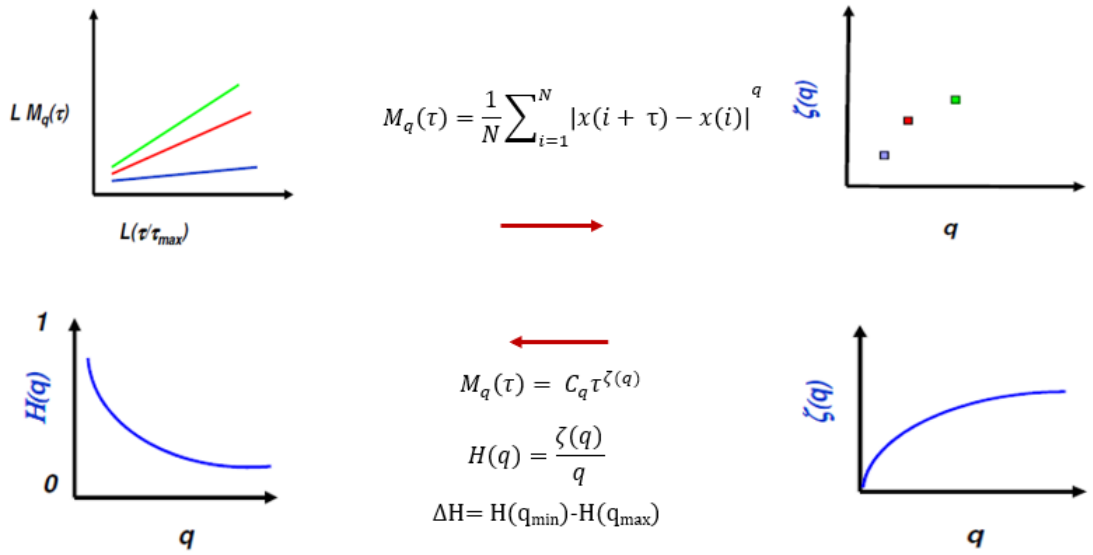

Figure 2.3: Exemplification for the last steps of how the generalized Hurst exponent is calculated using the generalized structure function. The process starts with the generalized variogram to finish calculating H(q) and ΔH.

2.3.3. Multifractal detrended fluctuation analysis

The main feature of multifractals is that a high variability characterises them over wide ranges of temporal or spatial scales associated with intermittent fluctuations and long-range power-law correlations. To undertake a multifractal analysis, Kantelhardt et al. (2002) developed Multifractal Detrended Fluctuation Analysis (MF-DFA). This method unlike the previous methods removes the local tendencies of the time series before calculating multifractal features.

The MF-DFA operates on x(i), where $i = 1,2,\ldots,N$ and N is the series's length. We represent the mean value with $\bar{x}$. We assume that x(i) are increments of a random walk process around the average $\bar{x}$. The integration of the signal, therefore, gives the profile:

$$y(i) = \sum_{k=1}^{i}[x(k) - \bar{x}] \qquad (19)$$

Furthermore, the integration will reduce the level of measurement noise present in observational and finite records. Next, the integrated series is divided into N_s

= int (N/s) non-overlapping segments of equal length s. We then calculate the local trend for each of the Ns segments by a least-squares fit. Finally, we determine the variance:

$$F^2(s,\nu) = \frac{1}{s}\sum_{i=1}^{s}\{y_{[(\nu-1)s+i]} - y_\nu(i)\}^2 \qquad (20)$$

For each segment ν, where $\nu = 1,\ldots,N_S$. Here, y_ν(i) is the fitting curve in segment ν, in this case, study a line was chosen. After detrending the series, we averaged over all segments to obtain the qth-order fluctuation function:

$$F_q(s) = \left\{\frac{1}{2N_s}\sum[F^2(s,\nu)]^{\frac{q}{2}}\right\}^{\frac{1}{q}} \qquad (21)$$

Where in general, the index variable q can take any real value except zero. In this case, we have selected real positive numbers. Repeating the procedure described above for several time scales s, $F_q(s)$ will increase with an increasing s. We can determine the fluctuation functions' scaling behaviour by analysing the log-log plots of Fq(s) versus s for each value of q (similar to log-log plots of previous methods). If the series x(i) is long-range power-law correlated, $F_q(s)$ increases for large values of s as a power law as shown below:

$$F_q(s) \propto s^{H(q)} \qquad (22)$$

H(q) is the generalised Hurst exponent in the function of q. *H(q)* is calculated for the time scales where the fluctuation functions increase linearly at a logarithmic scale. It starts at 32 days up to 512 days. Observing Equations (21) and (22), in the case that q=2, the equation will be as follows, where$F^2(s,\nu)$ comes from equation 20:

$$F_2(s) = \sqrt{\frac{1}{2N_s}\sum F^2(s,\nu)} \qquad (23)$$

$$F_2(s) \propto s^{H(2)} \qquad (24)$$

Therefore, H(2) correspond to the Hurst index estimated using MF-DFA as used by Li et al. (2017) and its calculation is exemplified in Figure 2.4.

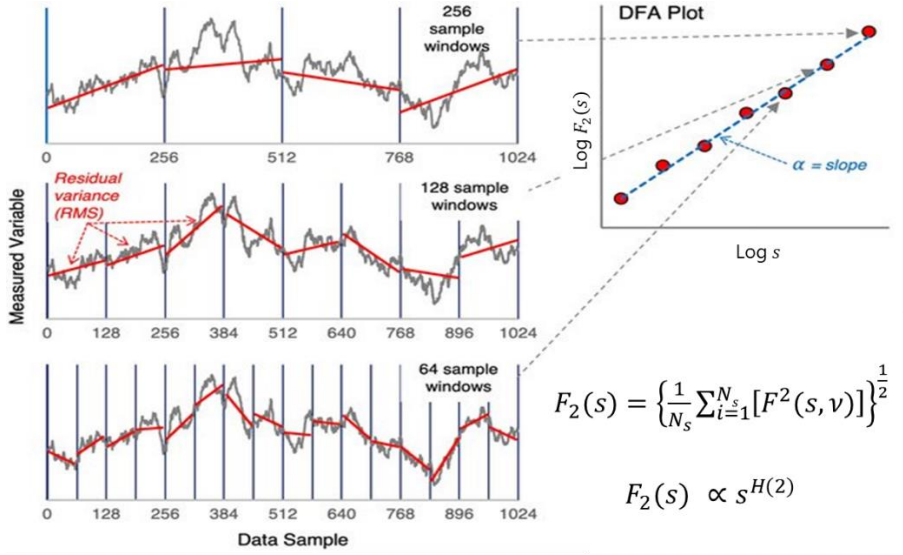

Figure 2.4: Exemplification for the last steps of how Hurst exponent (H2) is calculated using the Multifractal detrended fluctuation, but only for q=2, where H2 would be the slope.

As mentioned above, a monofractal series with compact support is characterised by *H(q)* independent of q. Different scaling of small and large fluctuations will yield a significant dependence of *H(q)* on q having higher ΔH, calculated as H(0.25)-H(4). The difference in scaling increases with increasing dependency. Once that H(q) is calculated, the scaling exponents function (ζ(q)) is derived from the expression H(q)/q (Kantelhardt et al., 2002).

There are two sources of multifractality (i) due to a broad probability density function and (ii) due to different long-range correlations (Kantelhardt et al., 2002). To test the study areas' multifractality sources, we use the shuffle series to eliminate any temporal correlation. If the shuffle series had any multifractality, that would be due to a broad probability density function (pdf). The shuffle series were obtained using a random array of the length of our time series. We ordered our time series to match the order of the random array. To test long-range correlations, we use surrogate series (or phase-randomised series). Surrogate series were calculated using the method iterated amplitude adjusted Fourier

transform (IAAFT, Schreiber and Schmitz, 2000, 1996). If the surrogate series exhibited multifractality, that would be due to long-range correlations. Ten surrogate and shuffle series were calculated and averaged to compare them with the original series, based on previous studies (Mali, 2015; Schreiber and Schmitz, 1996). The difference between the ΔH of the original and shuffle series (Hcor) is quantitatively related to the influence of broad pdf, and the difference of ΔH of the original and surrogate series (Hpdf) is related to the influence of long-range correlation (Movahed et al., 2006).

2.4. Machine learning

2.4.1. Variable selection for clustering

Summary statistics of the NDVI time series (first, second and third quartile and variance) were calculated to analyse vegetation dynamics, similar to Triscowati et al. (2019) and Uehara et al. (2020). However, the statistics were calculated at different year moments (phases) where NDVI behaves differently across the year. Three periods were chosen when the NDVI experienced more significant, following Sanz et al. (2021b). For the selected period, the mentioned summary statistics were calculated. Then, the Hurst exponent was calculated for the whole NDVI time series using two methods, R/S and DFA. Afterwards, clustering techniques were used on the selected summary statistics on their own and with each of the Hurst exponents. The results were compared to topographical data: elevation and slope.

Among all summary statistics and the Hurst exponents, a correlation matrix was run to select variables that did not have a strong correlation (i.e. <0.75). Principal Component Analysis was run when strong correlations were present to select the most explanatory variables. Upon selection, clustering analyses were run and compared.

2.4.2. Clustering

Clustering was made using two different unsupervised machine learning methods: k-means and unsupervised random forest (URF). The silhouette index was used to compare the different classification results and select the best option based on the partition and all proximities for all objects. Silhouette Index was calculated following equation 25, where for a cluster A and C, (i) is the average dissimilarity i to all other objects of cluster A, and b(i) is the minimum average dissimilarity of i to the centroid of cluster C.

$$SI(\mathrm{i}) = \frac{\mathrm{b}(i)-\mathrm{a}(i)}{\max\{a(i),\mathrm{b}(i)\}} \qquad (25)$$

To study the differences and similarities between the clusters adjusted rand index was used (Hubert and Arabie, 1985), from the R package “fossil v 0.4.0” (Vavrek, 2011), which determines whether two clusters are similar to each other using a contingency table of the two clusters doing an all pair-wise comparison.

2.4.2.1. K-means

K-means was developed by Stuart Lloyd in 1957 and published in 1982 (Lloyd, 1982). It is a non-hierarchical and one of the simplest methods to solve clustering problems. This method was first coined as k-means by James MacQueen in 1967 (MacQueen, 1967). This algorithm starts the clustering process by randomly assigning a K number of centroids. Secondly, it calculates the distance between the data points, and the closest centroid minimises the sum of the square as in equation 26):

$$d(x,y) = \frac{1}{2}\sum_i (x_i - y_i)^2 \qquad (26)$$

The algorithm repeats this process by adjusting the centroids based on the calculated distance, iterating a set number, and converging at a fixed point (MacKay, 2003). In this paper, Hartigan and Wong's method was used (Hartigan and Wong, 1979) with the R packages "stats v. 3.6.2" (Team, 2021). This method

reassigns point by point, considering the shift in the means after the reassignment of previous points, and it may reassign a point even if it already has an assigned centre.

2.4.2.2. Unsupervised Random Forest

Random forest (RF, Breiman, 2001) is a tree-based ensemble method. That is, methods that generate many classifiers and aggregate their results. It uses bootstrap aggregating (also called bagging Breiman (1996)) to calculate a large number of trees based on the fed predictor variables and selects the most voted trees. Random forest is a non-parametric method that builds each tree using a deterministic algorithm based on the three main variables: 1) the number of trees (*nt*); 2) the number of predictors tested on each node (*m*), and 3) the minimal size for each node (*nodesize*). A third of the bootstrap is left out in each node and is considered out-of-the-bag (OOB) data. This data is used to get a classification rate for each node. The variable importance is calculated for the averaged final tree based on the OOB data and their classification rate. Each tree presents different variable importance, but it is averaged (Breiman and Cutler, 2007). The R package "randomForest v. 4.6-14" was used (Liaw and Wiener, 2002) to calculate the RF as an unsupervised method, utilizing the proximity matrix as predictor variables.

2.5. Areas of study

This thesis has focused on the South-east of Spain, in Murcia and Almeria provinces Figure 2.5, as two of the aridest provinces in Spain (along with Alicante and Fuerteventura and Lanzarote, in the Canary Islands). We divided the thesis into two main blocks with two parts each. The first block would be the temporal response of vegetation indices to physical parameters such as precipitation and water soil content. This block is divided into the first part, the temporal response of NDVI to temperature and precipitation, and the second part the temporal

relationship of Z_{VCI} with Z_{WCI}. The second block uses fractal analyses and is divided into the third and fourth parts of this thesis. The third part is the scaling properties of vegetation indices (NDVI and NDVIa) and the fourth part is the clustering of rangelands using annual patterns and persistence of NDVI series. In the following sections, we describe the areas of study for each of these parts.

Figure 2.5: Selected provinces for this thesis (in blue). Both of them are characterized by arid climates.

2.5.1. Murcia Agricultural region- temporal response to precipitation of NDVI and scaling properties of NDVI

To study the temporal response of NDVI to temperature and precipitation and the scaling properties of NDVI, four plots were selected in Murcia province (Figure 2.6). The area has a Mediterranean arid climate with annual precipitation of less than 300 mm, although there are regional variations (Barceló and Nunes, 2009). Four square areas with 2.5 km sides (6.25 ha) were selected for this study. They are situated in the vicinity of a meteorological station, covering three

different agricultural regions of Murcia: Northeast, Segura River, and Northwest (Table 9.1, in Appendix 1). The average temperature varies amongst the four areas from 14.7 to 17.3 °C, and the average accumulated precipitation per eight-day period ranges from 262 to 348 mm.

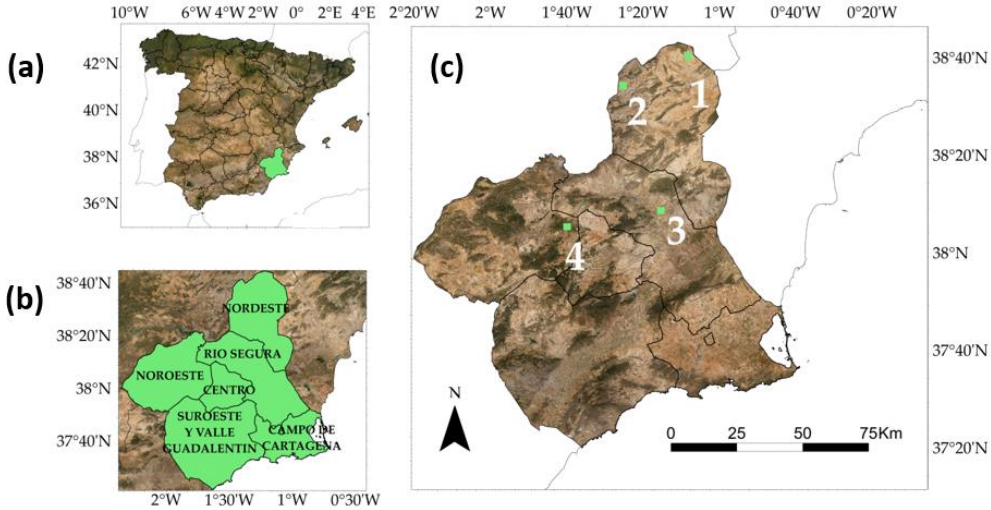

Figure 2.6. Location of the study area. (a) Autonomous Community of Murcia. (b) Agricultural regions of Murcia. (c) Selected areas in three agricultural regions of Murcia province. Numbers refer to the sampling areas.

All the areas are used as rangeland, two predominantly herbaceous (A1 and A2) and two mainly covered by shrubs or trees (A3 and A4). Area 1 (A1) is mostly covered by stubble from cereal crops. Area 2 (A2) is almost entirely covered by mixed croplands used for stubble grazing with some grassland and scrubland. Area 3 (A3) has a top grassy area mixed with shrubs and with few forested areas surrounded by tree crops with irrigation. Area 4 (A4) is mainly covered by coniferous open woodland with rainfed mixed crops on small patches (Figure 2.7).

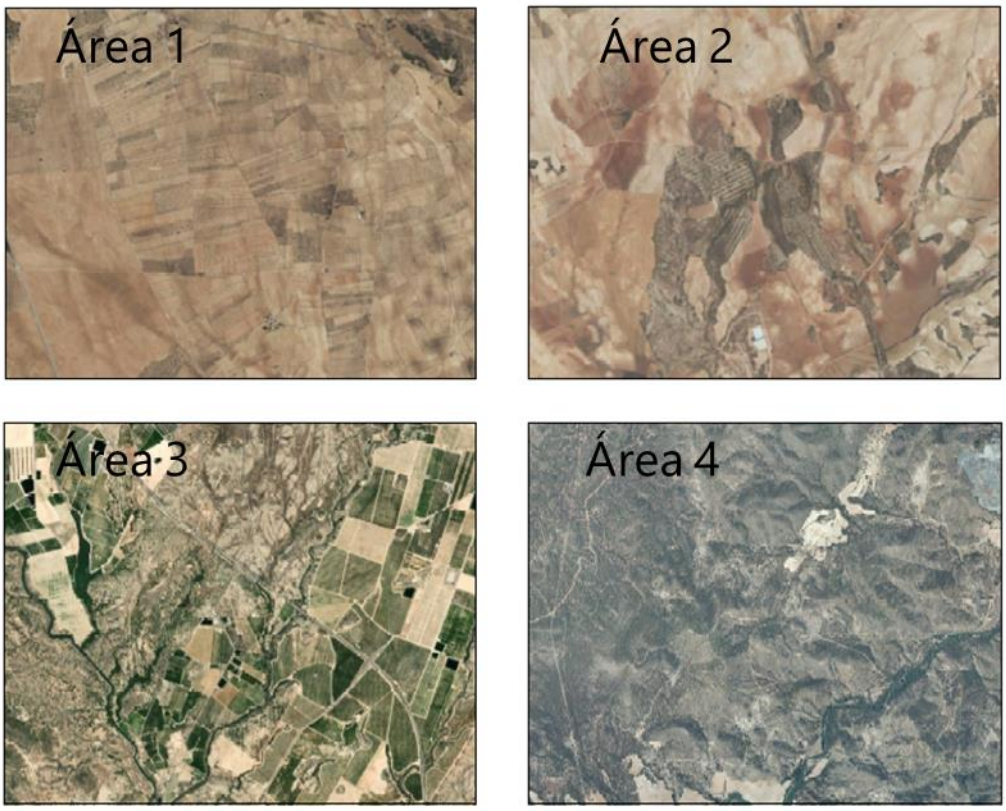

Figure 2.7. The four areas studied: (a) Area 1 with mostly stubble; (b) Area 2 with mixed crops and grasslands; (c) Area 3, with scrublands and mixed crops; (d) Area 4 with open woodland.

To study the temporal response of NDVI to temperature and precipitation, two spatial resolutions were selected. Low resolution with 500 m and 25 pixels for each area and MR with 250 m and 132 pixels for each of the four areas (according to the MODIS data availability). On the other hand, only the highest spatial resolution (MR) was used to study the scaling properties of NDVI and its anomaly (NDVIa). Additionally, with the temporal response of NDVI to temperature and precipitation, for A3, we removed pixels that were irrigated (Figure 2.7). Rainfed areas were selected coming up to a total of 11 (LR) and 61 pixels (MR) in A3 to eliminate the effects of irrigation in the NDVI dynamics. The rainfed pixels were selected based on each pixel's average NDVI for the summer months (June, July, and August). Pixels with a summer average below 30 and did not have peaks over 40 in their NDVI time series, were selected to be analysed, and these pixels match the grassy patch that crosses A3 from the top centre to the

right bottom corner. To study the scaling properties of NDVI and its anomaly (NDVIa) all pixels from A3 were used (with the highest spatial resolution). The other areas are mainly conformed of rainfed crops, grasslands, and reforestation that do not present irrigation (Fondo Español de Garantía Agraria, 2021). Therefore, all their pixels were used since no irrigation could affect their NDVI dynamics.

2.5.2. Los Velez (Almeria)- Z_{VCI} and Z_{WCI} relationship

To study the relationship between VCI and WCI anomalies a larger set of rangeland pixels was selected in Los Velez, in Almeria, southeast of Spain (Figure 2.8). The pixels had a spatial resolution of 250 m (MR). This area presents a mountainous landscape with a slope from 1-14%. With soils dominated by slightly acidic sandy soil (Xerochrept). This region has an overall Mediterranean climate. It has average monthly temperatures ranging from 5.4 to 24.1 with an average accumulated yearly precipitation of 373.8 mm (Fernández González, 2014). 621 pixels were selected. This rangeland pixel selection was provided by Tragsatec in collaboration with Entidad Nacional de Seguros Agrarios (ENESA).

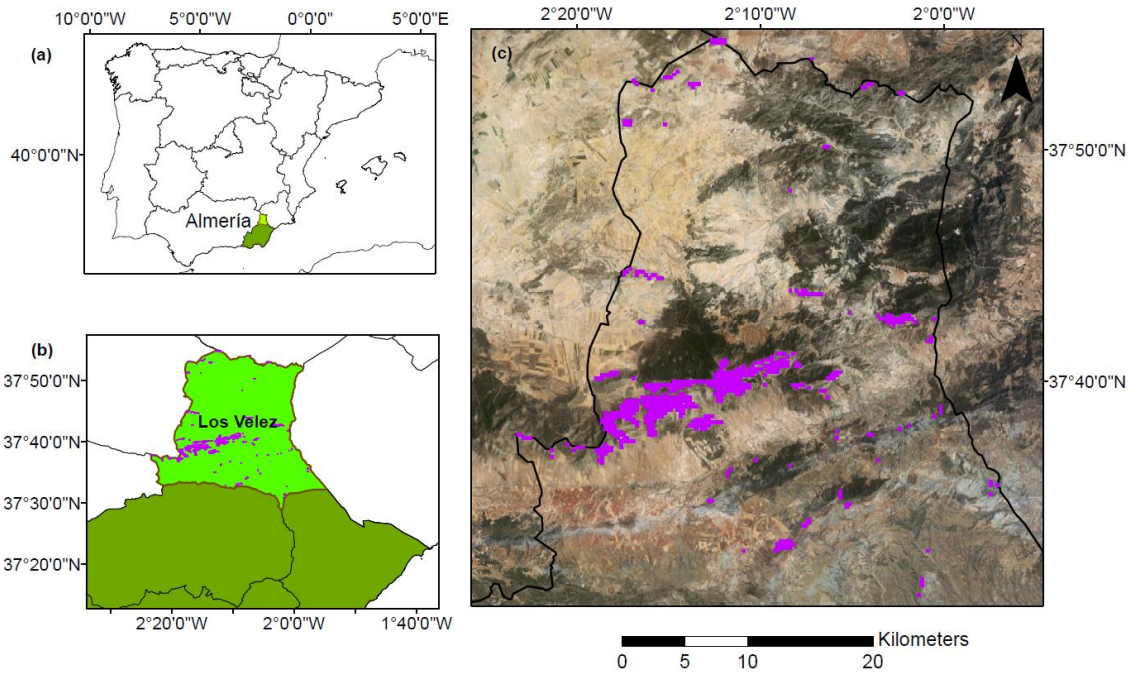

Figure 2.8.: Map representing the selected pixels in purple. In light green is the agricultural region and in dark green is the province of Almeria. a) Almeria province. b) Agricultural region Los Velez. c) Selected pixels.

2.5.3. South-eastern Spain –Clustering of rangelands based on NDVI annual patterns and their persistence

To study the clustering of rangeland pixels the dataset was collected covering three agricultural regions in two different provinces in the southeast of Spain (Figure 2.9). Los Velez in the province of Almería and Northwest and Northeast regions of the province of Murcia, which will be called Murcia-NW and Murcia-NE for clarity. These three regions have a Mediterranean arid climate with average annual precipitation of less than 300 mm, although with regional variations (Barceló and Nunes, 2009). The three regions are mainly placed in mountainous areas. The Murcia-NE region is mainly a mix of grassland and shrubland, Murcia-NW is dominated by sparse woodland mixed with shrubs, and in Los Velez grasslands and shrublands are the major vegetation with minimal areas of sparse woodland. These regions include areas with different aspects and changing slopes and elevations.

Pixels of 250 m were used. The pixel selection was provided by Entidad Estatal de Seguros Agrarios (ENESA, Ministerio de Agricultura, Pesca y Alimentación, Spain Government), by using Sistema de Información Geográfico de Parcelas Agrícolas (SIGPAC, Fondo Español De Garantia Agraria) and the Mapa Forestal Español (MFE, Spanish Forest Map). Firstly, pixels categorized as rangeland were selected using the SIGPAC and from this previous selection, pixels with a tree coverage higher than 15% were discarded to ensure a low tree coverage, based on the MFE. 3654 pixels of rangelands were obtained, divided into grasslands, shrublands, and open woodlands from this selection.

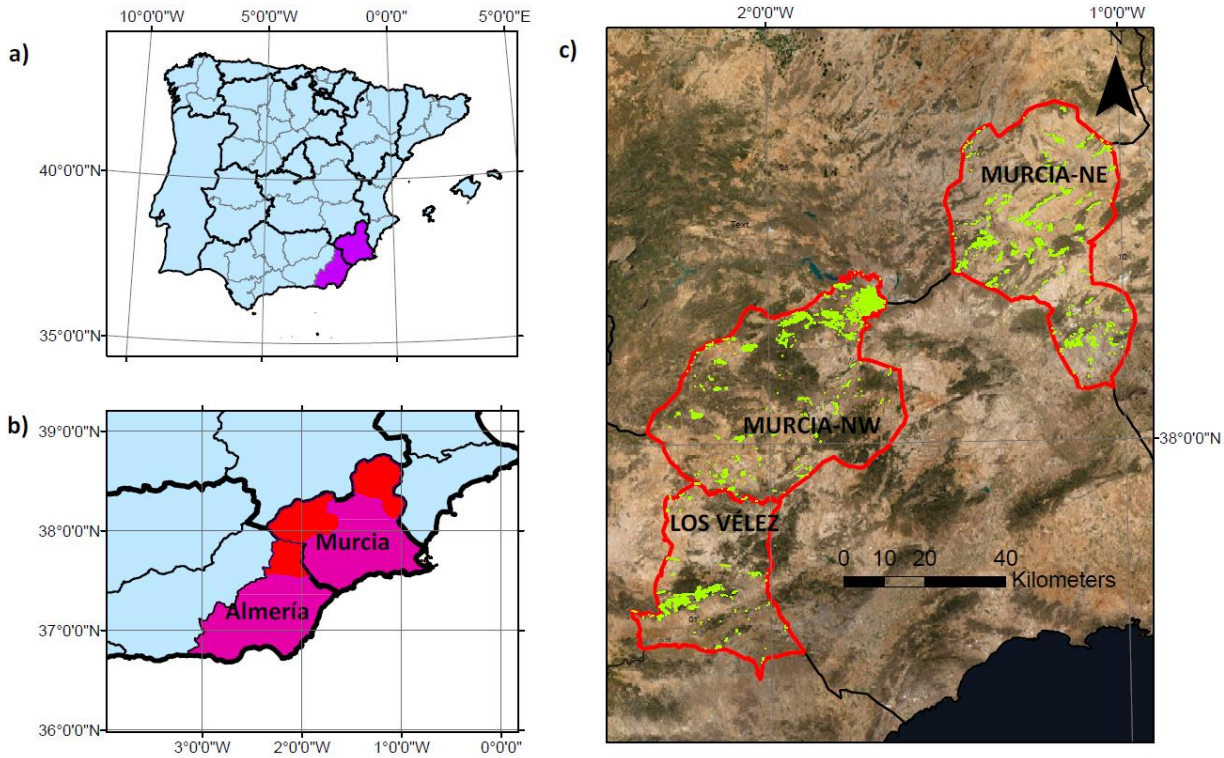

Figure 2.9. Location of the study area. (a) Selected Provinces (purple). (b) Selected agricultural regions of Almeria and Murcia (red). (c) Selected pixels in three agricultural regions of Almería and Murcia (light green).

3. TEMPORAL RESPONSE OF NDVI TO TEMPERATURE AND PRECIPITATION IN ARID RANGELANDS

3.1. Interannual variation

When yearly average NDVI, temperature, and precipitation were plotted at the two resolutions, different behaviours were found in these 18 years (Figure 3.1 and Figure 3.2). In all the areas (Murcia plots), NDVI at both resolutions were very similar. In A1 and A3, NDVI presents almost a constant value (A1 has around 20 and NDVI nearly 30) as does temperature (15 °C in every area, except A3 where it reaches 18 °C). Precipitation is constant in A1 while in A3 it shows an increasing trend (A3 presents the lowest precipitation, mostly below 300 mm and the remaining areas range between 300 and 400 mm). On the other hand, A2 and A4 NDVI present a slight increase (with values around 20 for A2 and 40 for A4). In both areas, temperature and precipitation show different trends.

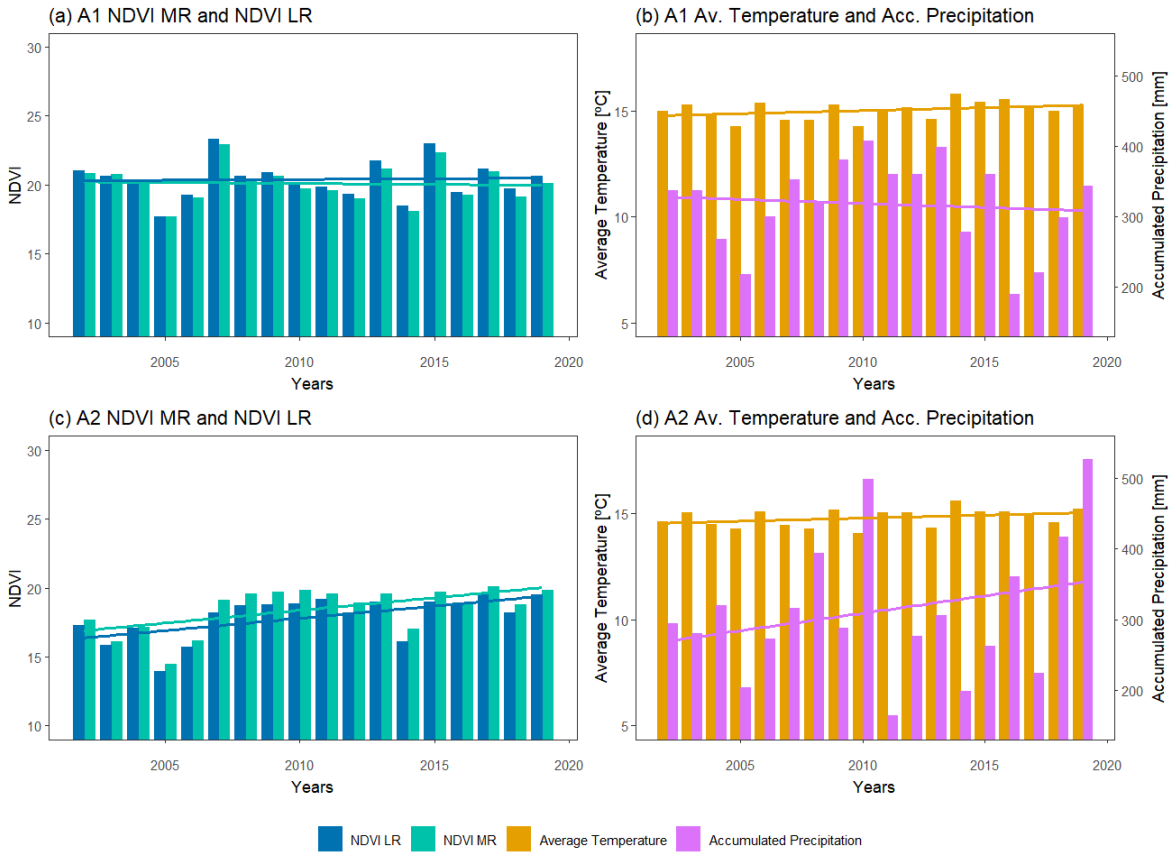

Figure 3.1. Bar plots of yearly average NDVI, temperature, and accumulated precipitation for A1 (a, b) and A2 (c, d) for Medium and Low resolutions.

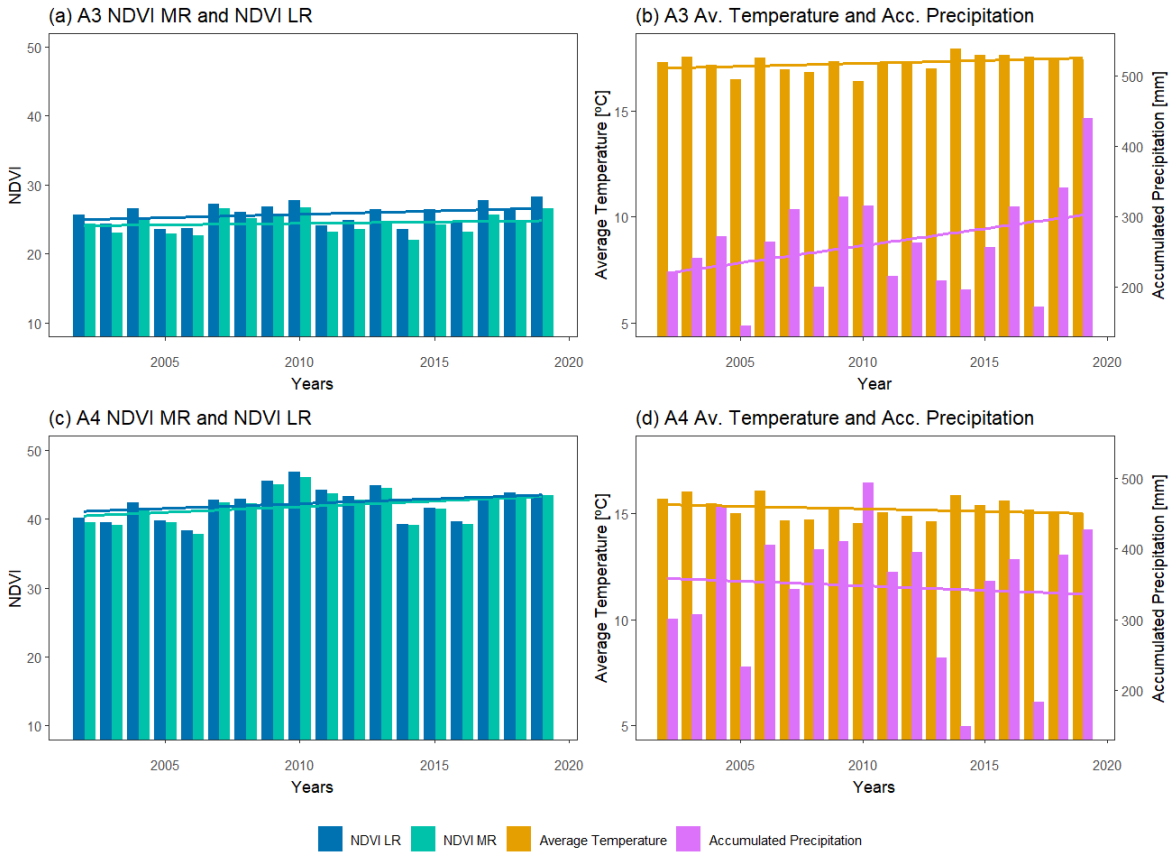

Figure 3.2. Bar plots of yearly average NDVI, temperature, and accumulated precipitation for A3 (a, b) and A4 (c, d) for Medium and Low resolutions.

To study whether these trends, visible in Figure 3.1 and Figure 3.2, are statistically significant, a Mann–Kendall test (Kendall, 1975; Mann, 1945) was applied in each area (Table 3.1). A1 shows a decreasing trend with NDVI MR and LR, but it is only significant with MR. On the other hand, A2 to A4 show an increasing trend, significant in both resolutions. The temperature increases in A1 to A3 and decreases in A4 and precipitation decreases in A1 and A4 and increases in A2 and A3. However, temperature and precipitation do not present significant trends, except for precipitation in A4, which decreases significantly.

Table 3.1. Mann–Kendall test results of the four areas with two spatial resolutions for NDVI, temperature and precipitation; * means that the trend was found significant; Temp: Temperature; Precip: Precipitation. MR: Medium resolution; LR: Low resolution. Areas: A1, rainfed croplands; A2, rainfed croplands+scrublands; A3, grassy+tree crops; and A4, open woodland+crops.

Areas	Trend	S-Statistics	Kendall's tau	*p*-Value
A1-MR	Decreasing *	−15,213	−0.04	<0.05
A1-LR	Decreasing	−7466	−0.02	0.34
A1-Temp	Increasing*	8849	0.03	<0.05
A1-Precip	Decreasing	−7547	−0.02	0.34
A2-MR	Increasing *	89,524	0.26	<0.05
A2-LR	Increasing *	98,292	0.28	<0.05
A2-Temp	Increasing	9115	0.02	0.25
A2-Precip	Decreasing	−4599	−0.01	0.55
A3-MR	Increasing *	18,649	0.05	<0.05
A3-LR	Increasing *	42,338	0.12	<0.05
A3-Temp	Increasing	9912	0.02	0.21
A3-Precip	Decreasing	−6017	−0.02	0.44
A4-MR	Increasing *	29,096	0.08	<0.05
A4-LR	Increasing *	24,762	0.07	<0.05
A4-Temp	Decreasing	−126	−0.0004	0.98
A4-Precip	Decreasing *	−17,068	−0.05	<0.05

3.2. Comparison of low and medium resolution series

The average NDVI time series with LR and MR are shown in the left column of Figure 3.1 and Figure 3.2 for the four areas studied. When the averages of all pixels for both resolutions are plotted, they tend to coincide. Nevertheless, we can differentiate them at the peaks and valleys of most years. In A1 and A2 (Figure 3.3), the two series are very similar. However, we can see some peaks where LR is higher for A1 and A2. This effect is more prominent in the A3 case. On the other hand, in A4, the differences are minor between the two resolutions (suggesting a larger homogeneity in this area). These peaks where LR is higher than MR are due to a few pixels and dates where the NDVI are much higher in both resolutions. However,

because the MR has more pixels averaged, the smoothing effect is more noticeable. Since not all pixels were used for A3, this rise of LR is more conspicuous.

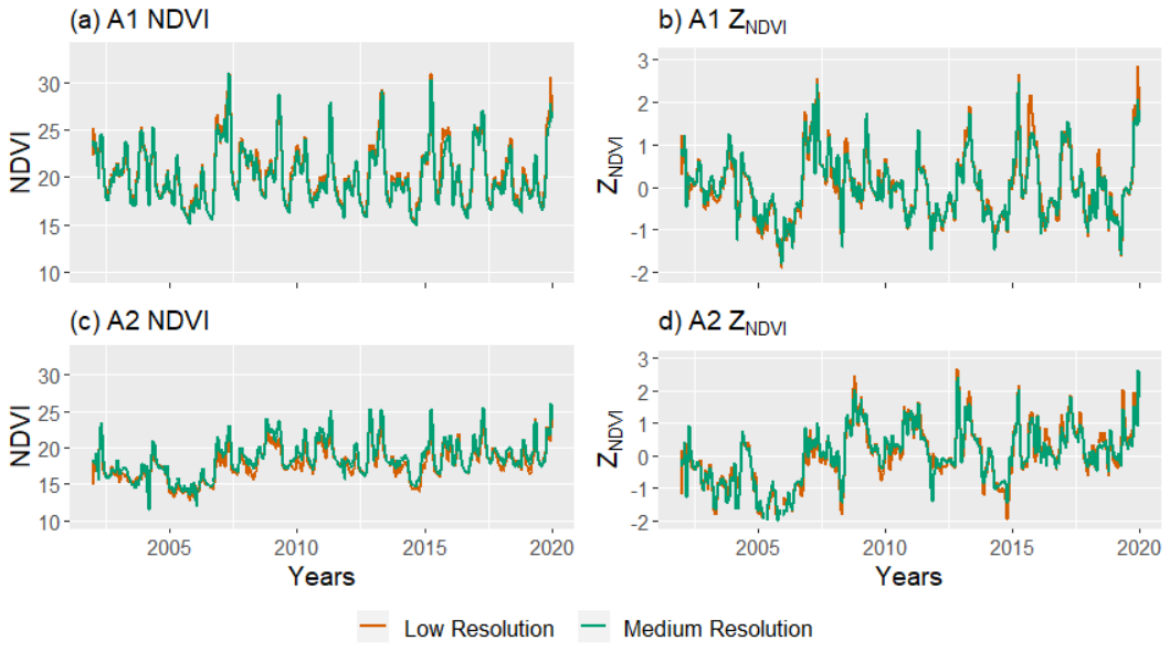

Figure 3.3. Series of average NDVI and Z_{NDVI} for A1 (a, b) and A2 (c, d) for both resolutions: orange shows low resolution (500 m) and green shows medium resolution (250 m).

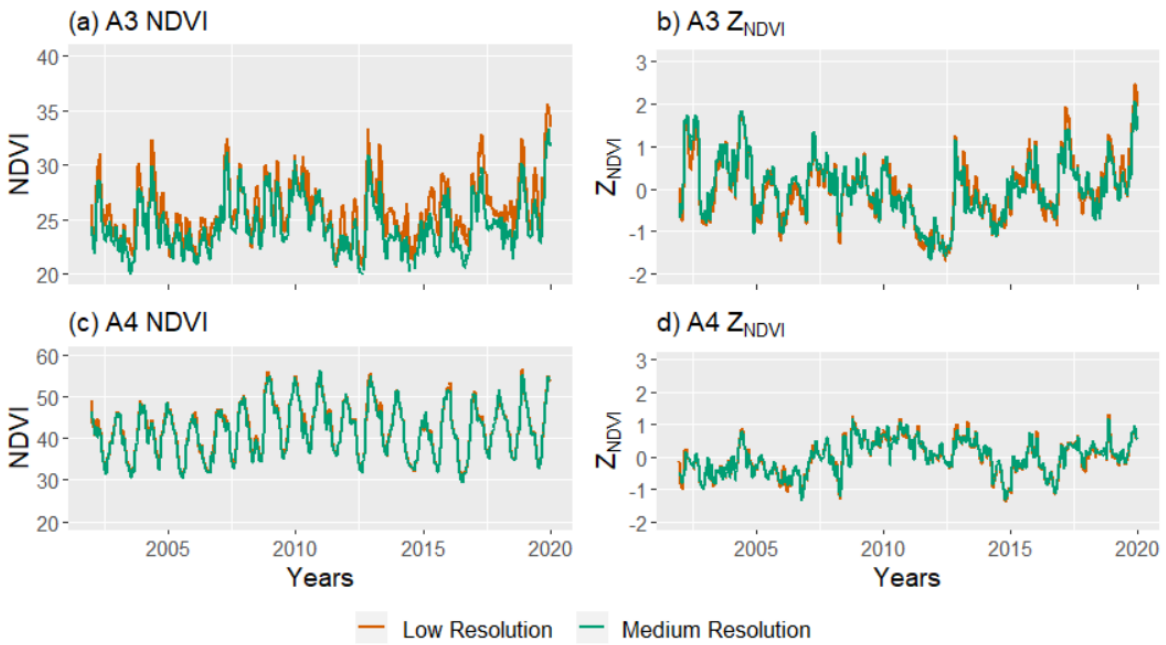

Figure 3.4. Series of average NDVI and Z_{NDVI} for A3 (a, b) and A4 (c, d) for both resolutions: orange shows low resolution (500 m) and green shows medium resolution (250 m).

In the right column of Figure 3.3 and Figure 3.4, we can observe the Z_{NDVI}. In all areas, there is a change in trend during 2006–2008. From 2000 until 2019, the year 2006 was one of the hottest, and after that, 2007 and 2008 were among the coolest years since 1996 (AEMET, 2020), as can be observed in Figure 3.1 and Figure 3.2. Looking at Figure 3.1 and Figure 3.3, A1 and A2 show Z_{NDVI} values in different years beyond +2 and −2. In these years, there are hotter temperatures for negative values with reduced precipitation. When Z_{NDVI} goes above 2, high peaks in precipitation and temperature are lower than in other years. Z_{NDVI} in A3 only goes above two once, at the end of 2019, coinciding with a strong peak in precipitation (Figure 3.2 and Figure 3.4). Area 4 does not show values beyond 2 or -2, although it shows how the series rises or drops with these events. Regarding the resolution in A1 to A3, we can see peaks and valleys where LR has a higher frequency of extreme values. These differences are smoother for A4. The use of Z_{NDVI} and its comparison to the NDVI series highlights the more significant changes during the series and the differences between the two resolutions. In particular, we find that extreme events are more pronounced in Z_{NDVI} when using LR, compared to MR.

The average NDVI values for LR and MR of MODIS display relatively strong similarities. However, differences between them in their series' peaks and valleys can be detected (Figure 3.3 and Figure 3.4). These differential patterns among areas suggest that it is caused by the difference of the averaged pixels within each area, showing that a finer scale is more representative of the area. On the other hand, some peaks and valleys are more pronounced, mainly when extreme meteorological events occur. These differences show a spatial difference among the pixels. These differences are confirmed with the following analysis: boxplots, Pearson correlation and regression analysis.

3.3. NDVI patterns in relation to meteorological variables

The LR and MR NDVI annual evolution and temperature and precipitation are shown in the following boxplots for each of the studied areas (Figure 3.5 to Figure 3.8). The LR and MR NDVI values in A1 and A2 are very similar, then A3 presents an increase in these values, and A4 has much higher NDVI values than the rest. This pattern may be, at least in part, explained by increasing tree coverage in those areas. In each graph, the year was divided into different phases as the NDVI average trend changed, as it did not match the change in climatic seasons (Table 3.2). Areas 1–3 were split into five phases, whereas A4 was split into four phases.

Table 3.2. Division of phases following the behaviour of NDVI. The selected phases in which there is an NDVI trend are shown in bold. Areas: A1, rainfed croplands; A2, rainfed croplands+scrublands; A3, grassy+tree crops; and A4, open woodland+crops.

Initial Dates	Area 1 to 3		Area 4	
	Phases	**NDVI Trend**	**Phases**	**NDVI Trend**
01-Jan	Phase 1	Steady	**Phase 1**	**Decreasing**
06-Mar	**Phase 2**	**Increasing**		
30-Mar			Phase 2	Steady
23-Apr	**Phase 3**	**Decreasing**		
17-May			**Phase 3**	**Decreasing**
28-Jul	Phase 4	Steady	**Phase 4**	**Increasing**
06-Sep	**Phase 5**	**Increasing**		

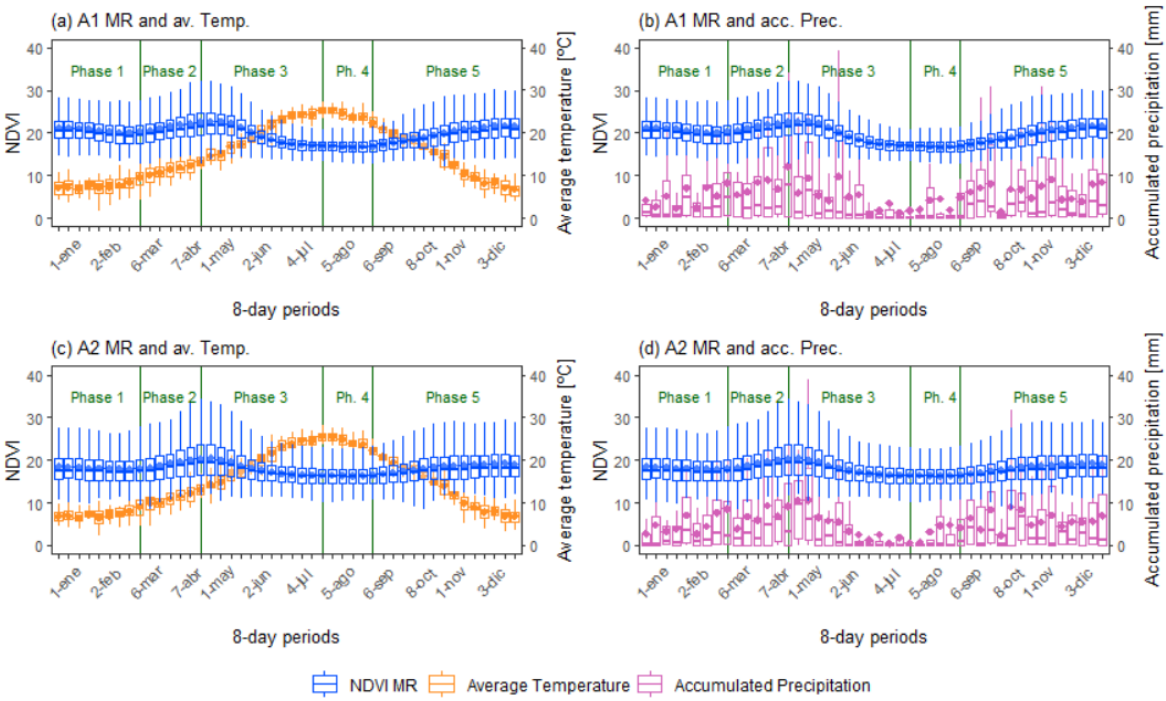

Figure 3.5. Boxplots of NDVI Medium Resolution (MR) for A1 (a, b) and A2 (c, d) in blue, average temperature in orange, and accumulated precipitation in purple.

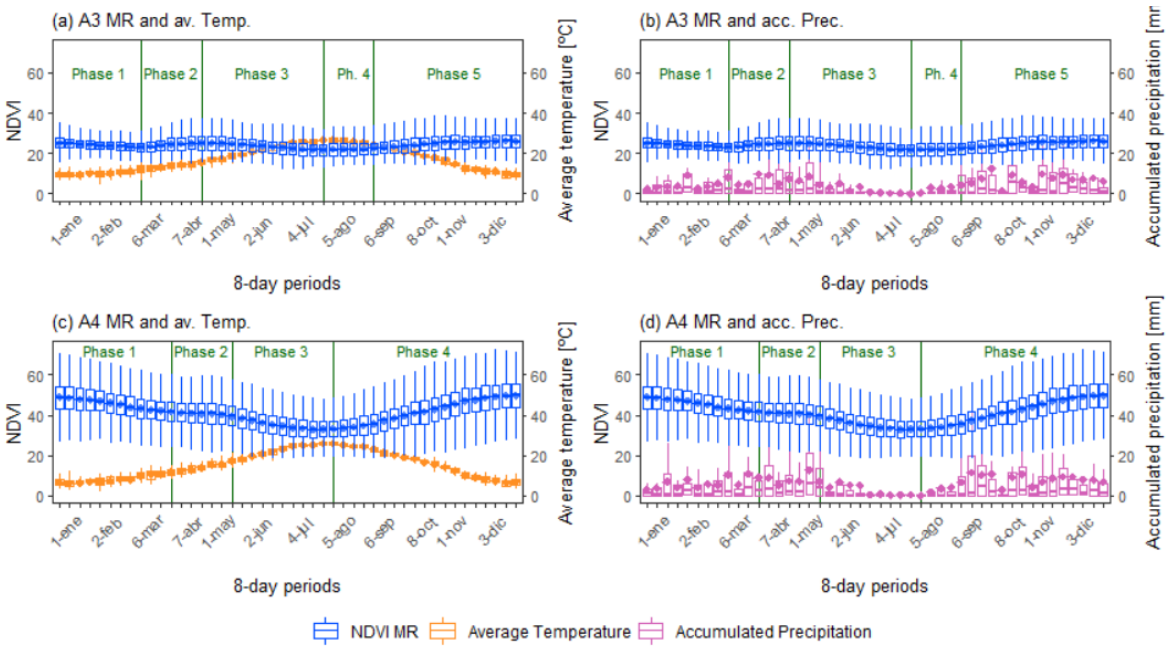

Figure 3.6. Boxplots of NDVI Medium Resolution (MR) for A3 (a, b) and A4 (c, d) in blue, average temperature in orange, and accumulated precipitation in purple.

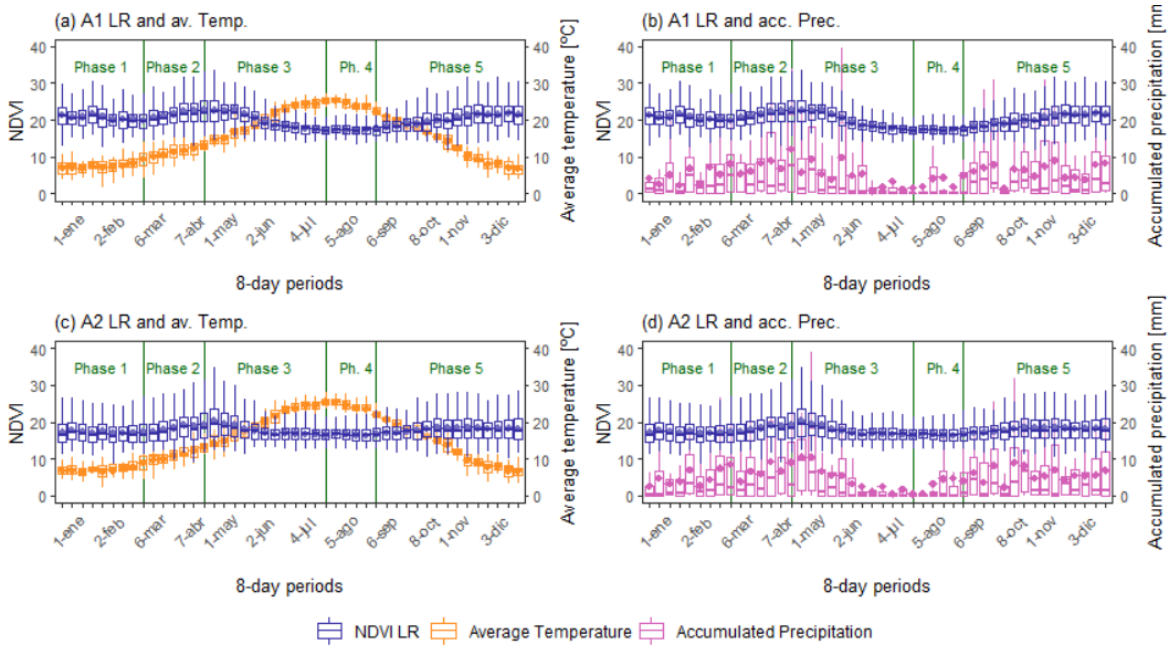

Figure 3.7. Boxplots of NDVI Low Resolution (LR) for A1 (a, b) and A2 (c, d) in dark blue, the average temperature in orange, and accumulated precipitation in purple.

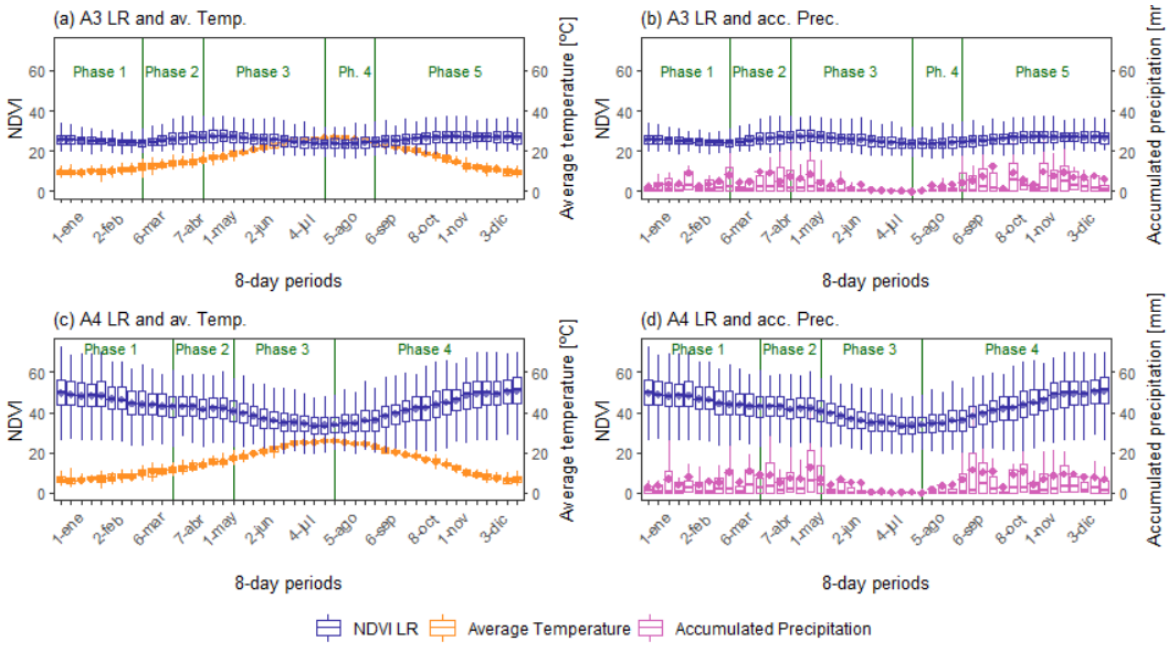

Figure 3.8. Boxplots of NDVI Low Resolution (LR) for A3 (a, b) and A4 (c, d) in dark blue, the average temperature in orange, and accumulated precipitation in purple.

A1 and A2 present a larger dispersion in NDVI during the spring (March, April, and May). This dispersion is present but less prominent in A3, probably due to its less abundant precipitation. A4 exhibits a more consistent dispersion of values

throughout the year with a reduction during the summer (June, July, and August), given by the almost complete tree coverage of this area. NDVI values decrease during the summer in all areas with a more visible trend in A4. NDVI and temperature appear to show a delay between their peak values. The average temperature peaks occur on July 28 in all the zones. The NDVI peaks on the July 20 in all the areas except A4, which showed it on July 12 (Figure 3.5 and Figure 3.7 for A1 and A2, and Figure 3.6 and Figure 3.8 for A3 and A4). Areas A1 to A3 are more heavily influenced by agricultural practices, which may cause the delay between NDVI and temperature, which only takes eight days. Area A4, as an open forest, does not have any irrigation regimes that can relate to an earlier peak of NDVI when temperatures rise. No different trends were found when boxplots were plotted for weeks, fortnights, months, or seasons (data not reported). Meteorological trends remain similar regardless of the temporal scale.

NDVI values are highly related to water availability, as stated by Holzapfel et al., (2006). NDVI responses are strongly linked to temperature in Mediterranean habitats, although this relationship weakens when precipitations are high (Alcaraz-Segura et al., 2009). In Murcia, the precipitations are scarce, with dry winters and almost no precipitation during the summer months. Furthermore, the temperature rises to its peak in July and August, leading to decreasing NDVI values. These values rise when the precipitation begins, and the temperature starts to descend. Our data show similar trends of higher NDVI values when precipitation increases, as highlighted by Chen and Weber (2014) and Iglesias et al. (2016). Area 4, located in the northwest county of Murcia, has relatively more water abundance and larger NDVI values.

We found differences in the boxplots among resolutions in A4, which is the most heterogeneous landscape, with a mix of tree-, scrub-, and grassy-dominated pixels. The medium resolution provided more significant results when studying their tendencies; the Mann–Kendall test for A1 with MR showed a tendency that was not

visible with LR. Regression analysis provided more robust results for the relationship of NDVI and climatic variables with MR in A2 and A3, while A1 and A4 had smoother results than A2 and A3. Additionally, MR NDVI had more delayed lagged correlations. The use of medium or low resolution may depend on the spatial heterogeneity of the areas of study. This is probably due to a more detailed depiction of NDVI values in MR, as a smaller pixel size allows us to separate areas that could be spatially diverse. MR allows emerging a more lagged correlation without being tampered with by the surroundings if an area dries at different times.

Using both resolutions shows a clearer image of the selected areas, especially highlighting those that are more heterogeneous. These results agree with Tarnavsky et al. (2008).

3.4. Intra-annual regression by phases

The regression analysis results between NDVI with temperature and precipitation by phases using the average of 18 years are shown in Figure 9.1–Figure 9.4 (in Appendix 2) for temperature and Figure 9.5–Figure 9.8 (in Appendix 2) for precipitation, a summary table of their R^2 are in Table 3.3. Phases 1 and 4 were eliminated in A1–A3 and Phase 2 in A4, since their NDVI values were steady (). The regression analysis shows that for A1 to A3 (Figure 9.1–Figure 9.3) temperature has a more substantial effect in NDVI in phases 2, 3, and 5, compared to phases 1 and 4, although phase 5 shows a slightly weaker relationship for A2, and especially A3. In A4, phases 3 and 4 show a strong relationship in the regression analysis and mild for phase 2 (Figure 9.4).

Table 3.3: R^2 from regression analyses shown in Appendix 2, for each area and spatial resolution. * was added when regression analysis was statistically significant (p-value<0.05). Phases in parentheses and green are for Area 4 which shows different vegetation dynamics to the other series. A1, rainfed croplands; A2, rainfed croplands+scrublands; A3, grassy+tree crops; and A4, open woodland+crops. Average Temperature (Temp) and Accumulated Precipitation (Pp).

Meteorological variables	Selected phases	Areas and spatial resolutions							
		A1		A2		A3		A4	
		LR	MR	LR	MR	LR	MR	LR	MR
Temp	Phase 2 (1)	0.98*	0.98*	0.89*	0.97*	0.99*	0.98*	0.91*	0.93*
	Phase 3	0.95*	0.97*	0.84*	0.96*	0.92*	0.98*	0.95*	0.99*
	Phase 5 (4)	0.97*	0.98*	0.68*	0.95*	0.7*	0.89*	0.99*	0.99*
Pp	Phase 2 (1)	0.04	0.057	0.31	0.07	0.007	0.055	0.21	0.21
	Phase 3	0.44*	0.55*	0.55*	0.69*	0.55*	0.69*	0.37	0.08
	Phase 5 (4)	0.003	0.009	0.00	0.03	0.01	0.001	0.001	0.008

The regression analysis for precipitation shows that for A1 to A3 (Figure 9.5–Figure 9.7), the herbaceous areas, NDVI in phase 3 is influenced by precipitation, while the others show a fragile relationship. No strong relationships are found in any phases in A4 (Figure 9.8). Due to the use of average values in the regression, differences between the two resolutions are small, although LR tends to have lower R^2 values than MR.

3.5. NDVI and meteorological series correlations

The Chow test confirmed significant structural differences between phases for all areas (Table 3.4). Medium- and low-resolution NDVI produced similar results in the previous analyses. However, there were differences, particularly regarding the lagged responses. This paragraph describes the results of MR NDVI correlation analysis and discusses the differences with LR NDVI. The correlation values mentioned are the highest lagged correlation (Table 3.5 and Table 3.6). NDVI has similar lags in each phase throughout A1 to A3. In phases 1 and 4, the NDVI values experience little change (with a difference within these phases between 4 and 10 in NDVI).

For this reason, temperature and precipitation have a minimal correlation with NDVI during these phases. Phase 2 shows a positive correlation between NDVI and temperature for these three areas: 0.32 for A1, 0.28 for A2, and 0.25 for A3. Phase 3 presents a moderate negative correlation for A1 and A2 (−0.73 and −0.61, respectively) and a low correlation (−0.12) in A3. Phase 5 has a low negative correlation for A1 (−0.32), A2 (−0.35), and A3 (−0.04). Area 4 always presents a negative correlation between temperature and NDVI, all lower than −0.4 except in phase 3, which has a stronger negative correlation of −0.73. Precipitation presents small positive values in all phases and areas, all below 0.35.

Table 3.4. Chow test of NDVI and time of all areas and phases, given with F-statistic and *p*-value for each continuous phase pair: phase 1 (P1), phase 2 (P2), phase 3 (P3), and phase 4 (P4). Areas: A1, rainfed croplands; A2, rainfed croplands+scrublands; A3, grassy+tree crops; and A4, open woodland+crops. F-stat: F-statistic, and p-val.: P-value.

Phases	**A1**		**A2**		**A3**		**A4**	
	F-stat.	***p*-val.**	**F-stat.**	***p*-val.**	**F-stat.**	***p*-val.**	**F-stat.**	***p*-val.**
P1–P2	7.05	0.001	7.44	0.001	6.31	0.002	71.16	0.000
P2–P3	4.67	0.010	3.33	0.037	4.54	0.011	108.00	0.000
P3–P4	60.96	0.000	33.81	0.000	22.64	0.000	99.95	0.000
P4–P5	53.44	0.000	34.65	0.000	48.39	0.000		

Table 3.5. Lagged correlations of medium resolution NDVI and meteorological parameters (Meteo) for A1 and A2. Only the phases with an increasing or decreasing NDVI trend are included. For each phase, bold values show the strongest correlations among the different time lags tested. Average Temperature (Temp) and Accumulated Precipitation (Pp).

Area	Meteo	Phase	Lag Time (Days)						
			0	8	16	24	32	40	48
A1	Temp	Phase 2	0.23	0.3	0.32	0.29	0.29	0.19	0.13
		Phase 3	−0.72	−0.72	−0.72	−0.72	−0.73	−0.7	−0.66
		Phase 5	−0.5	−0.52	−0.52	−0.51	−0.52	−0.51	−0.5
	Pp	Phase 2	0.11	0.19	0.26	0.24	0.28	0.28	0.2
		Phase 3	0.21	0.22	0.21	0.2	0.15	0.12	0.15
		Phase 5	0.08	0.08	0.11	0.13	0.17	0.23	0.25
A2	Temp	Phase 2	0.18	0.22	0.25	0.24	0.29	0.21	0.17
		Phase 3	−0.58	−0.58	−0.59	−0.59	−0.61	−0.58	−0.55
		Phase 5	−0.35	−0.35	−0.34	−0.34	−0.34	−0.33	−0.32
	Pp	Phase 2	0.12	0.12	0.15	0.19	0.17	0.15	0.03
		Phase 3	0.17	0.19	0.22	0.23	0.19	0.17	0.17
		Phase 5	0.23	0.3	0.32	0.29	0.29	0.19	0.13

Table 3.6. Lagged correlations of medium resolution NDVI and meteorological parameters (Meteo) for A3 and A4. Only the phases with an increasing or decreasing NDVI trend are included. For each phase, bold values show the strongest correlations among the different time lags tested. Average Temperature (Temp) and Accumulated Precipitation (Pp).

Area	Meteo	Phase	Lag Time (Days)						
			0	8	16	24	32	40	48
A3	Temp	Phase 2	−0.09	0.04	0.13	0.25	0.25	0.21	0.20
		Phase 3	−0.04	−0.06	−0.09	−0.12	−0.11	−0.09	−0.07
		Phase 5	−0.02	−0.03	−0.04	−0.04	−0.03	−0.02	−0.01
	Pp	Phase 2	0.28	0.22	0.14	0.01	0.07	0.10	0.09
		Phase 3	0.06	0.08	0.15	0.19	0.16	0.18	0.17
		Phase 5	0.12	0.10	0.10	0.08	0.08	0.13	0.14
A4	Temp	Phase 1	−0.14	−0.11	−0.07	−0.01	−0.04	0.04	0.09
		Phase 3	−0.71	−0.72	−0.73	−0.72	−0.73	−0.71	−0.69
		Phase 4	−0.31	−0.23	−0.17	−0.07	−0.02	0.00	0.03
	Pp	Phase 1	0.02	0.03	0.10	0.08	0.12	0.11	0.11
		Phase 3	0.25	0.24	0.25	0.25	0.24	0.21	0.23
		Phase 4	0.34	0.34	0.27	−0.05	−0.02	0.06	0.02

Lags on temperature for A1 to A3 in phases 1 and 4 range from 0 to 8 days, except for phase 4 in A2. All of these have very low values due to the constant behaviour of NDVI values. In phase 2, the highest correlation between NDVI and temperature is found with a 16-day lag in A1 and a 32-day lag in A2 and A3. Phase 3 has lags of 24 and 32 days for these three areas. Phase 5 differs more between areas, with a lag of 32 days for A1, eight days for A2, and 24 days in A3. Area 4 only shows a 16-day lag in phase 3, while the rest of its phases present no lag. The differences between the areas may be related to two factors, differences between their vegetation and their hydrological regimes. Precipitation correlation lags show small similarities between all four areas. The scattered precipitations of these habitats and water scarcity make it difficult to find a pattern across the areas. These disparities appear to be related to differences in heavy rains at specific times in each phase and area.

Comparing these results with the LR ones (Table 3.7 and Table 3.8), correlation exhibited one of our analyses' significant differences between the two resolutions. The lag presented by the highest correlation with temperature was similar for MR and LR, except for some cases where there was an approximate difference of 8-day lag. However, phases 4 and 5 present more significant differences with a lag of 16 and 32 days, in some cases. The precipitation variable presents an almost constant smaller lag in the LR, ranging from 8 to 48 days. A partial correlation with NDVI, temperature and precipitation was made, but no significant differences were found (Table 9.2 and Table 9.3, in Appendix 3).

Table 3.7. Lagged correlations of Low Resolution (LR) NDVI and meteorological parameters (Meteo) for A1 and A2. Only the phases with an increasing or decreasing NDVI trend are included. For each phase, bold values show the strongest correlations among the different time lags tested. Average Temperature (Temp) and Accumulated Precipitation (Pp).

Area	Meteo	Phase	Lag Time (Days)						
			0	**8**	**16**	**24**	**32**	**40**	**48**
A1	Temp	Phase 2	0.2	0.25	0.34	0.25	0.33	0.32	0.16
		Phase 3	−0.67	−0.66	−0.66	−0.65	−0.66	−0.64	−0.61
		Phase 5	−0.41	−0.43	−0.44	−0.44	−0.44	−0.42	−0.41
	Pp	Phase 2	0.18	0.16	0.23	0.26	0.18	0.19	0.18
		Phase 3	0.19	0.19	0.19	0.21	0.15	0.13	0.18
		Phase 5	0.17	0.1	0.11	0.13	0.16	0.23	0.24
A2	Temp	Phase 2	0.16	0.16	0.23	0.2	0.3	0.33	0.22
		Phase 3	−0.45	−0.46	−0.46	−0.46	−0.48	−0.46	−0.46
		Phase 5	−0.18	−0.2	−0.19	−0.19	−0.17	−0.16	−0.15
	Pp	Phase 2	0.19	0.06	0.16	0.2	0.15	0.03	−0.03
		Phase 3	0.13	0.12	0.21	0.27	0.18	0.2	0.15
		Phase 5	0.2	0.25	0.34	0.25	0.33	0.32	0.16

Table 3.8. Lagged correlations of Low Resolution (LR) NDVI and meteorological parameters (Meteo) for A3 and A4. Only the phases with an increasing or decreasing NDVI trend are included. For each phase, bold values show the strongest correlations among the different time lags tested. Average Temperature (Temp) and Accumulated Precipitation (Pp).

Area	Meteo	Phase	Lag Time (Days)						
			0	8	16	24	32	40	48
A3	Temp	Phase 2	0.09	0.12	0.12	0.12	0.01	0.05	0.09
		Phase 3	−0.40	−0.41	−0.41	−0.42	0.41	−0.39	−0.36
		Phase 5	−0.28	−0.28	−0.27	−0.26	−0.24	−0.20	−0.16
	Pp	Phase 2	0.31	0.29	0.27	0.18	0.15	0.21	0.14
		Phase 3	−0.08	−0.02	0.04	0.09	0.08	0.12	0.15
		Phase 5	0.16	0.14	0.16	0.15	0.15	0.20	0.19
A4	Temp	Phase 1	−0.17	−0.10	0	0.05	−0.07	0.00	0.02
		Phase 3	−0.66	−0.65	−0.67	−0.66	−0.67	−0.64	−0.63
		Phase 4	−0.29	−0.14	−0.13	−0.01	0.02	0.05	0.08
	Pp	Phase 1	0.14	−0.01	0.03	0.06	0.13	0.09	0.09
		Phase 3	0.25	0.25	0.22	0.26	0.22	0.18	0.22
		Phase 4	0.41	0.30	0.18	−0.09	−0.07	0.01	−0.02

Our correlation analysis shows that NDVI data are strongly and negatively correlated to average temperature when precipitation is strongly limited. The intraseasonal variation of the relationship between the NDVI and the meteorological variables has been approached by using different phases based on the NDVI behaviour. The patterns of NDVI correlations with temperature change depending on the land use and the phase selected. Phases 1 and 4 show weak correlation values because the NDVI presents a steady pattern. On the other hand, phases 2, 3, and 5 have either increasing or decreasing NDVI trends. These phases present negative values except for phase 2 for A1 to A3 when the spring precipitation occurs. The correlations for NDVI and precipitation are very low, all below 0.35. However, the regression analysis highlights a stronger relationship for A1 to A3 for phase 3, when the precipitation starts high and steadily drops as

temperature increases. A4, covered with trees, does not show a strong relationship between NDVI and precipitation where its precipitation in phase 2 is more limited than in the other areas. These changes among phases suggest that one of the critical factors affecting NDVI is water availability, matching other areas with semiarid and arid climates (He et al., 2015; Mahyou et al., 2010)

3.6. Aridity index and NDVI

After characterizing the climatic variables and NDVI dynamics, we approached how the NDVI was affected by the AI, as a combination of precipitation and potential evapotranspiration, reflecting the temperature as well. This relation was established by accumulating the average NDVI and AI for each phase, defined in the different areas. The NDVI and AI was plotted in a cumulative graph. This allowed us to see how the different vegetation types representing each area responded differently to water availability. Figure 3.9 shows the four areas clustered into two groups. On one side, we find A1 and A2 intermingling. These two areas present lower cumulative NDVI than A3 and A4, and higher cumulative values of AI than A4 and A3, representing different types of crops: A1 and A2 show a smaller NDVI in response to a similar AI than A3 and more remarkably A4.

The AI for A4 was calculated based on its four phases, instead of five as was done for the other areas. However, this change does not affect the pattern and slope of this graphic. In the upper part of Figure 3.9, we find A3 and A4 showing a more efficient use of water resources. Their higher slope reflects the increase of NDVI as AI rises. With more typical Mediterranean vegetation (as opposed to crops in A1 and A2), A3 and A4 have more efficient water use, particularly A3 with xerophilous shrubs like esparto, as opposed to less xeric shrub vegetation, such as rosemary found in A4.

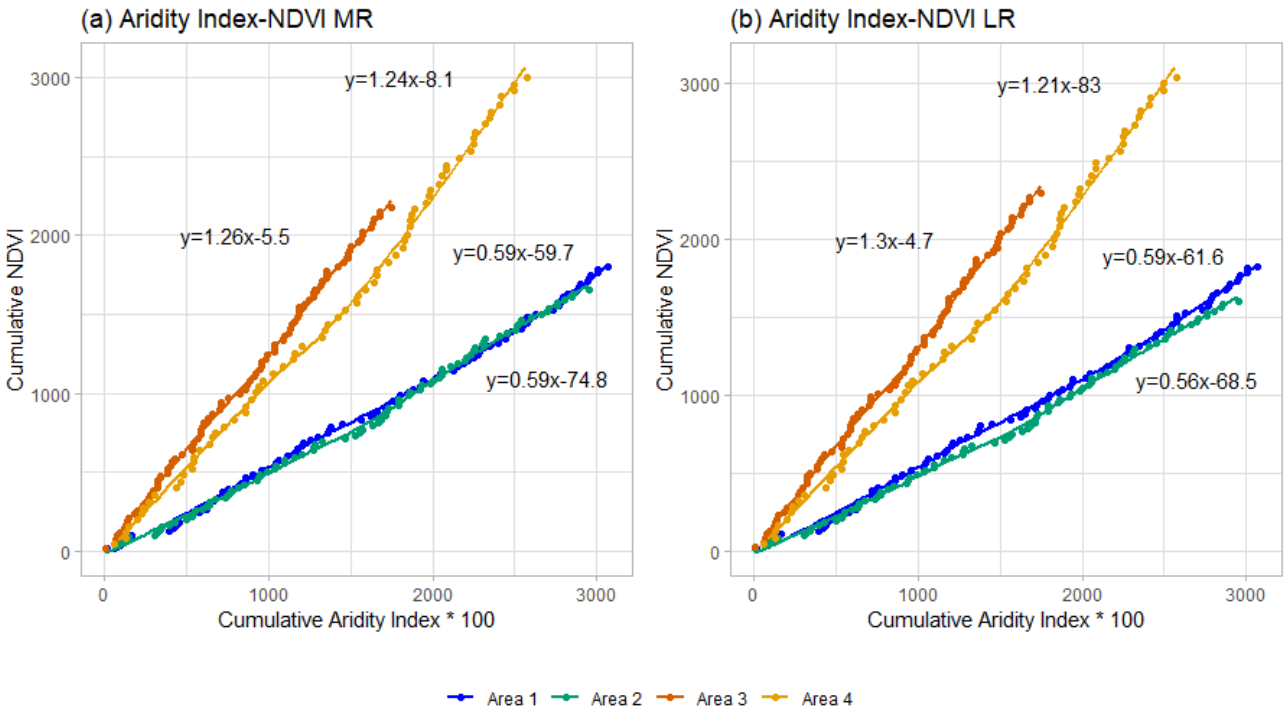

Figure 3.9. Linear regression analysis of cumulative aridity index and cumulative NDVI of all areas for medium resolution (a), and low resolution (b). All R^2 values are above 0.99.

4. SOIL WATER CONTENT AND VEGETATION. THE TEMPORAL RELATIONSHIP BETWEEN Z_{WCI} AND Z_{VCI}

4.1. Water and vegetation condition indices

Firstly, we studied the dynamics of VCI and WCI without the anomalies of Los Velez in Almeria province. Figure 4.1 shows how the vegetation growth increases during the end of Summer and the beginning of autumn, then decreases until February and increases again until April. Therefore, as the dynamics of VCI do not match the season (a rise and a drop are seen for example during the Autumn). Following Sanz et al. (2021a) four phases were proposed to analyse the vegetation and soil dynamics. In phases 1 and 2 the VCI and WCI have more similar dynamics among them, while in phases 3 and 4 the VCI increases and decreases, respectively, while the WCI shifts during these periods are subtler. This concurs with the increase in temperature that occurs in phases 3 and 4 (Figure 4.2), while in phases 1 and 2, the temperature is not as high and precipitations tend to be more common, at least compare to phase 4. In phase 3 precipitations are abundant but temperature and evapotranspiration play an important role in superficial soil water content, obscuring the relationship between precipitation and water soil content (Sanz et al., 2021a; Wang et al., 2003).

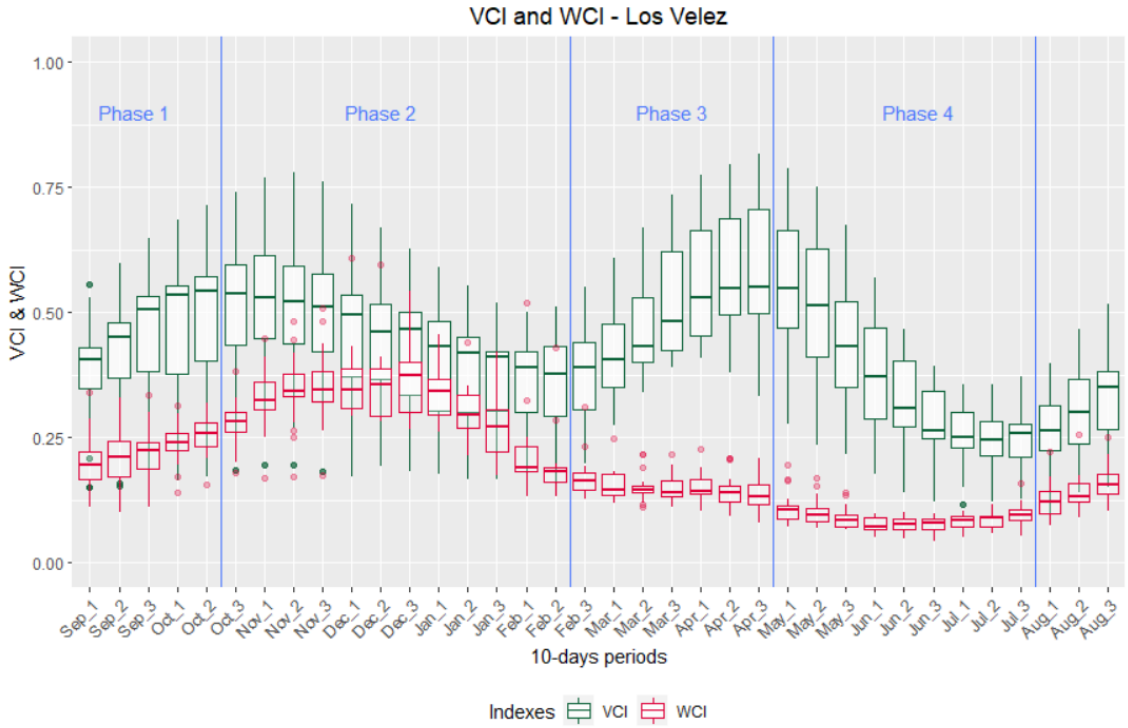

Figure 4.1. Boxplots for vegetation condition index (VCI) and water condition index (WCI) for each 10-day period of the year (e.g. Sep_1/2/3 represent the first, second, and third ten days periods of September). VCI is represented in dark green and WCI in maroon. The blue vertical lines represent the phases split based on the VCI dynamics.

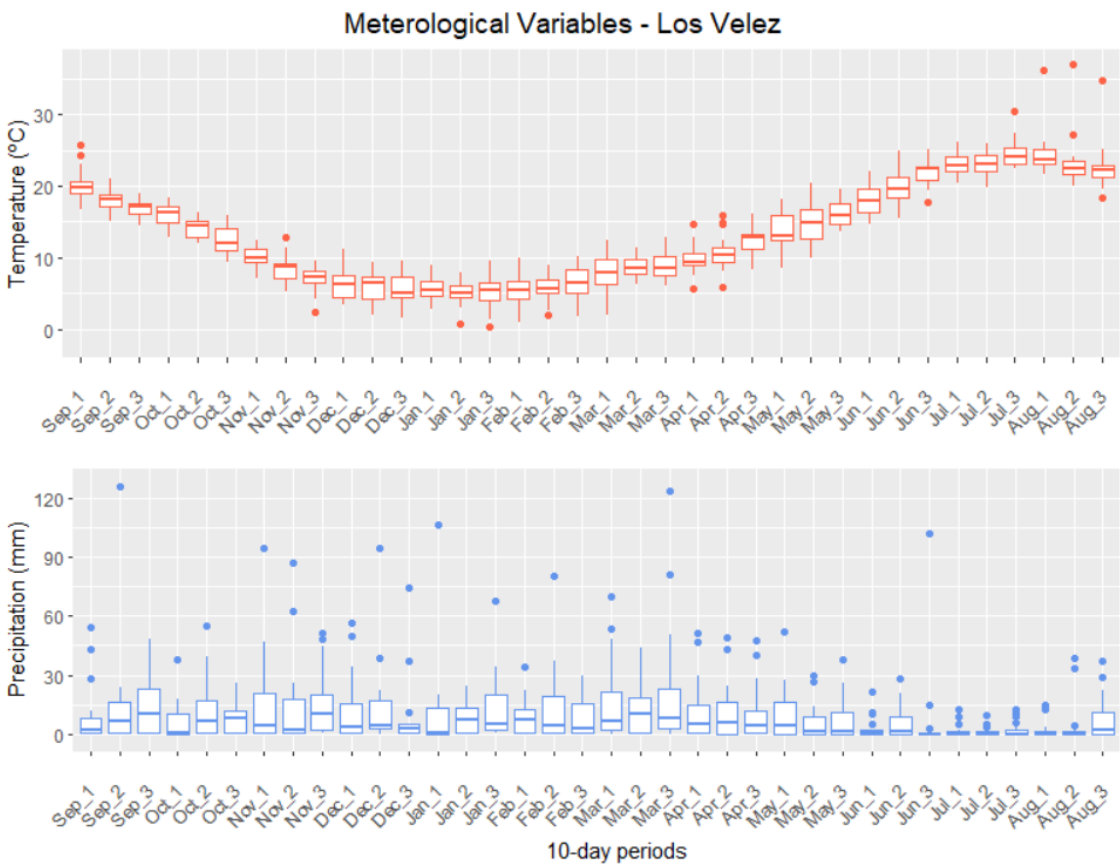

Figure 4.2. Boxplots for Temperature (orange) and precipitation (blue) for each 10-day period of the year (e.g. Sep_1/2/3 represent the first second and third 10-day periods of September).

Secondly, we studied the time series of the anomaly indices for the average of the region, as well as their severity at the three selected thresholds. Z_{VCI} is more continuous and smoother than Z_{WCI}, which presents a rougher profile with higher peaks (Figure 4.3).

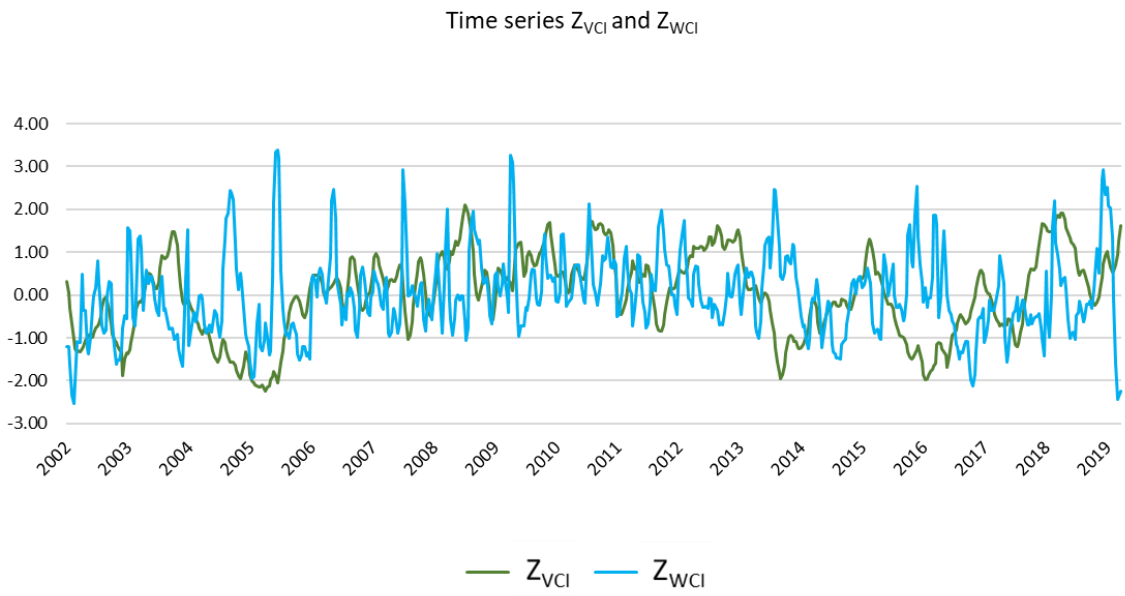

Figure 4.3. Time series Z score for the average of the selected pixels of Los Velez. In green, we can observe the Z_{VCI} and in blue Z_{WCI}.

Figure 4.4 shows the probability of each threshold for Z_{VCI} to occur for each 10-day period. The chance of passing the first threshold increases from December to the end of May, peaking in April. On the other hand, the probability for Z_{VCI} to pass below -1 is kept rather constant for most of the year, increasing approximately from 15 % to 25 % from September to mid-October. This provides a basic risk for each period, the base probability. A similar graphic, but for Z_{WCI} is presented in Figure 4.5. The probabilities are larger for the -0.5 threshold for Z_{WCI}, while the threshold -1 shows more oscillations with more periods with 0, compared to Z_{VCI}. However, a similar pattern is shown for thresholds -0.5 and -0.7 of Z_{WCI}, compared to those thresholds in Z_{VCI}, although the higher probabilities are located from December to June, with drops in between.

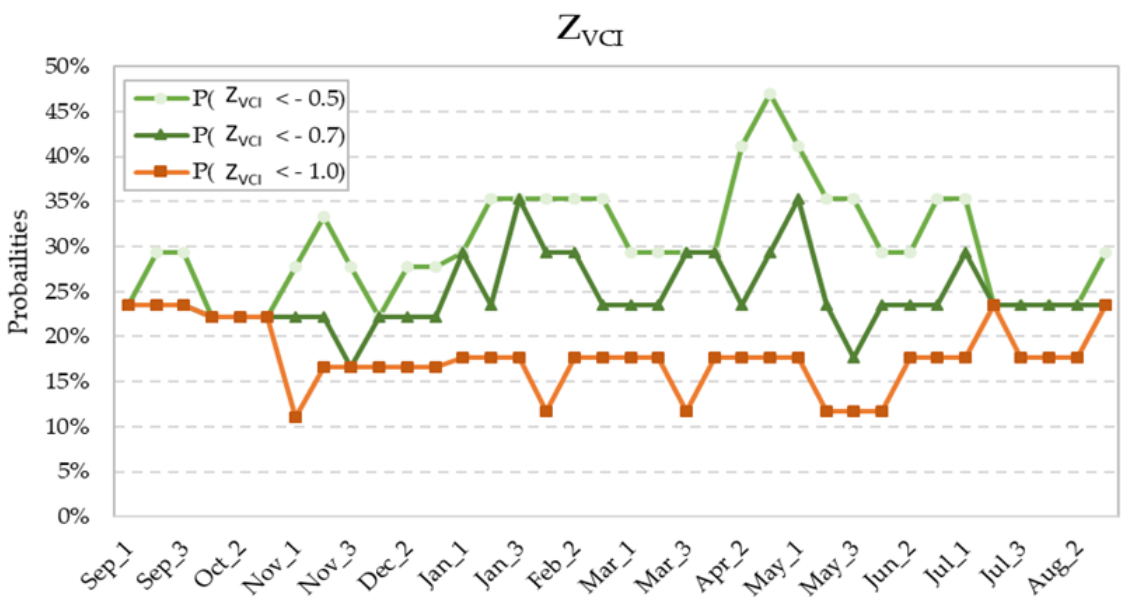

Figure 4.4. Probabilities for the Z_{VCI} to pass below the three thresholds for each 10-day period. Threshold -0.5 in light green, -0.7 in dark green, and -1 in orange.

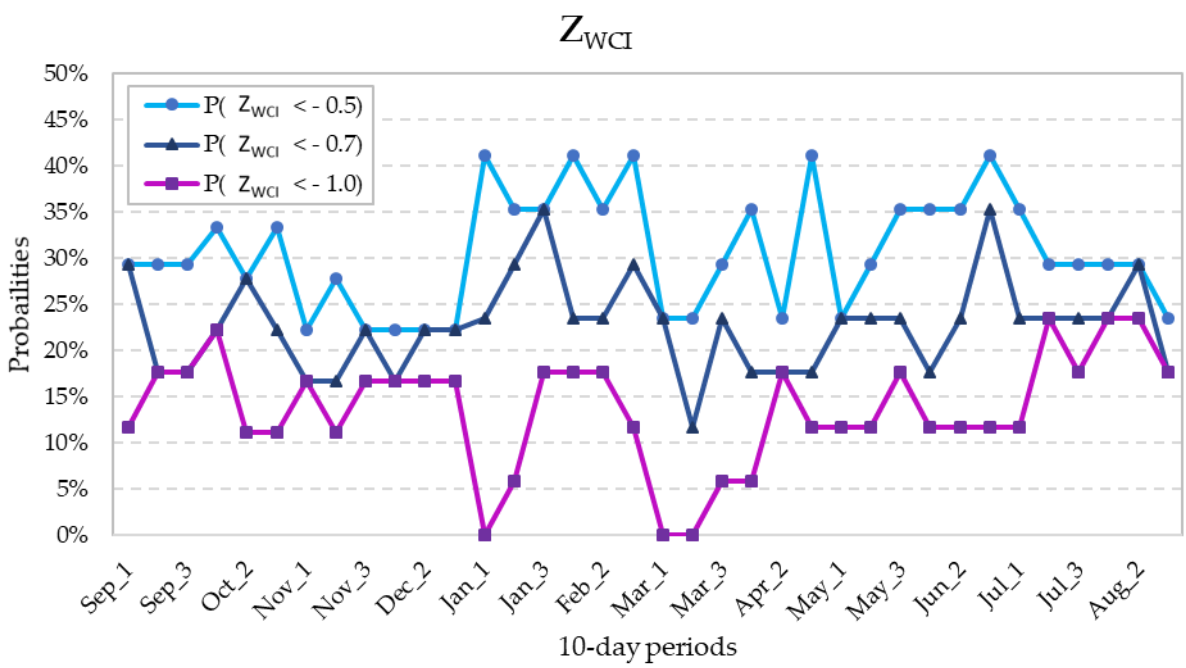

Figure 4.5. Probabilities for the Z_{WCI} to pass below the three thresholds for each 10-day period. Threshold -0.5 in light blue, -0.7 in dark blue, and -1 in purple.

4.2. Relationship of VCI and WCI anomalies

For each threshold, the base probability of Z_{VCI} and the conditional probability are shown in Figure 4.6 to Figure 4.8. For all thresholds, the conditional probability is higher from September to April, without considering the lags. When positive lags are calculated for Z_{VCI}, the probability compared to no lag probability is higher from September to January and some periods of March. The increase in probability is larger with smaller anomalies (-0.5), reaching often from 50% to 80% of conditional probability from September to January (compared to an average of 30% of base probability for -0.5). These probabilities decrease when we use -0.7, especially, with -1 as the threshold reaching a maximum of 67%. And decreasing the probabilities in general, but still staying above the base probability, as the base probability also decreases when the thresholds lower.

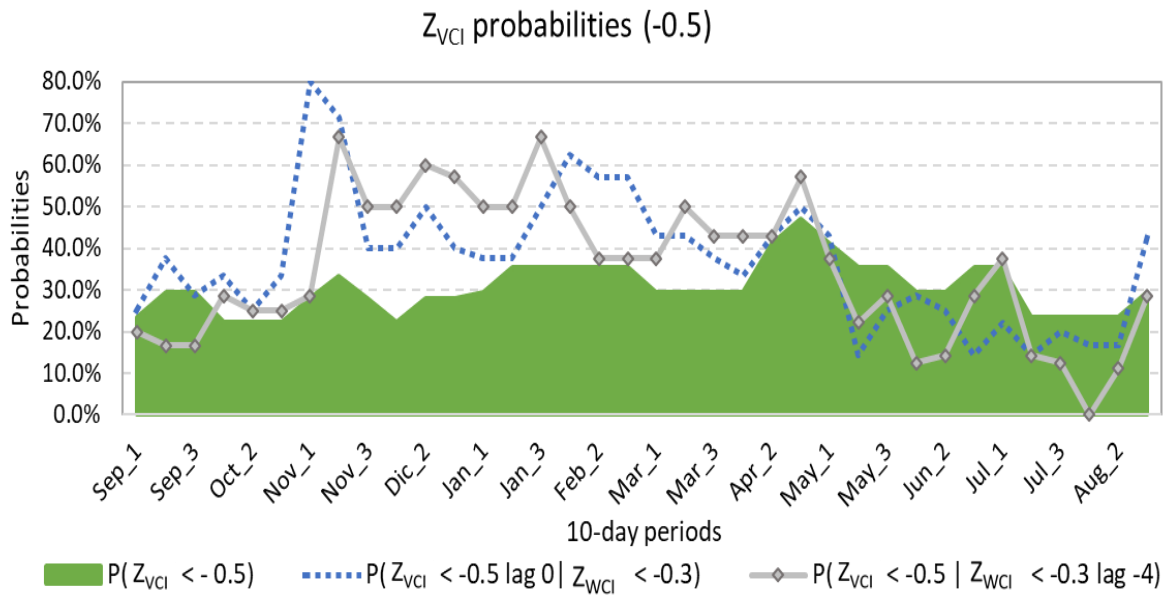

Figure 4.6. Probability for Z_{VCI} to be below -0.5 (light green), conditional probability without lag (dotted blue) and condition probability for lag 4 (grey).

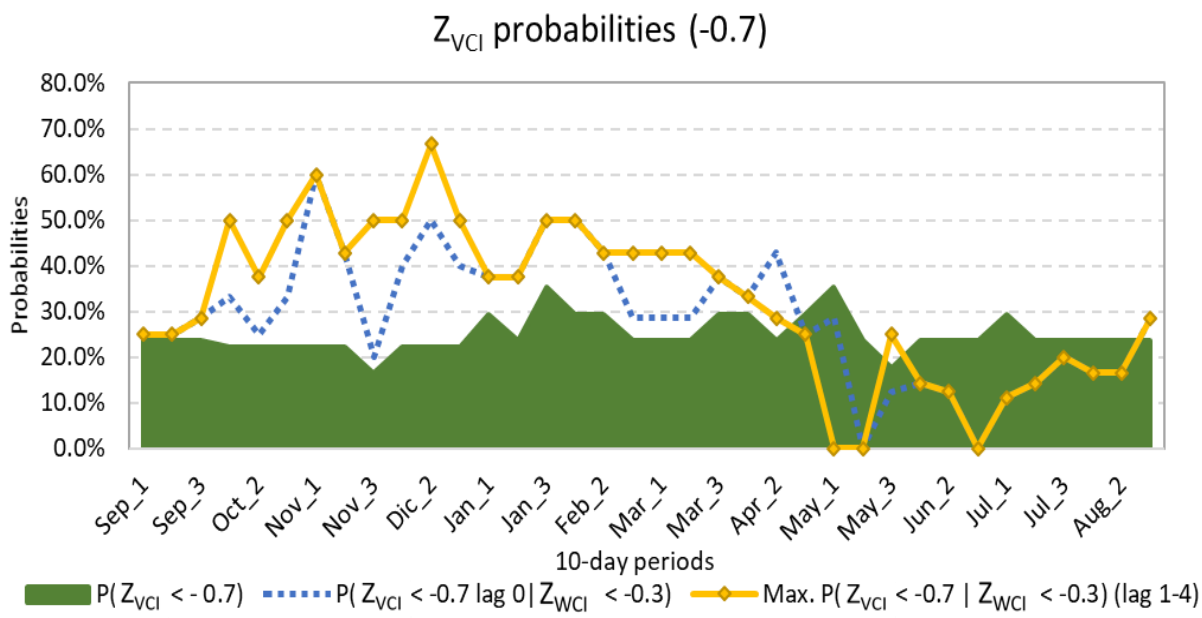

Figure 4.7. Probability for Z_{VCI} to be below -0.7 (dark green), conditional probability without lag (dotted blue) and maximum condition probability for lag 4 (yellow).

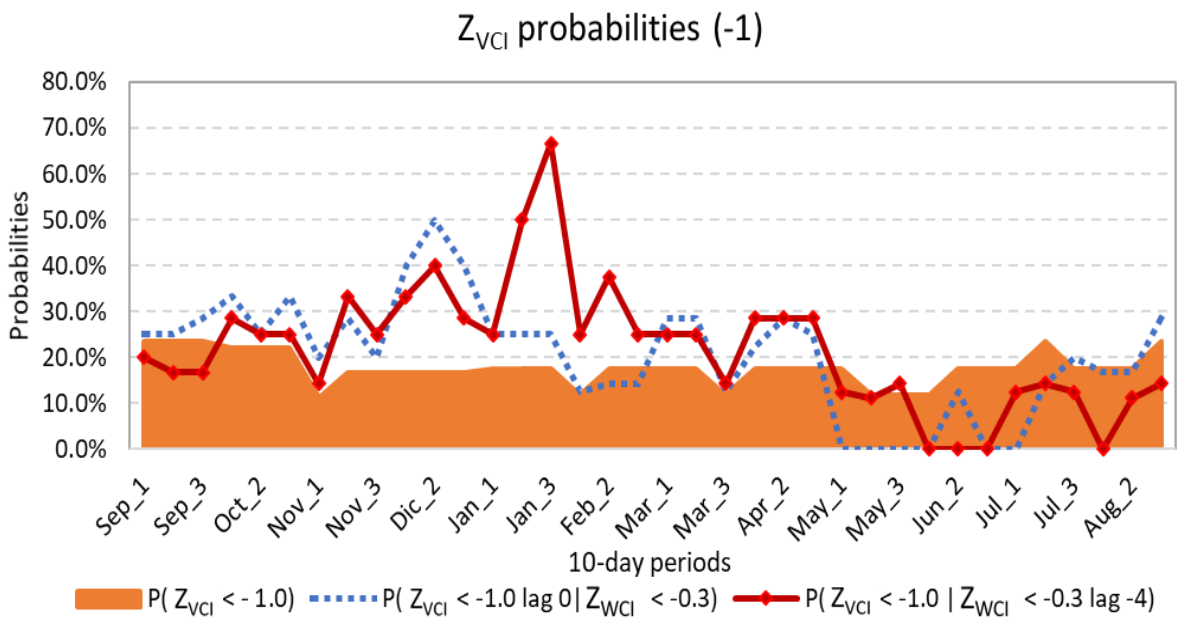

Figure 4.8. Probability for Z_{VCI} to be below -1 (orange), conditional probability without lag (dotted blue) and maximum condition probability for lag 4 (dark red).

For all thresholds from September to April, the conditional probability is higher than the base probability for those periods. Threshold -0.5 has a larger increase in predictability from September to November and from the second period of January to March, while the increase in predictability is the highest in December and the first period of January for threshold -1. This is shown in Figure 4.9. From September to March the precipitation is more or less abundant but they concur with low temperatures. From April, while the precipitations are still falling the temperature increases until the end of Summer. Therefore, this could explain why the predictability of vegetation anomalies using the water soil content index is improved in the months where temperature and evapotranspiration play a major role in water soil content (Cui and Shi, 2010; Sanz et al., 2021a; Wang et al., 2003).

In Table 4.1 the average predictability for each month and the whole year is shown. There it summarizes the months where using Z_{WCI} and Z_{VCI} increases the predictability compared to the base probability and therefore these indices could be used as a warning system. Further research is needed to expand to other areas and different vegetations and ecoregions.

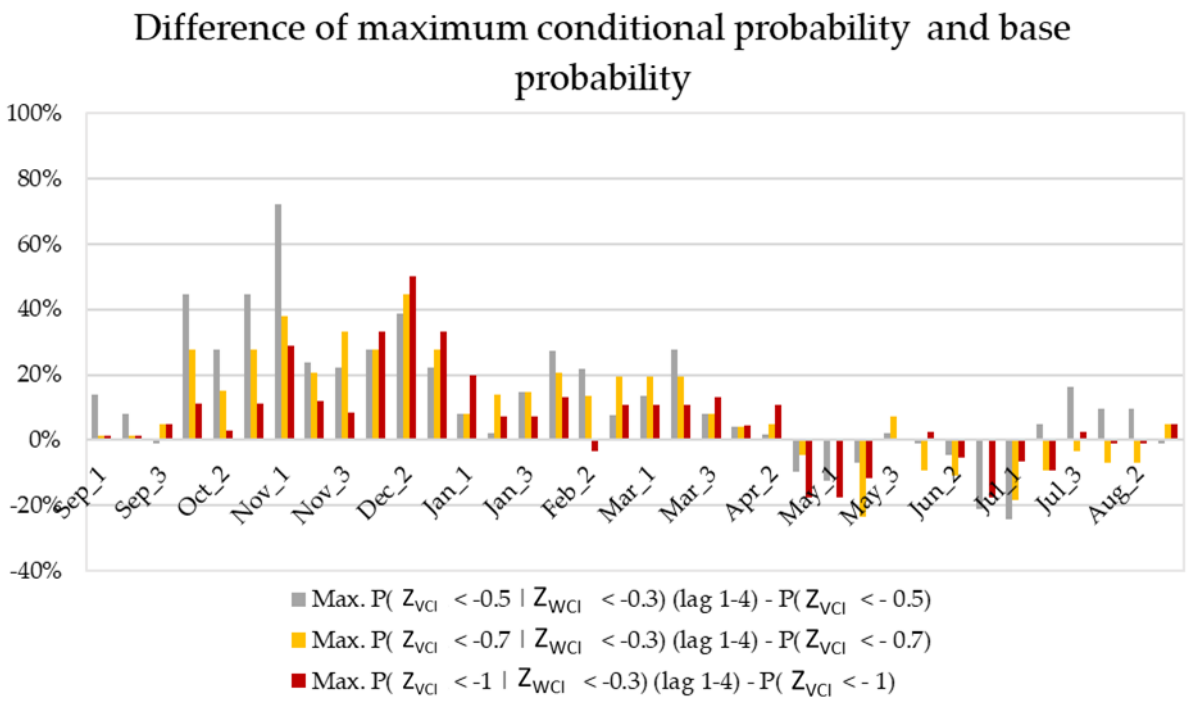

Figure 4.9. Difference of the maximum conditional probability using lags and the base probability for each threshold (grey -0.5, yellow -0.7, and red -1).

Table 4.1. The average increase in predictability for each month of the year.

Periods	**Change in predictability**		
	-0.5	**-0.7**	**-1**
September	7%	3%	3%
October	39%	24%	8%
November	39%	31%	16%
December	30%	33%	39%
January	8%	12%	12%
February	19%	18%	7%
March	16%	16%	12%
April	-1%	2%	-1%
May	-6%	-8%	-10%
June	-9%	-10%	-7%
July	-1%	-10%	-4%
August	6%	-3%	1%
Whole year	12%	10%	6%

5. MULTIFRACTAL CHARACTER OF NDVI AND ITS ANOMALY

5.1. Temporal trend analysis

As in the study of the temporal response of NDVI to temperature and precipitation, the Mann-Kendall test was calculated to the original series and the anomaly series (Murcia plots), but instead of using the Z-score, we calculated the anomaly (NDVIa) by only subtracting the yearly average for each date. Similar Mann-Kendall results were found in all four parcels from Murcia province. However, in A3 we used all pixels instead of the selection of the shrubland without the croplands that surround it, to include wider variation for fractal analyses. This area provided the only difference, which switch from decreasing (when using only the selected crop pixels) to increasing (when all pixels were used (Table 5.1). All four areas exhibit a significant trend. The Pettitt test found a shift in the trend in the four areas: A1 and A2, in the autumn of 2006; A3, in the autumn of 2007 and A4, in the autumn of 2008 (Figure 5.1 and Figure 5.2).

The change in the used anomaly was made to compare anomalies without seasonality but maintained the differences between areas with different vegetation that are normalized when using Z-score. This was reflected in the trend present in the original series was also found in NDVIa. These trends may be due to changes in land uses, vegetation evolution or climate change effects worthy of further consideration.

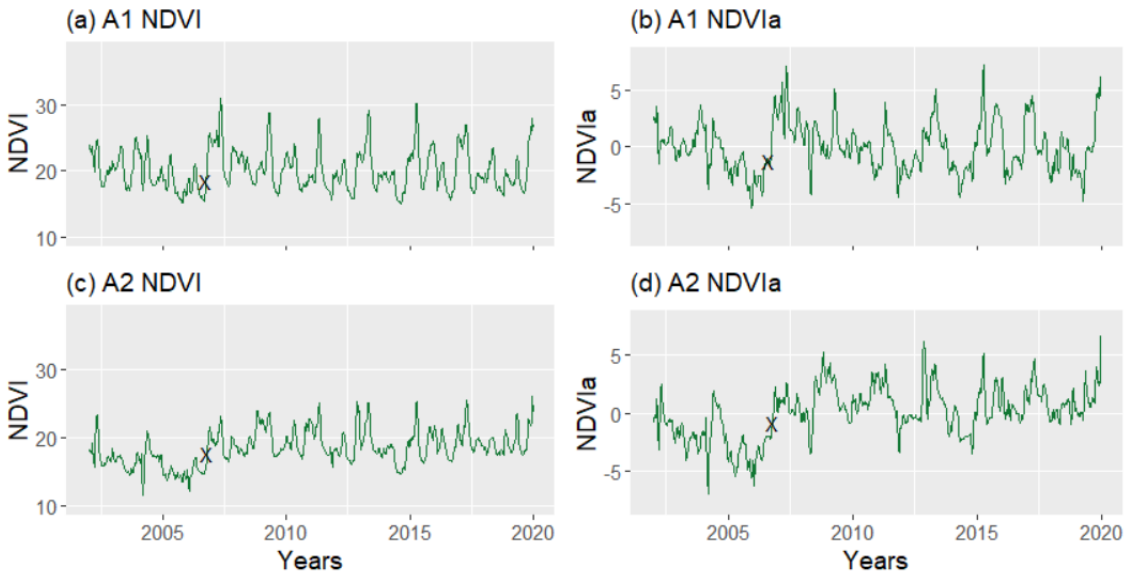

Figure 5.1. Series of average NDVI (a-c) and NDVIa (b-d) for A1, rainfed croplands and A2, rainfed croplands+scrublands. The X signal represents the point where the Pettitt test indicated a trend shift.

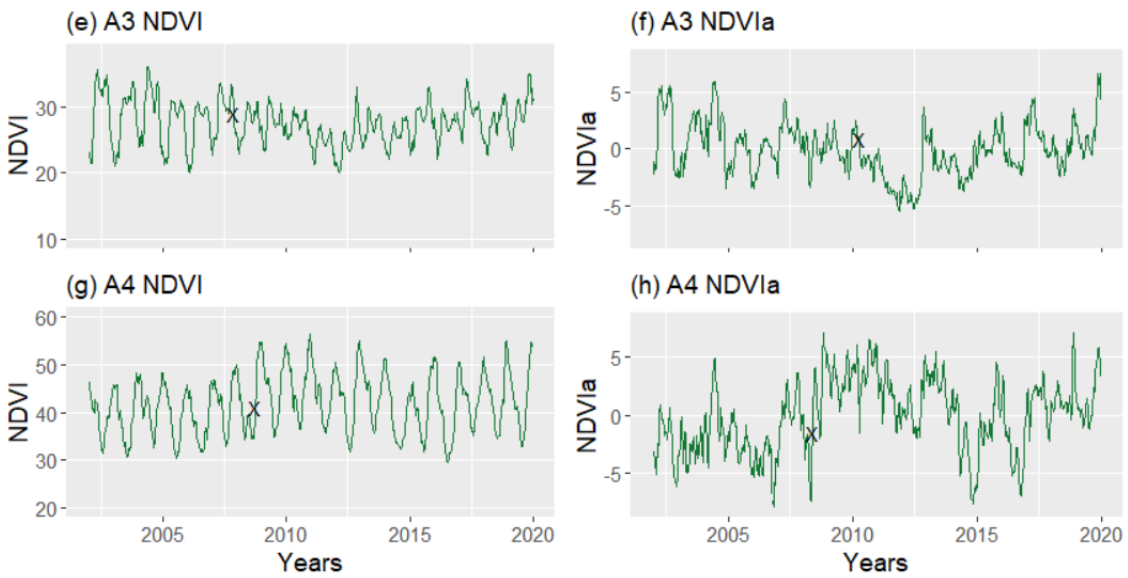

Figure 5.2. Series of average NDVI (a-c) and NDVIa (b-d) for A3, grassy+tree crops; and A4, open woodland+crops. The X signal represents the point where the Pettitt test indicated a trend shift.

Table 5.1. Mann-Kendall test results of the four study areas: A1, rainfed croplands; A2, rainfed croplands+scrublands; A3, grassy+tree crops and A4 woodland+crops. The same results were obtained using NDVI and NDVIa. All results were statistically significant.

Areas	Trend	Kendall's tau	*p*-Value
A1	Decreasing	−0.04	<0.05
A2	Increasing	0.26	<0.05
A3	Decreasing	−0.05	<0.05
A4	Increasing	0.08	<0.05

5.2. Hurst index

The HI (Table 5.2), ranging between 0.68 (NDVI) and 0.91 (NDVIa), indicates a persistent character for NDVI and NDVIa series in study areas. However, some differences were found between the original NDVI and the NDVIa. The most significant changes between the HIs of NDVI and NDVIa are found in A4, where persistence increased by roughly 0.2 when NDVIa was used. Meanwhile, smaller increases, between 0.02 and 0.12, are observed in the other areas. Considering NDVI, A2 is the most persistent (the highest HI), followed by A3, A4, and A1. Nevertheless, when NDVIa was analysed, a different order emerged, and A4 appeared as the most persistent. Its more extensive tree cover and woodland nature are less prone to a high variability showing a higher persistence. On the other hand, the other areas remained with similar values and maintained the same order as NDVI (A2, A3, and then A1).

Table 5.2. Corrected R/S Hurst indices (HI), Generalized Hurst exponent for q=2 (H(2)) based on Generalised Structure Function(GSF) and Multifractal Detrended Fluctuation Analysis(MF-DFA) for the original NDVI and NDVIa from different study areas: A1, rainfed croplands; A2, rainfed croplands+scrublands; A3, grassy+tree crops and A4 woodland+crops.

Areas	HI		GSF		MF-DFA	
	NDVI	NDVIa	NDVI	NDVIa	NDVI	NDVIa
A1	0.684	0.736	0.677	0.578	0.430	0.348
A2	0.863	0.893	0.758	0.644	0.504	0.367
A3	0.762	0.845	0.767	0.614	0.490	0.287
A4	0.728	0.907	0.829	0.608	0.638	0.295

5.3. Generalized structure function

Unlike the Hurst index (a monofractal technique), in this section and the next two sections, we use multifractal analyses. The fluctuation functions for any moment order q reveals the multifractality of a series by its power-law behaviour. Plotting the fluctuation function in log-log scales shows the multifractality by its linear behaviour from 0.25 to 4. The scaling exponent was calculated at four different time scales (τ): 8, 16, 32, and 64 days (Figure 5.3, only A3 for illustrative purposes).

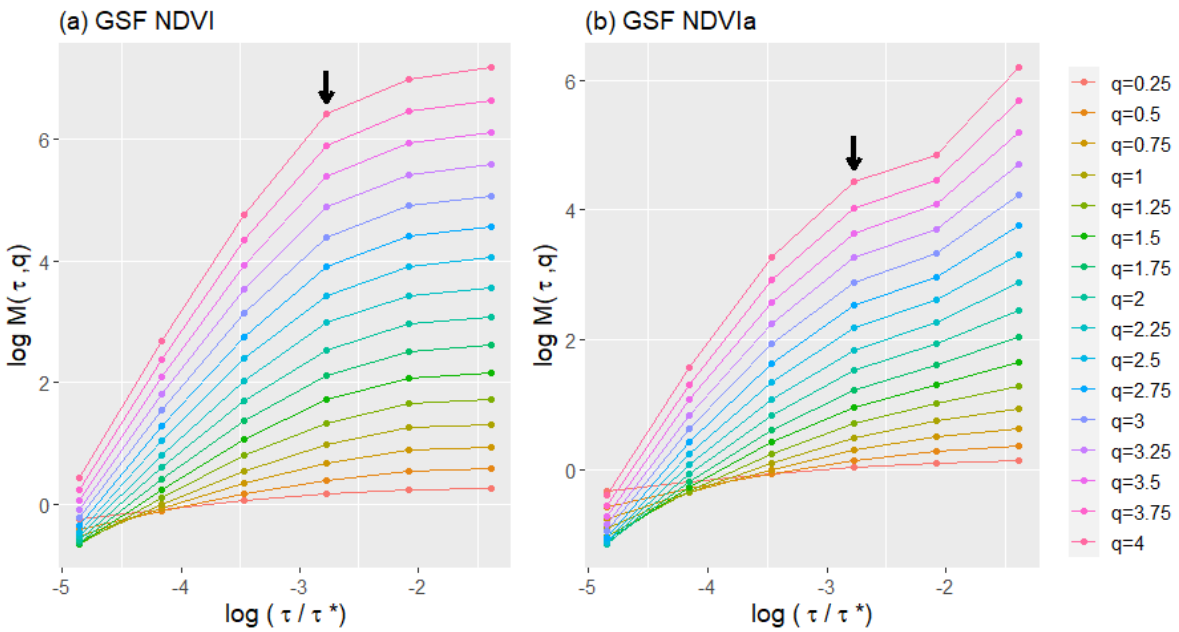

Figure 5.3. Log-Log plot of moments function (M(τ,q)) versus lag time scale (τ) normalised with the maximum lag time scale (τ*), for Generalised Structure Function (GSF), with q ranging 0.25 to 4 for NDVI (a) and NDVIa (b)of A3, grassy+forested+crops. The arrow marks the last point included in the linear regression. All the regressions obtained an $R^2 \geq 0.97$.

Observing the scaling exponent for NDVI, A4 appears on the plot top as the least multifractal, while A1 is the most multifractal and A2 and A3 stay in between (Figure 5.4). For NDVIa, the scaling exponent showed slight differences between A2, A3 and A4, while A1 appears further below the others.

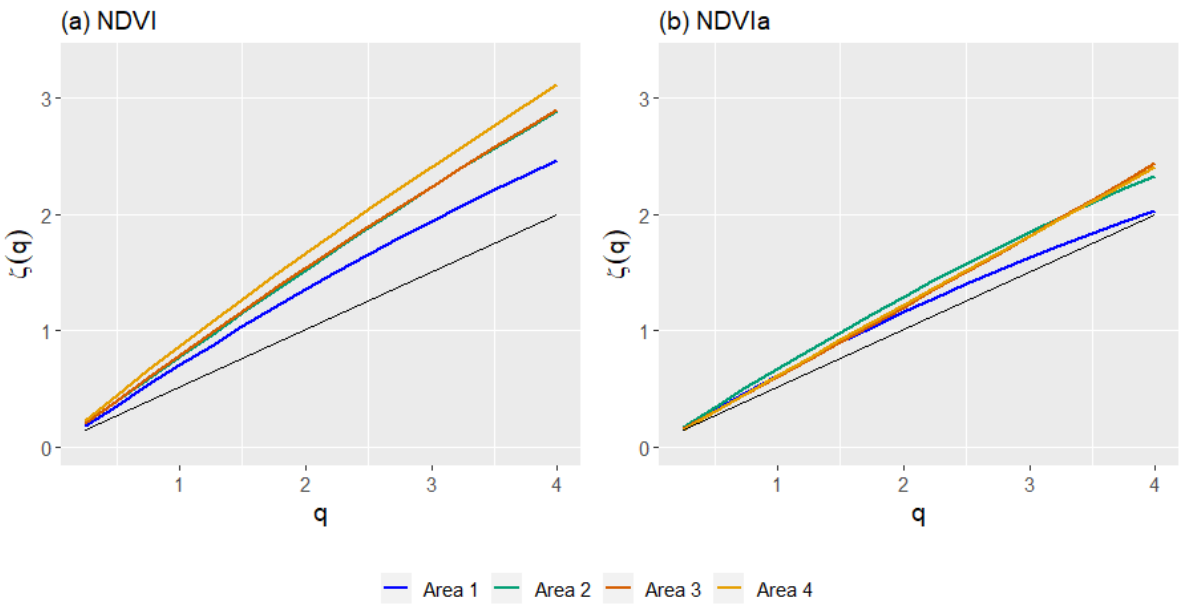

Figure 5.4. General Structure Function (GSF) scaling exponents ζ(q) for NDVI (a) and NDVIa (b) for the study areas: A1, rainfed croplands; A2, rainfed croplands+scrublands; A3, grassy+tree crops; and A4, open woodland+crops. In black, it is the scaling exponent of a Brownian motion.

The results of the generalised Hurst exponent with GSF produced similar results when compared to R/S analysis. The HI and H(2) from these analyses show minor differences when applied to the NDVI series, with disparities ranging from 0.007 to 0.12 (Table 5.2). These differences were higher when NDVIa series were used, with a difference ranging from 0.12 to 0.3. The NDVI series with GSF was more persistent than the NDVIa series. In both cases, the analysis revealed a persistent character in all four areas. Comparing the NDVI series of the four areas (Figure 5.5), A1 appears as the least persistent, A2 and A3 have a very similar pattern, with A4 showing a more persistent character than the other areas.

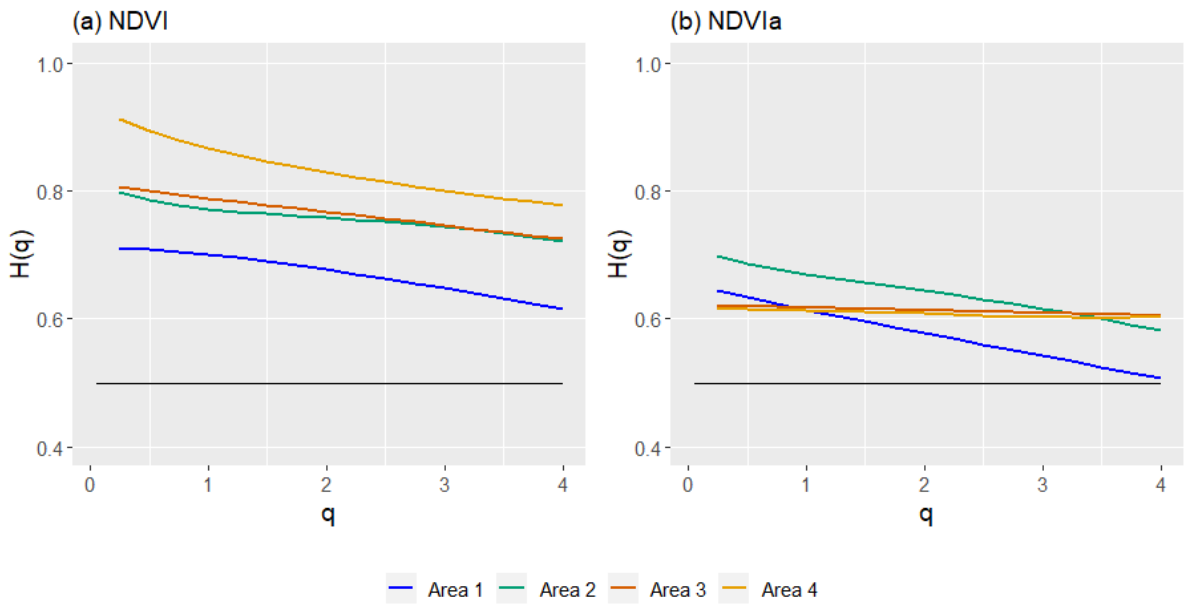

Figure 5.5. Generalised Hurst exponents H(q) for the study areas from Generalised Structure Function (GSF), for NDVI (a) and NDVIa (b) for each area: A1, rainfed croplands; A2, rainfed croplands+scrublands; A3, grassy+tree crops; and A4, open woodland+crops. In black is the H(q) of a Brownian motion to compare.

On the other hand, NDVIa results were more similar among them. Area 2 appears as the most persistent, A3 and A4 in the middle and A1 as the least persistent. Furthermore, A1 and A2 show a similar pattern, while A3 and A4 present a more constant profile, very similar between them.

The ΔH for NDVI with GSF has a minimum of 0.063 and a maximum of 0.116 (Table 5.3). There are differences between NDVI and NDVIa. Whilst A4 and A1 are the most multifractal with NDVI, followed by A3 and then A2, with NDVIa, a different order emerges. A1 and A2 show the highest ΔH with 0.137 and 0.116, respectively. On the other hand, A3 and A4 exhibit small values (0.015 and 0.012, respectively). These results match the different patterns between NDVI and NDVIa observed in the generalised Hurst exponents.

Table 5.3. Multifractality strength based on ΔH, using the generalized structure function (GSF) and multifractal detrended fluctuation analysis (MF-DFA), for all original NDVI and NDVIa series from different study areas: A1, rainfed croplands; A2, rainfed croplands+scrublands; A3, grassy+forested+crops; and A4, open woodland+crops.

Areas	GSF		MF-DFA	
	NDVI	NDVIa	NDVI	NDVIa
A1	0.094	0.137	0.386	0.304
A2	0.063	0.116	0.409	0.259
A3	0.075	0.015	0.338	0.236
A4	0.116	0.012	0.360	0.206

5.4. Multifractal detrended fluctuation analysis

The fluctuation functions revealed the multifractality of the series when analysed with GSF and MF-DFA. The generalised Hurst exponent was calculated for four (NDVI) and five (NDVIa) different time scales (s): 32, 64, 128, 256, and 512 days (Figure 5.6, only A2 for illustrative purposes). As different time scales were used for the GDF and MF-DFA, due to differences in their fluctuation functions, the comparison among these results should be taken cautiously. Due to the trends in most series, we used MF-DFA to avoid the effects on the Hurst exponent and compare the different series for fractal character and persistence or antipersistence. In opposition to the GSF results, the generalised Hurst exponent of MF-DFA indicated mainly an antipersistent character. For NDVI, A4 appears the most persistent area, A2 and A3 appear in the middle, with A1 as the most antipersistent (Figure 5.7). All of them start above 0.5 but, except A4, they all dropped below 0.5 for $q \geq 2$, reflecting an antipersistent character. A more antipersistent plot emerged when NDVIa was used, A1 and A2 start above 0.5 and immediately decrease to the antipersistent as q grows. A3 and A4 have a similar pattern but with more antipersistent profiles. Moreover, both NDVI and NDVIa A1 and A2, and A3 and A4 have two different patterns. Although for NDVI, each group keeps the same pattern at a different persistency level. The ΔH

for MF-DFA, compared to the GSF, tends to have higher values, ranging from 0.206 to 0.409. ΔH decreased when NDVIa was used for study areas, with a more significant difference in A2 (Table 5.3). The common patterns mentioned are reflected in their ΔH. A1 and A2 have a higher ΔH, and A3 and A4 have a lower ΔH for both series. The generalized Hurst exponents diverged between the GSF and MF-DFA. The GSF characterized the series as low-level multifractal and persistent. However, when MF-DFA was applied, a larger multifractality and an antipersistent character were observed for the same series.

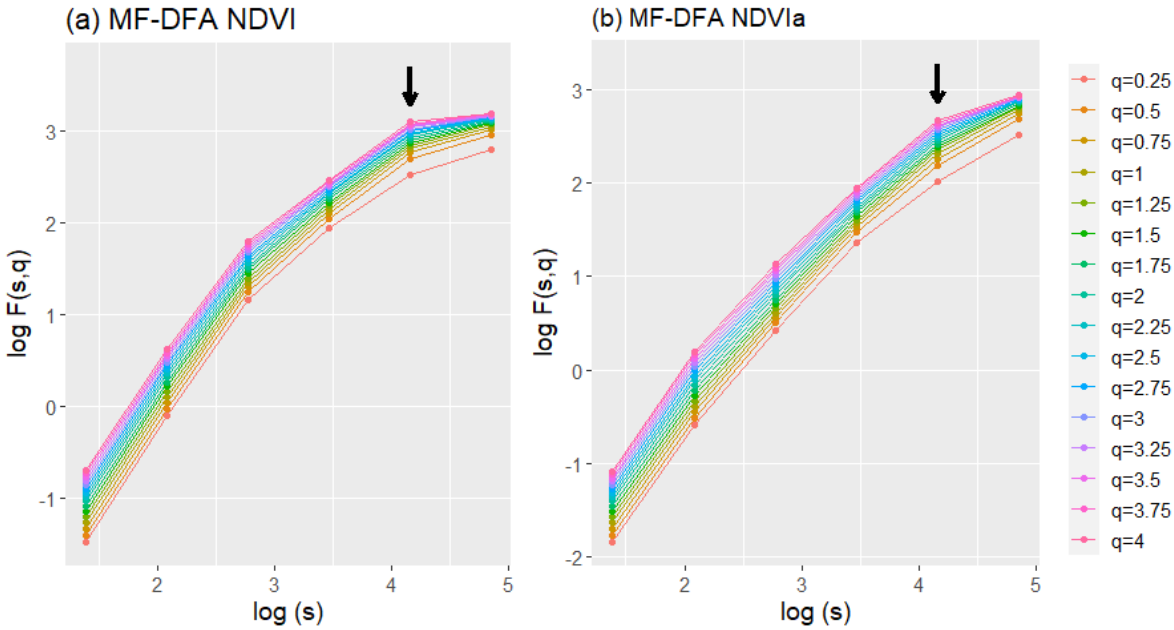

Figure 5.6. Log-Log plot of fluctuation function (F(s,q)) versus time scale (s), for multifractal detrended fluctuation analysis (MF-DFA), with q ranging from 0.25 to 4 for NDVI (a) and NDVIa (b) of A2, rainfed croplands +scrublands. The arrow marks the last point included in the regression line. All the regressions obtained an $R^2 \geq 0.97$.

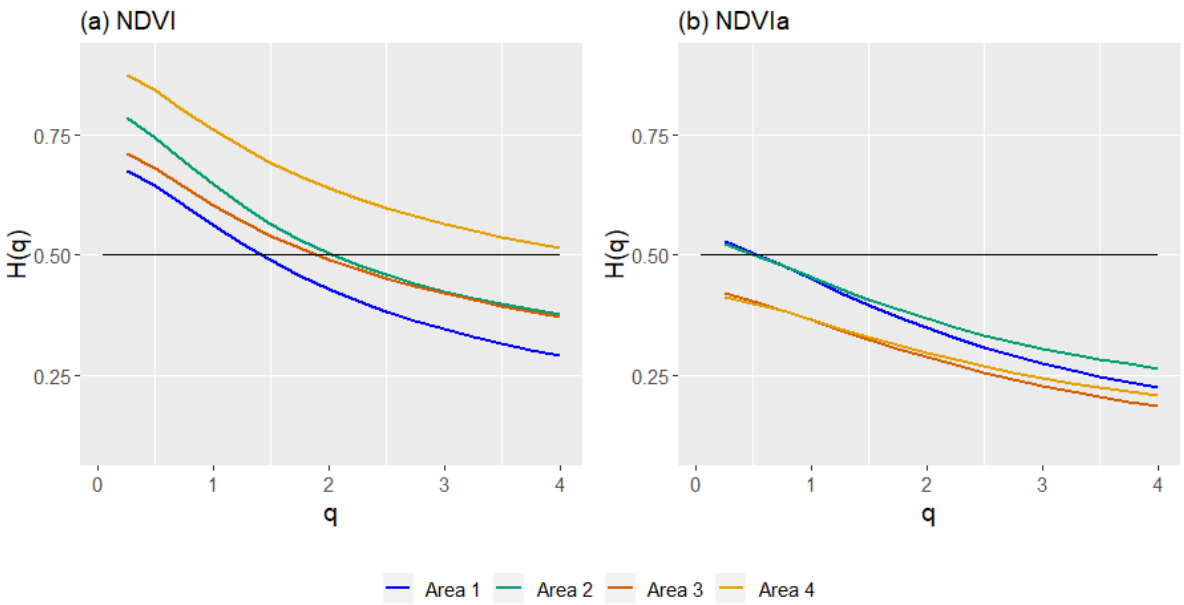

Figure 5.7. Generalised Hurst exponent (H(q)), from the Multifractal Detrended Fluctuation Analysis (MF-DFA), for NDVI (a) and NDVIa (b) for each area: A1, rainfed croplands; A2, rainfed croplands+scrublands; A3, grassy+tree crops; and A4, open woodland+crops. In black is the H(q) of a Brownian motion to compare.

The scaling exponent (ζ(q)) of the four study areas shows a stronger multifractal character than GSF results, especially for NDVIa. For NDVI, A1 has the most multifractal profile, with A2 and A3 on top and A4 as the least multifractal. This order shifts with NDVIa, where all of them show a more multifractal character, while A4 changes from the least to the most multifractal, right below A1 (Figure 5.8).

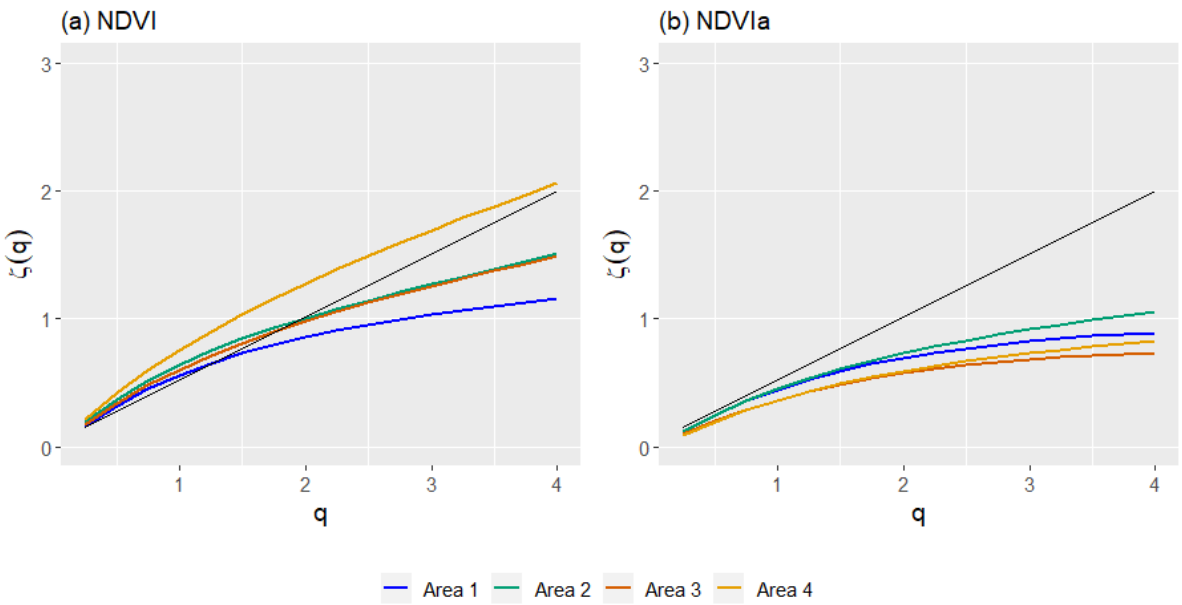

Figure 5.8. Scaling exponents ζ(q), from Multifractal Detrended Fluctuation Analysis (MF-DFA), for NDVI (a) and NDVIa (b), for the study areas: A1, rainfed croplands; A2, rainfed croplands+scrublands; A3, grassy+tree crops; and A4, open woodland+crops. In black, there is the scaling exponent of a Brownian motion.

5.5. Sources of multifractality

The shuffle and surrogate NDVI series analyses revealed similar patterns across the study areas (Figure 5.9). Generally, all shuffle series had generalised Hurst exponents very close to 0.5, similar to a Brownian motion. The surrogate series reported generalised Hurst exponents with a smaller multifractality (ΔH) than the original series (Table 5.4). However, some differences in their patterns are worth mentioning. A1 and A2 presented a surrogate series that diverged more heavily from the original series. At lower-order statistical moments (q=1, 2), the shuffle series was slightly lower than a typical Brownian motion. On the other hand, A3 and A4 surrogate series were very similar to the original series, and their shuffle series were almost always at 0.5.

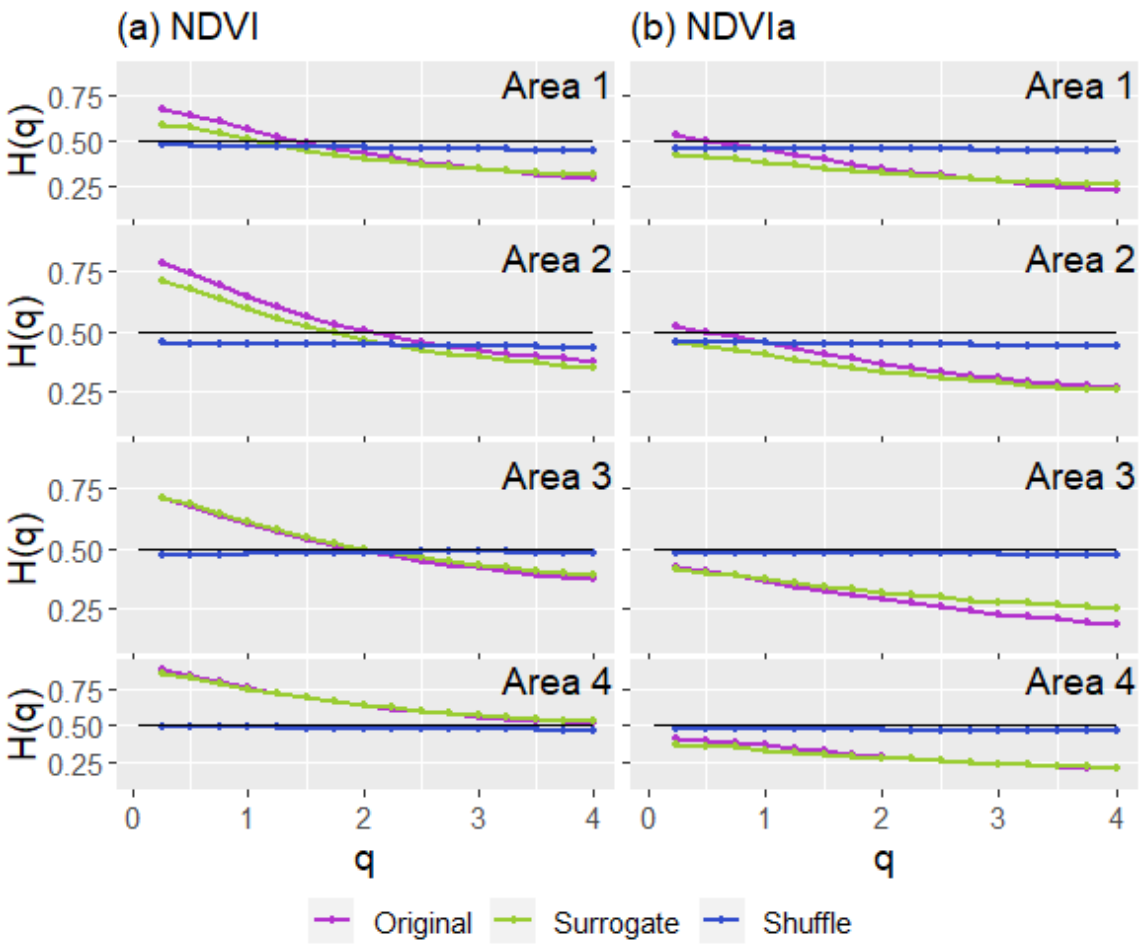

Figure 5.9. Generalised Hurst exponents (H(q)), from multifractal detrended fluctuation analysis (MF-DFA), for NDVI (a) and NDVIa (b), for the study areas: A1, rainfed croplands; A2, rainfed croplands+scrublands; A3, grassy+tree crops; and A4, open woodland+crops. The original series is in dotted purple, the surrogate series is in dotted green, and the shuffle series is in dotted blue. To compare the figures, the H(q) of a Brownian motion is in solid black.

Table 5.4. Multifractal strength measure by ΔH of Multifractal Detrended Fluctuation Analysis (MF-DFA), for original series (NDVI and NDVIa), surrogated series (NDVI_su and NDVIa_su), and shuffle series (NDVI_sh and NDVIa_sh). Study areas: A1, rainfed croplands; A2, rainfed croplands+scrublands; A3, grassy+tree crops; and A4, open woodland+crops.

Areas	NDVI	NDVI_su	NDVI_sh	NDVIa	NDVIa_su	NDVIa_sh
A1	0.386	0.284	0.029	0.304	0.172	0.017
A2	0.409	0.361	0.019	0.259	0.198	0.017
A3	0.338	0.317	0.001	0.236	0.162	0.014
A4	0.360	0.326	0.017	0.206	0.157	0.013

NDVIa results were similar to the mentioned NDVI results. However, the original and surrogate series presented a more antipersistent character, and the difference between the surrogate and the original series was more conspicuous for A3 and A4. Whilst similar to NDVI, A3 NDVIa presented a more divergent pattern between these series in higher-order statistical moments (q>2). A4 presented a more significant difference in the smaller order statistical moments (q<2). To analytically examine the influence of both sources of multifractality, Hcor and Hpdf were calculated (Table 5.5). Study areas present a higher dominance of long-range correlation multifractality, although A1 present a mix of both sources with a Hpdf>0.1.

Table 5.5. Difference between the ΔH of the original and surrogate series (Hpdf) and the difference of ΔH of the original and shuffle series (Hcor) for NDVI and NDVIa for the study areas: A1, rainfed croplands; A2, rainfed croplands+scrublands; A3, grassy+tree crops; and A4, open woodland+crops.

Areas	Hcor		Hpdf	
	NDVI	NDVIa	NDVI	NDVIa
A1	0.357	0.287	0.103	0.132
A2	0.390	0.241	0.048	0.061
A3	0.337	0.222	0.021	0.074
A4	0.343	0.193	0.035	0.049

Differences in multifractality between the NDVI and NDVIa were observed with ΔH and the scaling exponent patterns. The results indicate that part of the multifractality is due to seasonality. Nevertheless, long-range correlations affected the multifractality observed with the NDVI and NDVIa surrogate series (i.e., before and after removing seasonality). On the other hand, there was a limited impact of the broad probability density function for all study areas. The NDVIa presented a more decisive influence from the broad probability density function than the NDVI, particularly in A1, where its multifractality based on the broad probability density function of the NDVI series was higher than in other study areas. Therefore, we can appreciate two types of long-range correlations

based on (i) seasonal and (ii) annual or longer memory processes. We found a greater difference in ΔH between the original series of the NDVI and NDVIa, compared to the difference between the original and respective surrogate for each index (NDVI and NDVIa). This larger difference between the NDVI and NDVIa indicates that seasonality had a decisive influence on overall multifractality in all areas, except for A1. In this case, the NDVIa series presented more multifractality than its surrogate NDVI series. This is likely due to the almost complete herbaceous nature of A1. Vegetation in A1 is entirely rainfed and cannot take full advantage of deeper soil water compared to arboreal vegetation. Therefore, its behaviour is more dependent and similar to precipitation, which is more related to a broad probability density function, unlike air temperature or humidity (Baranowski et al., 2015). Area 2, while it is also dominated by herbaceous crops, presents a grassland area with few shrubs and some reforested pixels that will maintain greener vegetation when precipitation is scarce.

6. CLUSTERING ARID RANGELANDS BASED ON NDVI ANNUAL PATTERNS AND THEIR PERSISTENCE

6.1. Variable selection approach

For the pixels from Almería and Murcia provinces, all summary statistics between the three selected phases (periods where NDVI rose or decreased, from chapter 3 and Sanz et al. (2021a)) presented a robust linear correlation (>0.75) except for the three variances (Figure 6.1). Principal component analyses (PCA) were performed with our statistic variables, including the Hurst exponents (HI and H2). Moreover, among those variables with a strong correlation, quartile 3 of phase 5 was chosen for its higher explanatory power (Table 6.1 and Table 6.2). The three variances and quartile 3 of phase 5 were used separately with HI and H2, and with neither of them for the clustering analyses.

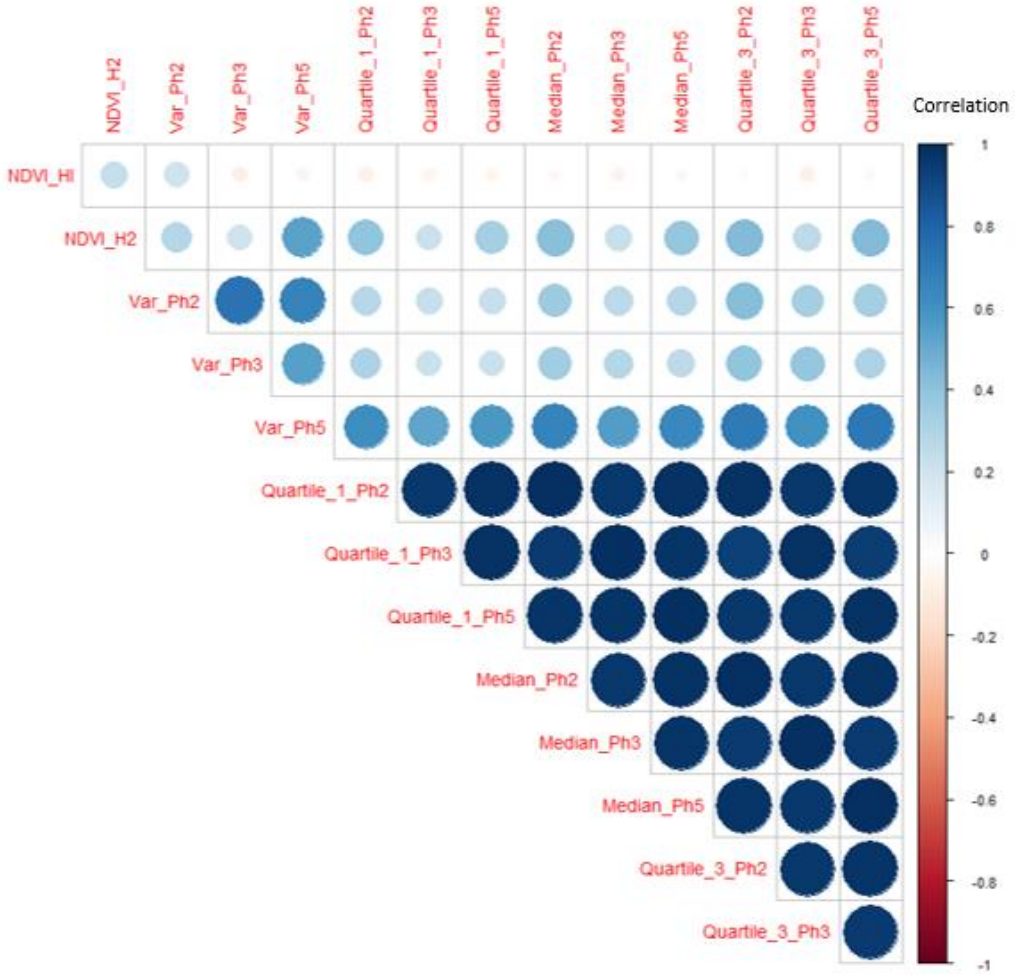

Figure 6.1. Correlation matrix of all variables tested for the three study regions. Large, dark blue circles indicate a high correlation, while small, light blue circles indicate a low correlation. Ph2/3/5 stands for Phase 2/3/5, and Var for variance.

Table 6.1. Three first principal components from the PCA for all the NDVI time series variables and H2. Shaded are highlighted those variables with higher explanatory power for each principal component.

Variables	PC1	PC2	PC3
NDVI_H2	0.14	-0.27	0.84
Var_Ph2	0.13	-0.59	-0.22
Var_Ph3	0.13	-0.56	-0.37
Var_Ph5	0.23	-0.38	0.17
Quartile_1_Ph2	0.32	0.01	0.03
Quartile_1_Ph3	0.31	0.19	-0.13
Quartile_1_Ph5	0.31	0.16	001
Median_Ph2	0.32	0.05	0.2
Median_Ph3	0.31	0.14	-0.14
Median_Ph5	0.31	0.11	0.04
Quartile_3_Ph2	0.32	-0.01	0.01
Quartile_3_Ph3	0.32	0.08	-0.17
Quartile_3_Ph5	0.33	0.05	0.07
Standard deviation	3.10	1.36	0.95
Proportion of Variance	0.74	0.14	0.07
Cumulative Proportion	0.74	0.88	0.94

Table 6.2. Three first principal components from the PCA for the selected variables after removing the variables with strong correlation for the summary statistics with the least explanatory power. Highlighted those variables with higher explanatory power for each principal component.

Variables	PC1	PC2	PC3
NDVI_H2	0.36	-0.54	0.74
Var_Ph5	0.47	0.45	0.13
Var_Ph3	0.43	0.54	0.07
Var_Ph2	0.54	-0.13	-0.16
Quartile_3_Ph5	0.12	-0.43	-0.64
Standard deviation	1.72	1.02	0.76
Proportion of Variance	0.59	0.21	0.12
Cumulative Proportion	0.59	0.79	0.91

6.2. Clustering Analysis

6.2.1. K-Means

The k-mean method was applied, using the aforementioned selected variables, for three and four clusters based on the elbow method. The elbow method is a heuristic method to determine the number of clusters in a dataset (Ng, 2012), as shown in Figure 6.2. K-means clustering was different when three (three-cluster analyses) and four (four-cluster analyses) clusters were used. However, for each cluster number, the results were identical whether no Hurst exponent, H2 or HI were used. The clustering results presented an adjusted Rand Index of 1 among the three-cluster analyses and an adjusted Rand Index of 0.84 when comparing the results of three- and four-cluster analyses. The new fourth cluster included very few pixels, and those pixels had a low Silhouette Index, as shown in Figure 6.3. The Silhouette Index was the same in all k-means analyses with three- and four-cluster analyses (Table 6.3).

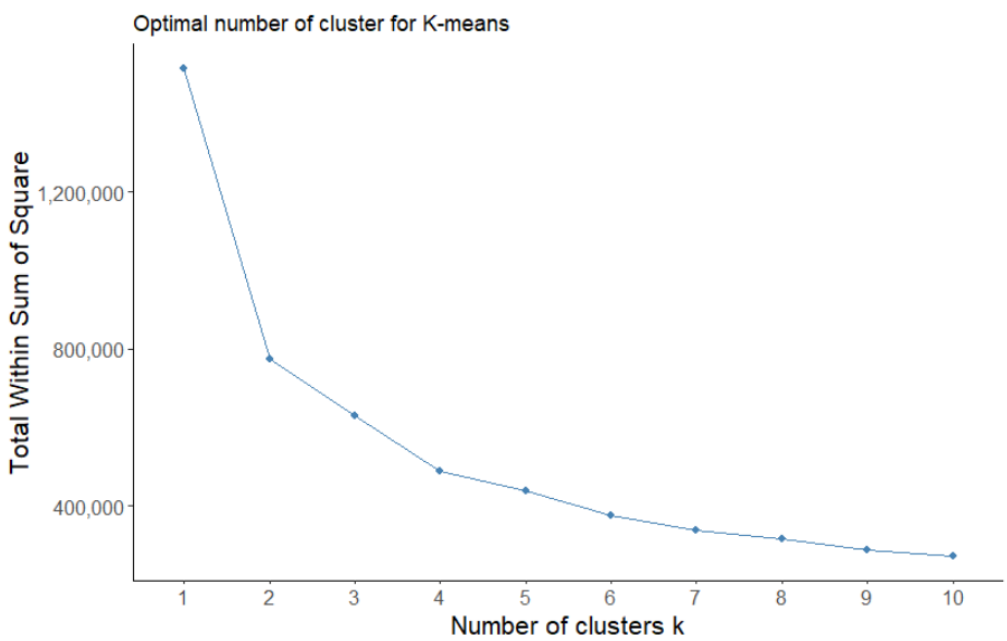

Figure 6.2. Elbow method on the selected variables using k-means clustering. Three- and four-cluster analyses were performed.

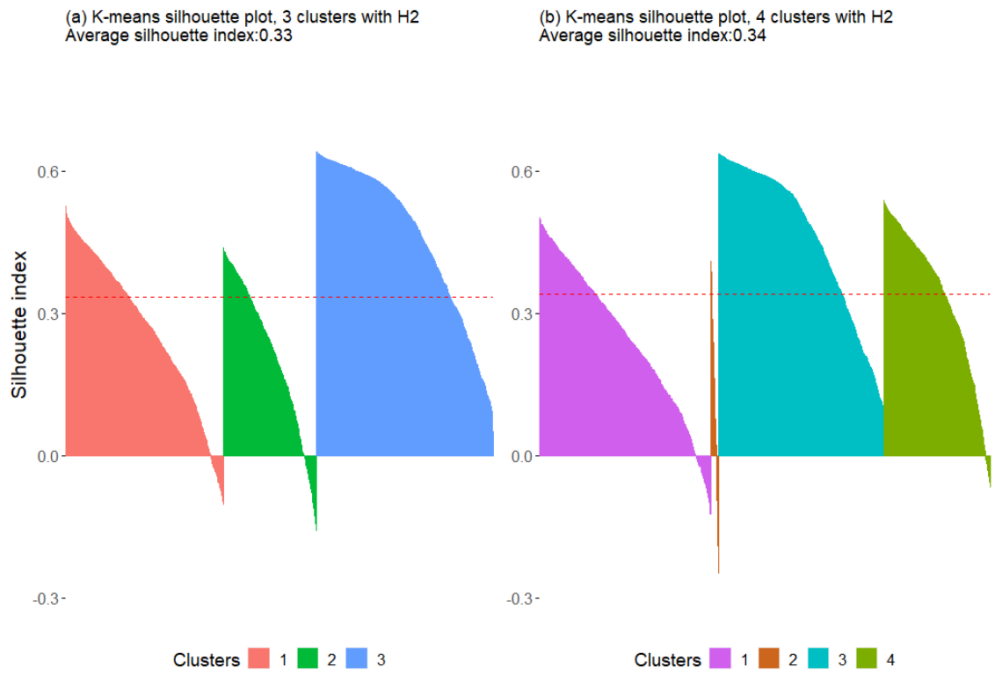

Figure 6.3. Silhouette plots for all pixels using k-means for three (a) and four clusters (b), showing the Silhouette Index (*y*-axis) for all pixels for each cluster represented on the *x*-axis with H2. The same results were obtained when k-means were run with HI or without HI/H2.

6.2.2. Unsupervised Random Forest

Using the elbow method with the partitioning around medoids method showed a similar graphic as using the k-means method, indicating that three and four clusters may be the most appropriate to use (Figure 6.4).

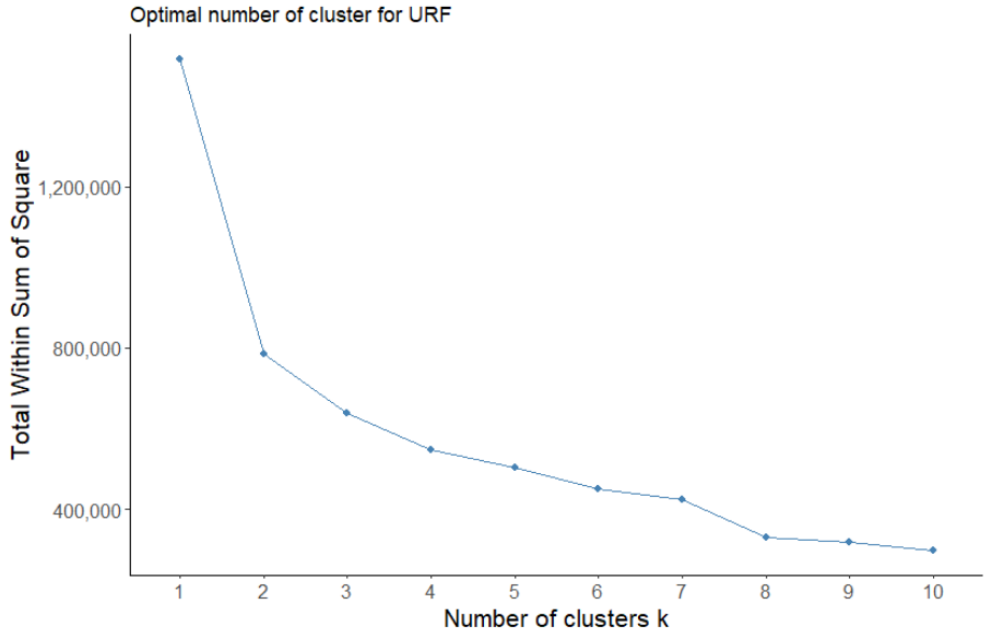

Figure 6.4. Elbow method of the selected variables using partitioning around medoids clustering, where three and four clusters were selected.

The URF has more variables that affect the results: the number of trees (nt) and several variables (m) used for splitting branches. Three or four clusters were used and H2, HI, and no Hurst exponent analyses were calculated. For each combination, URF was calculated for different nt and m to obtain the analysis with the highest Silhouette Index (Appendix 4). Compared with k-means, URF showed higher variability between the results, whether using H2, HI, or no Hurst exponent. The silhouette values from URF were consistently higher when three groups were used for the three analyses with the Hurst exponent from DFA (H2) (Table 6.3). When four clusters were used in our analyses, the additional fourth cluster showed a low Silhouette Index for that cluster (Figure 6.5). Therefore, only the URF clustering for three clusters will be discussed with and without the Hurst exponents, focusing on the cluster with the highest Silhouette Index (H2).

Table 6.3. Average Silhouette Indices for 3 and 4 clusters for k-means and optimised unsupervised random forest.

Analysis	K-Means		Unsupervised Random Forest	
	3 Clusters	4 Clusters	3 Clusters	4 Clusters
Without H2/HI	0.33	0.34	0.51	0.49
With H2	0.33	0.34	0.62	0.47
With HI	0.33	0.34	0.50	0.45

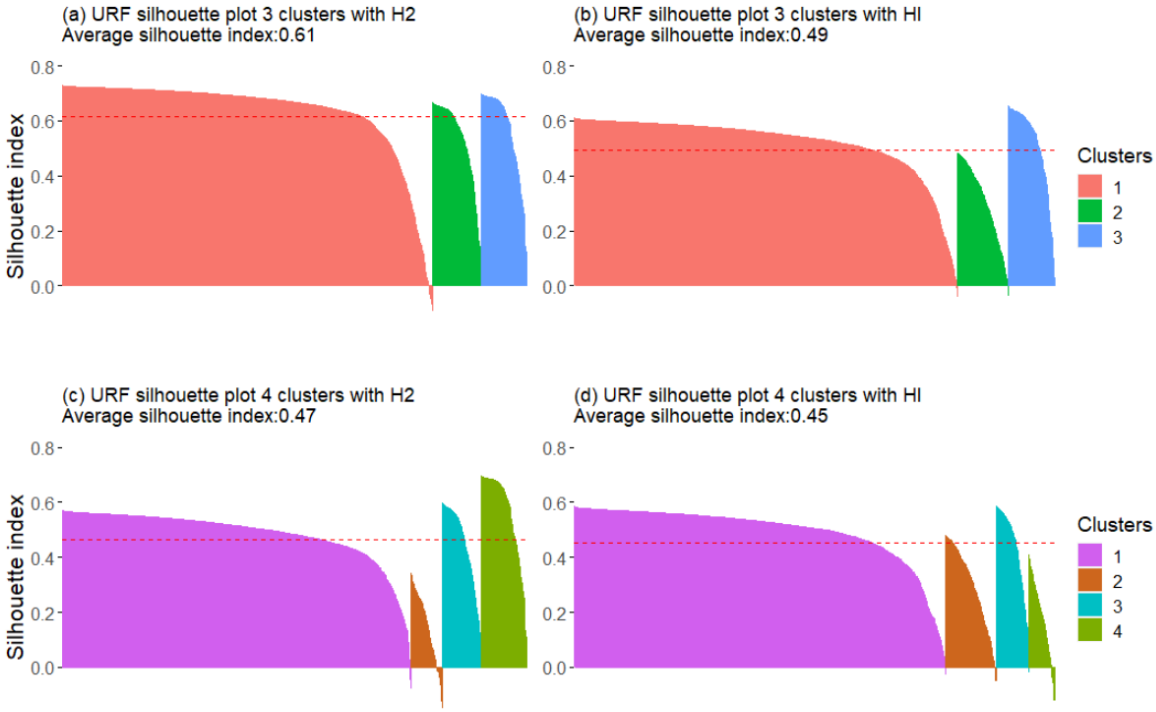

Figure 6.5. Silhouette plots for the different analyses performed with unsupervised random forest (URF). On the left are those performed with H2, from DFA; the analyses performed with HI, from R/S, are on the right. The top graphics are for three clusters and the bottom graphics are for four. Silhouette plots show the Silhouette Index (*y*-axis) for all pixels for each cluster represented on the *x*-axis.

The clustering results were more similar between the analyses done with HI and no Hurst exponent than when H2 or HI was used, presenting 0.82 and 0.74 in the adjusted Rand Index, respectively. For all cases, cluster 1 was the most predominant, and cluster 2 had a higher NDVI and variance, while the opposite can be said for cluster 3. These differences were more remarkable when H2 was

used. The difference in Hurst exponent (HI or H2, respectively) between the three clusters was more evident when H2 was used. The major differences in clustering among these three analyses were found in cluster 2, with the highest H2 and NDVI (Figure 6.6 and Figure 6.7). These distinct pixels were found mainly in the Murcia-NW region (Figure 6.8, and Figure 9.12 to Figure 9.14 in Appendix 5).

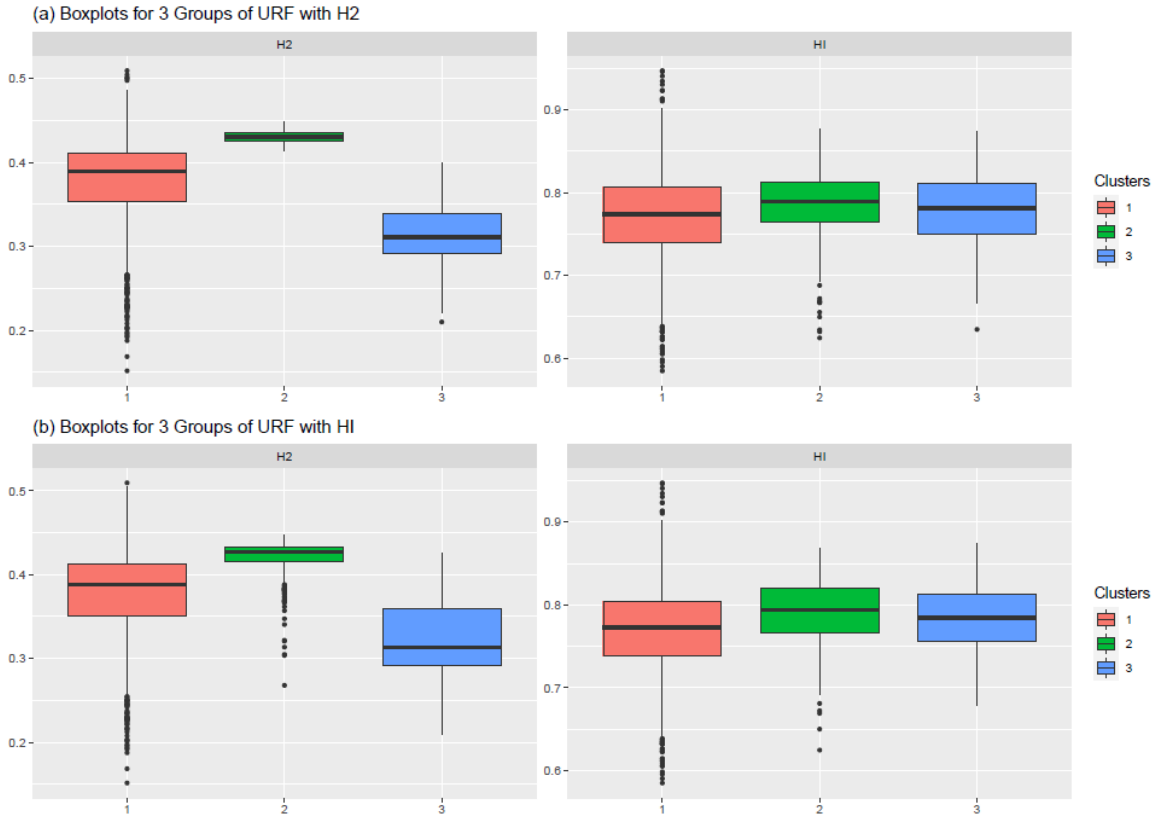

Figure 6.6. Comparison of H2 and HI for all clusters when unsupervised random forest (URF) was used with H2 (top) and HI (bottom) in all study areas.

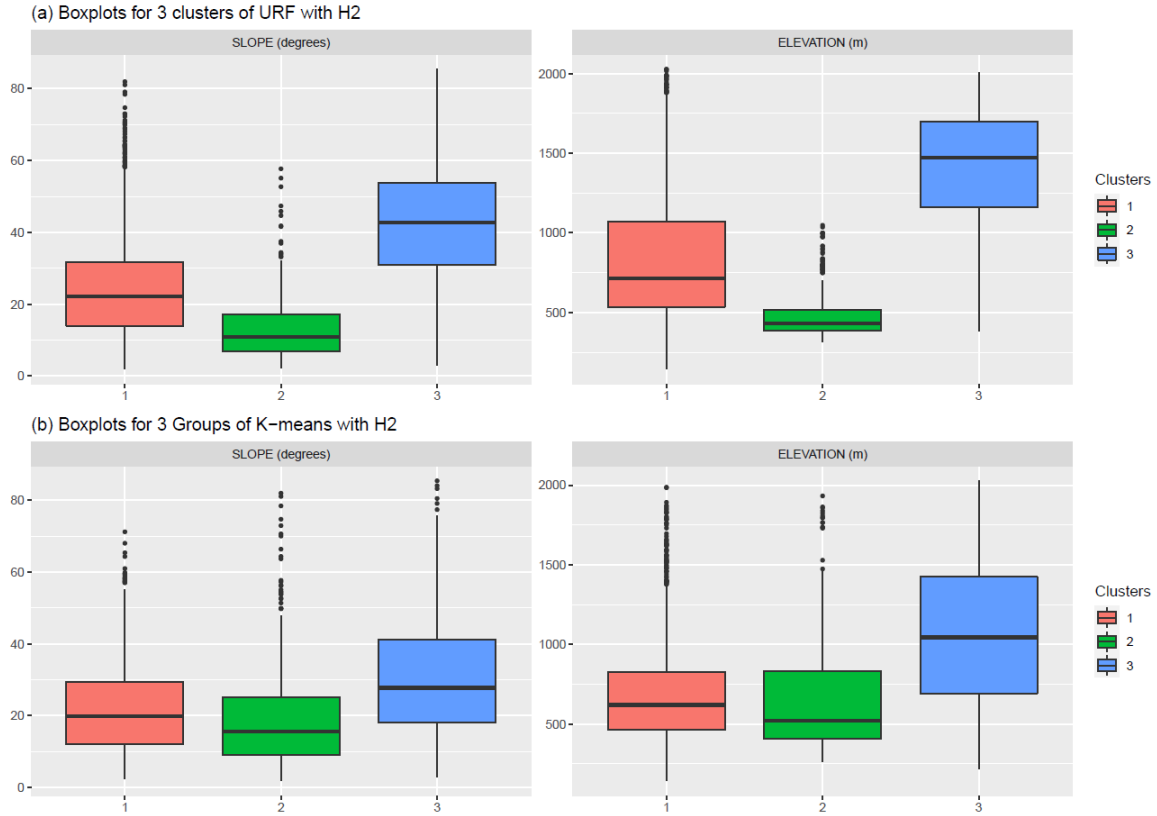

Figure 6.7. Slope and elevation comparison for all clusters when unsupervised random forest (URF) (a) and k-means (b) were used with H2 in all study rangelands.

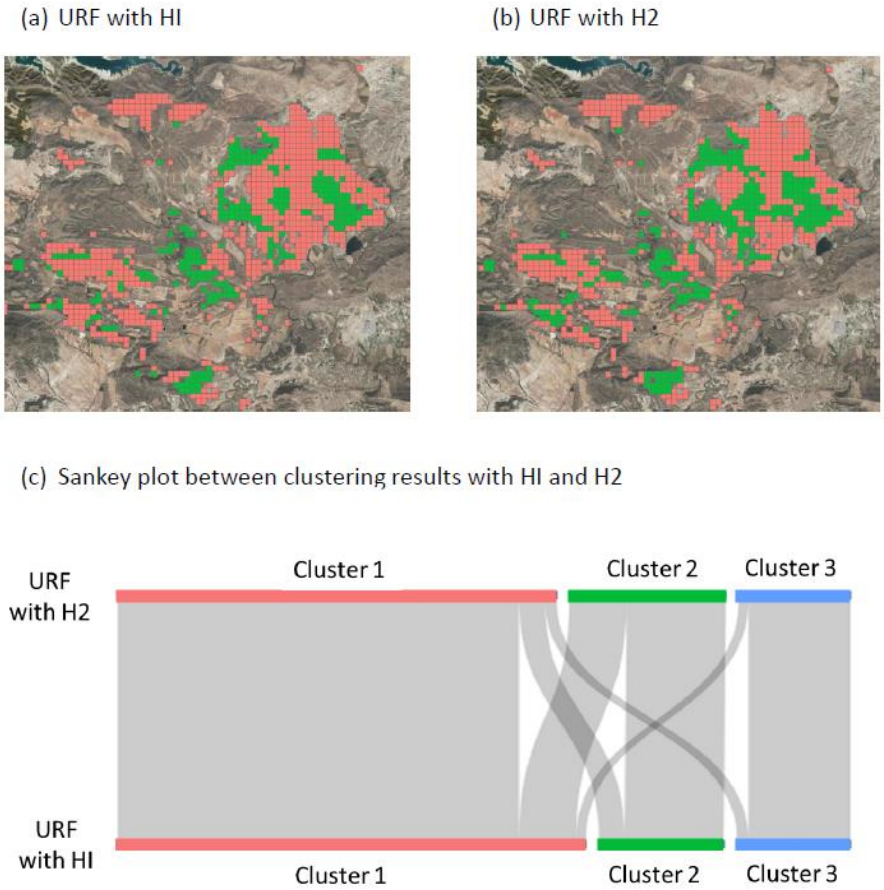

Figure 6.8. (**a**) On the top are the clustering results of unsupervised random forest (URF) in the Murcia-NW when HI (a) or H2 (b) was used, showing clusters 1 and 2 present in this region, while cluster three was not present in this area. (c) compares the differences in clustering when HI (bottom) and H2 (top) were used in URF for all the study areas.

6.2.3. Cluster Characterisation and their relevance

The link between elevation and the Hurst exponent was previously reviewed by Peng et al. (2012), who found a good relationship between HI and elevation. The Hurst exponent from DFA showed a stronger linear correlation with elevation and slope than HI (negatively: the higher or more sloppy terrain would present a lower Hurt exponent, especially with H2 from DFA). The same occurred with the selected variables used for the clustering analyses (Table 6.4), the variances from phases 5 and 2 (those with the highest correlation to H2 and HI, respectively). These correlations were reflected in the clustering process. When URF with H2 was used, slope and elevation were more heavily differentiated for

clusters 2 and 3. These differences were not found when k-means was used since the clustering outcome was the same when H2 substituted HI, or no Hurst exponent was used. Furthermore, slope and elevation showed a more considerable overlap between the clusters on the three-cluster analyses when k-means was used (Figure 6.7). In this study, the stronger correlation of H2 with NDVI time-series variances, compared with HI, suggests the importance of detrending in fractal analyses when studying vegetation time series. Differences between R/S and DFA were previously reported (Guo et al., 2015), as DFA is less affected by size effects or spurious correlation of non-stationary time series (Coronado and Carpena, 2005; Guo et al., 2015). Our results support these findings, highlighting the relevance of detrending, especially when studying different vegetation types.

Table 6.4. Correlations between H2 and HI with elevation, slope, and variances from phases 5 and 2.

Hurst Exponent	Elevation	Slope	Var_Ph5	Var_Ph2
H2	−0.81	−0.53	0.54	0.29
HI	−0.25	−0.07	0.05	0.21

When H2 was used, the three-cluster analyses presented more significant differences. These differences are shown in their dynamics, as seen in the variances calculated separately for each cluster, phase, and NDVI (Figure 6.9), where some pixels were distinct. These differences were still found when all pixels were averaged for each cluster (Figure 6.7 and Figure 6.9). These differences in NDVI are reflected in the type of vegetation found dominating each pixel. Cluster 1, where we found the majority of pixels, reflects a great variation from woodlands to grasslands. In this region with an arid climate, patchy landscapes with different vegetation are typical and they can occur along an ecological continuum, rather than as well-defined and separated ecosystems

(Ludwig and Tongway, 2000; Tongway and Ludwig, 1997). Cluster 2 shows a vast majority of thick forests, while cluster 3 consists mainly of grassland (Table 6.5), despite cluster 1 having both grassland and woodland, as reflected by an intermediate average NDVI for cluster 1, the pixels with higher NDVI in this cluster present more dispersed forest mixed with shrubs

Table 6.5. Percentages of vegetation type of the selected pixels, based on the National Forest Map. Results for each cluster are based on URF with H2.

Cluster	Woodland	Shrubland	Grassland
1	48.0	7.7	44.3
2	99.7	0.3	0.0
3	15.5	4.4	80.1

Figure 6.9. Time series of cluster prototypical pixels in (a) the cluster type (selected based on their vegetation type: mixed shrubland for cluster 1, open woodland for cluster 2 and grassland for cluster 3); (b) the average of each cluster; and (c) the variances for each cluster and phase, based on the NDVI dynamics following (Sanz et al., 2022).

The Mann–Kendall test was performed for all the pixels and the area. Although all three clusters showed that most pixels had a significant positive trend, cluster 2 had 90% of the pixels in that category, while clusters 1 and 3 only had 67% and 64%, respectively (Table 6.6).

Table 6.6. Percentages of Mann–Kendall results for each cluster based on URF with H2.

Significance	Cluster 1	Cluster 2	Cluster 3
Significant decrease	6.2 %	0 %	2.2 %
Not significant	26.5%	10 %	34.3 %
Significant increase	67.3%	90 %	63.5 %

Limited differences in pixel clustering were found in both methods of calculating the Hurst exponent in areas dominated by grasslands, suggesting that a tendency is not present in this NDVI series probably due to the grazing effect on these areas. On the other hand, more significant differences in areas with more trees were found. In this case, grazing does not limit the vegetation growth of trees, showing a trend in their vegetation time series.

Arid rangelands are spatially heterogeneous (Bird et al., 2002; Vetter, 2005), and land degradation and overgrazing can affect the landscape creating a grassland/woodland continuum (Martens et al., 2000; Schwinning and Parsons, 1999). This effect is reflected in the overlapping clusters, showing that discrete areas can have similar vegetation. However, differences among the majority of the pixels of each cluster in persistence, elevation, and slope were found. In further research, other factors relating to elevation and slope could be considered, such as availability for the use of heavy machinery in agriculture (easier on flatter areas), rainfall, soil depth, or erosion. These factors should be considered in land management.

Clustering vegetation dynamics and comparing those clusters with vegetation type illustrate the tendencies related to each vegetation. Understanding these

processes is key to the spatiotemporal interactions between human and natural systems (Aide et al., 2019; Woodward and Lomas, 2004). Most pixels were categorised as antipersistent and with a significantly increasing trend. Land managers should make special efforts to avoid further land degradation. Pixels categorised as the least antipersistent and with an increasing NDVI trend (as no persistent pixels were found) can be used as reference. These pixels can be studied to see if different management practices are in place leading to differences in persistence and NDVI trends.

The variability in arid areas was expected since minor changes in slope, rainfall, or other characteristics, mean a significant difference in water availability and plant growth (le Houérou et al., 1988; Stavi et al., 2008). Using URF to study rangelands can improve our understanding of the area even when fieldwork is unavailable, highlighting areas with different dynamics, crucial when monitoring vegetation. These techniques can also cluster a more extensive range of land uses, not only limited to rangeland since they will have more distinctive spectral signatures. The inclusion of larger arid areas would clarify whether this method can allow us to analyse previous land classification, prioritise areas for future surveys, and improve management action.

7. CONCLUSIONS

7.1. General and specific conclusions

The following paragraphs return to this thesis's specific goals to explain and answer the specific and general goals:

1. Which is the temporal response of NDVI to temperature and precipitation in arid areas and how does it change through the year?

The relationship between NDVI and meteorological variables shifts across the years' time. Two spatial scales were studied: MODIS MOD09Q1.006 (MR) and MOD09A1.006 (LR) showing that NDVI is scale-dependent. These resolutions show differences, particularly when studying correlation and regression analysis. The results suggest that medium resolution is more suited for spatial and lagged temporal patterns. However, when averaged, the trends are similar between these two resolutions. Lower resolution scales can be used when the studied areas are not spatially heterogeneous for temporal trend analysis, but larger resolution scales are recommended on spatially diverse areas.

Among the climatic variables used, temperature shows the strongest relationship with average NDVI. Our results reveal **that complex interactions of precipitation and temperature may explain real-time NDVI evolution**. However, their behaviours vary across the selected phases. **The use of phases based on NDVI patterns, instead of seasons, allows us to describe a more realistic depiction of the arid environments, based on their vegetation dynamics**. The study shows a strong positive correlation of NDVI with temperature when high precipitation occurs. Precipitation, however, shows a weak correlation with NDVI. The behaviour of both climatic variables points to water availability as one of the major drivers of NDVI in Murcia, as it is suggested by the positive correlations of temperature and NDVI during phases where heavier precipitation occurs.

Aridity index and NDVI allowed us to cluster our four areas into two large groups, A1 and A2; mainly grazed wastelands showed a low increase of NDVI with a high aridity index. In contrast, A4 and A3 with a similar or lower aridity index presented a higher NDVI accumulation, showing more efficient use of available water; A3, especially, presented a higher slope than A4. However, more rangelands and other ecosystems should be analyzed to determine whether or not these differences can discriminate and characterize other types of rangelands and land uses.

The intraseasonal relationship of NDVI with climatic variables was studied by splitting the analyses according to NDVI patterns. This allowed for viewing NDVI dynamics that were obscured when the seasonal division was followed. **Intraseasonal and interseasonal characteristics should be taken into consideration in the definition of agrometeorological indices in rangelands**. This study provides a discriminating technique for rangeland management and policymakers. It is expected that future research will expand the knowledge of NDVI drivers at different scales, to develop tools and indices that can help further comprehend vegetation communities of agricultural lands.

2. How does the soil water content index time series relate to the vegetation index throughout the year? Can we use the water content index as a warning index before vegetation damage?

Soil water content and vegetation indices show more similar dynamics in the months with lower temperatures (from Autumn to the beginning of Spring), in these months given the low temperatures, precipitation leads the vegetation growth. In the later months when the temperature rises the fall of precipitation and water availability depends on the evapotranspiration and type of vegetation.

The stronger relationship between precipitation and vegetation from Autumn to the beginning of Spring is reflected in the feasibility of Z_{WCI} to aid

prediction of vegetation index anomalies. During these months the use of Z_{WCI} and Z_{VCI} as warning indices has been shown to be possible for Los Velez region, in Almeria. Particularly, the months of October, November and December showed an average increase of more than 30% in the predictability of vegetation index anomalies. More areas are currently being researched to expand and improve this research and develop a warning index system.

3. How is the memory structure of vegetation time series, do different methods provide distinct results?

When comparing NDVI and NDVIa time series, we found similar trends in all study areas, which provides evidence of an inherent trend caused by land-use changes or climate change effects. When this inherent trend is present, MF-DFA allows us to study multifractality once the local trend is subtracted, and shows a multiscaling pattern, whilst the GSF can be affected by the inherent trend. Our analysis produced similar results to previous research conducted in semi-arid areas with analogous land uses and vegetation degradation (Igbawua et al., 2019). Using the NDVI, the MF-DFA $H(q)$ showed that the area with herbaceous crops had a slight antipersistent character. The areas with **open forests presented a more persistent character, while those with mixed uses appeared in the middle**. Examining the MF-DFA $H(q)$ for the NDVIa, we could discriminate among different land types, as those that are herbaceous and more heavily cropped had a steeper slope, resulting in a higher ΔH. Simultaneously, those with tree coverage, whether it is an open forest or a tree crop, showed a more antipersistent $H(q)$ but a smaller ΔH than then herbaceous-dominated areas. The use of surrogate and original series for the NDVIa produced different patterns for each study area, highlighting the heavier influence of probability density function on herbaceous croplands' multifractality, compared to those with at least partial tree coverage. **MF-DFA has been proven to enhance our skills in monitoring and discriminating among different land types for rangelands**,

supporting more accurate land use and management optimization. This research focused on the global description of each study area, and further work should focus on the spatial heterogeneity of each area. Our approach provides relevant information on vegetation dynamics that can inform policymakers and assist in the design of risk management programs such as index insurance systems.

4. Is it feasible to use annual patterns and persistence to cluster rangelands with different vegetation types?

Two methods (R/S and DFA) were used to calculate the Hurst exponent (HI and H2). The results were compared using two clustering methods, with summary statistics from the NDVI time series. The combination providing the best results was obtained based on the Silhouette Index and cluster characteristics. URF with the Hurst exponent from DFA (H2) showed the best outcome, compared with URF performed with the Hurst exponent calculated with R/S (HI), URF made without the Hurst exponent and all the k-means results.

URF found differences when different Hurst exponent methods were used, while k-means found no differences. URF with H2 showed greater differences between areas with higher tree coverage and those with a mix of grassland and shrubland. Additionally, the **H2 time series presented a stronger linear correlation with slope and elevation**, an essential aspect of vegetation dynamics in arid environments.

The clustering performed with URF and H2 provided three groups that presented a sort of continuum in Hurst exponent. On one hand, two clusters presented the lowest and the highest Hurst exponent. And those two clusters would show a higher representation of grassland (more antipersistent, closer to 0) and woodland (closer to random, near but all below 0.5), respectively. On the other hand, the last cluster would be mostly in between those clusters, showing a wide range of H2. These clusters were classified as woodland, shrubland or

grassland. Most likely linked to areas that show vegetation succession at different stages, as well as a mix of vegetation within the pixels.

Detrended fluctuation analyses produced significant differences when calculating the Hurst exponent in time series that presented a tendency. **Detrending time series allows for a better understanding of the dynamics of vegetation time series**, as well as rangeland evolution and future trends. **Rangeland persistence is a key aspect to consider in rangeland management and research**. Thus, future research should explore more rangeland, and other land uses, and compare different land management practices.

This thesis shows that NDVI time series can be used to study time and spatial variability and vegetation dynamics in arid rangelands, and how the interactions of vegetation with temperature, precipitation and soil water content. Furthermore, multifractal analysis has great potential to assess the complexity of vegetation time series. However, detrending methods are recommended to compare areas of different vegetations as distinctive vegetations present different slopes of temporal trends. It is demonstrated that persistence can be used as a tool for monitoring rangelands. And can inform management and policy-making regarding eco- and agrosystems.

7.2. Limitations and further research

7.2.1. Limitations

This study presents several limitations some due to remote sensing techniques others due to the research time limit and the limits of the areas of study:

- MODIS spatial resolution is much larger than most land plots in this region. Despite available remote-sensing data with a higher spatial resolution, 250 and 500 m spatial resolution was chosen. Both of them share the same temporal resolution and time series length. The length of the MODIS time series is longer than those with higher spatial resolution.

- Besides the spatial resolution issue, temporal lengths are limited by satellite data availability, a common problem in remote sensing. Longer time series will provide more robust multifractal results.
- Land use maps used such as the Spanish forest map and SIGPAC represented a single moment. The land use could have changed over time which could affect the results when comparing analyses of time series. Additionally, there were certain levels of mismatching between the land use classifications.

7.2.2. Further research

Further research should consider using more climatic variables to understand vegetation dynamics as especially soil water content measurements. In this research, the OPTRAM model has been used to estimate superficial water content, but field measurements would help calibrate the model and further understand vegetation and soil dynamics. Regarding clustering vegetation pixels with more multifractal metrics should be tested and studied in a larger number of vegetation types.

Additionally, more multifractal tools could be implemented such as multifractal detrended cross-correlation. This enables the study of the power-law behaviour of the correlation between two recorded time series, such as two different vegetation indices or vegetation indices with temperature or precipitation.

8. REFERENCES

Adegoke, J.O., Carleton, A.M., 2002. Relations between Soil Moisture and Satellite Vegetation Indices in the U.S. Corn Belt. J Hydrometeorol 3, 395–405. https://doi.org/https://doi.org/10.1175/1525-7541(2002)003<0395:RBSMAS>2.0.CO;2

AEMET, 2020. Vigilancia del clima [WWW Document]. Agencia Estatal de Meteorología (AEMET). URL http://www.aemet.es/es/serviciosclimaticos/vigilancia_clima

AghaKouchak, A., Farahmand, A., Melton, F.S., Teixeira, J., Anderson, M.C., Wardlow, B.D., Hain, C.R., 2015. Remote sensing of drought: Progress, challenges and opportunities. Reviews of Geophysics 53, 452–480. https://doi.org/https://doi.org/10.1002/2014RG000456

Aide, T.M., Grau, H.R., Graesser, J., Andrade-Nuñez, M.J., Aráoz, E., Barros, A.P., Campos-Cerqueira, M., Chacon-Moreno, E., Cuesta, F., Espinoza, R., 2019. Woody vegetation dynamics in the tropical and subtropical Andes from 2001 to 2014: Satellite image interpretation and expert validation. Glob Chang Biol 25, 2112–2126. https://doi.org/https://doi.org/10.1111/gcb.14618

Al-Bakri, J.T., Suleiman, A.S., 2004. NDVI response to rainfall in different ecological zones in Jordan. Int J Remote Sens 25, 3897–3912. https://doi.org/https://doi.org/10.1080/01431160310001654428

Albergel, C., Udiger, C.R., Pellarin, T., Calvet, J.-C., Fritz, N., Froissard, F., Suquia, D., Petitpa, A., Piguet, B., Martin, E., 2008. Hydrology and Earth System Sciences From near-surface to root-zone soil moisture using an exponential filter: an assessment of the method based on in-situ observations and model simulations, Hydrol. Earth Syst. Sci. https://doi.org/10.5194/hess-12-1323-2008

Alcaraz-Segura, D., Cabello, J., Paruelo, J., 2009. Baseline characterization of major Iberian vegetation types based on the NDVI dynamics. Plant Ecol 202, 13–29. https://doi.org/10.1007/s11258-008-9555-2

Allaby, M., 2014. Droughts. Infobase Publishing.

Almeida-Ñauñay, A.F., Benito, R.M., Quemada, M., Losada, J.C., Tarquis, A.M., 2021. The Vegetation–Climate System Complexity through Recurrence Analysis. Entropy 23, 559. https://doi.org/10.3390/e23050559

Almeida-Ñauñay, A.F., Villeta, M., Quemada, M., Tarquis, A.M., 2022. Assessment of Drought Indexes on Different Time Scales: A Case in Semiarid Mediterranean Grasslands. Remote Sens (Basel) 14. https://doi.org/10.3390/rs14030565

American Meteorological Society, 2004. AMS statement on meteorological drought. Bull Am Meteorol Soc 771–773.

American Meteorological Society, 1997. Meteorological drought—Policy statement. Bull Am Meteorol Soc 847–849.

Amri, R., Zribi, M., Lili-Chabaane, Z., Duchemin, B., Gruhier, C., Chehbouni, A., 2011. Analysis of vegetation behavior in a North African semi-arid region, using SPOT-VEGETATION NDVI data. Remote Sens (Basel) 3, 2568–2590. https://doi.org/10.3390/rs3122568

Anderson, A.N., McBratney, A.B., Crawford, J.W., 1997. Applications of fractals to soil studies. Advances in Agronomy 63, 1–76. https://doi.org/10.1016/S0065-2113(08)60241-2

Anyamba, A., Tucker, C.J., 2012. Historical perspective of AVHRR NDVI and vegetation drought monitoring. Remote sensing of drought: Innovative monitoring approaches 23, 20.

Babaeian, E., Sadeghi, M., Franz, T.E., Jones, S., Tuller, M., 2018. Mapping soil moisture with the OPtical TRApezoid Model (OPTRAM) based on long-term MODIS observations. Remote Sens Environ 211, 425–440. https://doi.org/10.1016/j.rse.2018.04.029

Bannayan, M., Sanjani, S., Alizadeh, A., Lotfabadi, S.S., Mohamadian, A., 2010. Association between climate indices, aridity index, and rainfed crop yield in northeast of Iran. Field Crops Res 118, 105–114. https://doi.org/10.1016/j.fcr.2010.04.011

Baranowski, P., Krzyszczak, J., Slawinski, C., Hoffmann, H., Kozyra, J., Nieróbca, A., Siwek, K., Gluza, A., 2015. Multifractal analysis of meteorological time series to assess climate impacts. Clim Res 65, 39–52. https://doi.org/10.3354/cr01321

Barceló, A.M., Nunes, L.F., 2009. Atlas Climático Ibérico - Iberian Climate Atlas 1971-2000, Atlas Climático Ibérico - Iberian Climate Atlas.

Baret, F., Guyot, G., 1991. Potentials and limits of vegetation indices for LAI and APAR assessment. Remote Sens Environ 35, 161–173. https://doi.org/10.1016/0034-4257(91)90009-U

Ba, R., Song, W., Lovallo, M., Lo, S., Telesca, L., 2020. Analysis of multifractal and organization/order structure in Suomi-NPP VIIRS Normalized Difference Vegetation Index series of wildfire affected and unaffected sites by using the multifractal detrended fluctuation analysis and the Fisher-Shannon analysis. Entropy 22. https://doi.org/10.3390/E22040415

Bastin, G.N., Chewings, V.H., Pearce, G., McGregor, F., 1999. Assessment of grazing impact on the Barkly tablelands: vegetation index and software.

Bird, S.B., Herrick, J.E., Wander, M.M., Wright, S.F., 2002. Spatial heterogeneity of aggregate stability and soil carbon in semi-arid rangeland. Environmental Pollution 116, 445–455. https://doi.org/10.1016/S0269-7491(01)00222-6

Birth, G.S., McVey, G.R., 1968. Measuring the color of growing turf with a reflectance spectrophotometer. Agron J 60, 640–643. https://doi.org/10.2134/agronj1968.00021962006000060016x

Birtwistle, A.N., Laituri, M., Bledsoe, B., Friedman, J.M., 2016. Using NDVI to measure precipitation in semi-arid landscapes. J Arid Environ 131, 15–24. https://doi.org/10.1016/j.jaridenv.2016.04.004

Booth, D.T., Tueller, P.T., 2003. Rangeland monitoring using remote sensing. Arid Land Research and Management. Arid Land Research and Management 17, 455–467. https://doi.org/10.1080/15324980390225539

Borchers, H.W., Borchers, M.H.W., 2019. Package 'pracma.'

Boyd, C.S., Svejcar, T.J., 2009. Managing complex problems in rangeland ecosystems. Rangel Ecol Manag 62, 491–499. https://doi.org/10.2111/08-194.1

Braswell, B.H., Schimel, D.S., Linder, E., Iii, B.M., 1997. The Response of Global Terrestrial Ecosystems to Interannual Temperature Variability. Science (1979) 278, 870–872. https://doi.org/10.1126/science.278.5339.870

Breiman, L., 2001. Random forests. Mach Learn 45, 5–32. https://doi.org/10.1023/A:1010933404324

Breiman, L., 1996. Bagging predictors. Mach Learn 24, 123–140. https://doi.org/10.1007/BF00058655

Breiman, L., Cutler, A., 2007. Random forests-classification description [WWW Document]. Department of Statistics, Berkeley. URL http://stat-www.berkeley.edu/users/breiman/RandomForests/cc_home.htm (accessed 1.21.22).

Breman, H., de Wit, C.T., 1983. Rangeland productivity and exploitation in the Sahel. Science (1979) 221, 1341–1347. https://doi.org/10.1126/science.221.4618.1341

Briske, D.D., 2017. Rangeland systems: processes, management and challenges. Springer Nature.

Briske, D.D., Fuhlendorf, S.D., Smeins, F.E., 2003. Vegetation Dynamics on Rangelands: A Critique of the Current Paradigms, Source: Journal of Applied Ecology. https://doi.org/10.1046/j.1365-2664.2003.00837.x

Brown, J.H., Gupta, V.K., Li, B.-L., Milne, B.T., Restrepo, C., West, G.B., 2002. The fractal nature of nature: power laws, ecological complexity and biodiversity. Philos Trans R Soc Lond B Biol Sci 357, 619–626. https://doi.org/10.1098/rstb.2001.0993

Byun, H.-R., Wilhite, D.A., 1999. Objective quantification of drought severity and duration. J Clim 12, 2747–2756. https://doi.org/10.1175/1520-0442(1999)012<2747:OQODSA>2.0.CO;2

Canedo Rosso, C., Hochrainer-Stigler, S., Pflug, G., Condori, B., Berndtsson, R., 2018. Early warning and drought risk assessment for the Bolivian Altiplano agriculture using high resolution satellite imagery data. Natural Hazards and Earth System Sciences Discussions 1–23. https://doi.org/10.5194/nhess-2018-133

Cao, X.M., Chen, X., Bao, A.M., Wang, Q., 2011. Response of vegetation to temperature and precipitation in Xinjiang during the period of 1998-2009. J Arid Land 3, 94–103. https://doi.org/10.3724/SP.J.1227.2011.00094

Chambers, J.C., Allen, C.R., Cushman, S.A., 2019. Operationalizing ecological resilience concepts for managing species and ecosystems at risk. Front Ecol Evol 7, 241. https://doi.org/10.3389/fevo.2019.00241

Chen, F., Weber, K.T., 2014. Assessing the impact of seasonal precipitation and temperature on vegetation in a grass-dominated rangeland. Rangeland Journal 36, 185–190. https://doi.org/10.1071/RJ13098

Chow, G.C., 1960. Tests of equality between sets of coefficients in two linear regressions. Econometrica 591–605. https://doi.org/10.2307/1910133

Cornell, H. v, Karlson, R.H., 1997. Local and Regional Processes as Controls of Species Richness. Spatial Ecology: The Role of Space in Population Dynamics and Interspecific Interactions 250. https://doi.org/10.1515/9780691188362

Coronado, A. v, Carpena, P., 2005. Size effects on correlation measures. J Biol Phys 31, 121–133. https://doi.org/10.1007/s10867-005-3126-8

Costantini, E.A.C., L'Abate, G., Faz Cano, A., Mermut, A., Arocena, J., Ortiz Silla, R., 2009. A soil aridity index to assess desertification risk for Italy. Land Degrataion and Rehabilitation—Dryland Ecosystems. Advances in GeoEcology 40, 231–242.

Cui, L., Shi, J., 2010. Temporal and spatial response of vegetation NDVI to temperature and precipitation in eastern China. Journal of Geographical Sciences 20, 163–176. https://doi.org/10.1007/s11442-010-0163-4

Curran, P.J., Dungan, J.L., Gholz, H.L., 1992. Seasonal LAI in slash pine estimated with Landsat TM. Remote Sens Environ 39, 3–13. https://doi.org/10.1016/0034-4257(92)90136-8

Davis, A., Marshak, A., Wiscombe, W., Cahalan, R., 1994. Multifractal characterizations of nonstationarity and intermittency in geophysical fields: Observed, retrieved, or simulated. Journal of Geophysical Research: Atmospheres 99, 8055–8072. https://doi.org/10.1029/94JD00219

Dean, W.R.J., Macdonald, I.A.W., 1994. Historical changes in stocking rates of domestic livestock as a measure of semi-arid and arid rangeland degradation in the Cape Province, South Africa. J Arid Environ 26, 281–298. https://doi.org/10.1006/jare.1994.1030

Desai, B., Maskrey, A., Peduzzi, P., de Bono, A., Herold, C., United Nations Office for Disaster Risk Reduction (UNISDR), 2015. Making development sustainable: the future of disaster risk management, global assessment report on disaster risk reduction. United Nations Office for Disaster Risk Reduction (UNISDR), Geneve, Switzerland.

Dhakar, R., Sehgal, V.K., Pradhan, S., 2013. Study on inter-seasonal and intra-seasonal relationships of meteorological and agricultural drought indices in the Rajasthan State of India. J Arid Environ 97, 108–119. https://doi.org/https://doi.org/10.1016/j.jaridenv.2013.06.001

Downing, B.H., 1978. Environmental consequences of agricultural expansion in South Africa since 1850. S Afr J Sci 74, 420–422.

Eldridge, D.J., Bowker, M.A., Maestre, F.T., Roger, E., Reynolds, J.F., Whitford, W.G., 2011. Impacts of shrub encroachment on ecosystem structure and functioning: towards a global synthesis. Ecol Lett 14, 709–722. https://doi.org/10.1111/j.1461-0248.2011.01630.x

Ellis, E.C., Ramankutty, N., 2008. Putting people in the map: anthropogenic biomes of the world. Front Ecol Environ 6, 439–447. https://doi.org/https://doi.org/10.1890/070062

Escribano Rodríguez, J.A., Hernández Díaz-Ambrona, C.G., Tarquis Alfonso, A.M., 2014. Selection of vegetation indices to estimate pasture production in dehesas. Pastos 44, 6–18.

Fay, P.A., Carlisle, J.D., Knapp, A.K., Blair, J.M., Collins, S.L., 2003. Productivity responses to altered rainfall patterns in a C4-dominated grassland. Oecologia 137, 245–251. https://doi.org/10.1007/s00442-003-1331-3

Feder, J., 2013. Fractals. Springer Science & Business Media.

Fernández González, J., 2014. Caracterización de las comarcas agrarias de España. Provincia de Almería. Ministerio de Agricultura, Alimentación y Medio Ambiente. Madrid.

Fern, R.R., Foxley, E.A., Bruno, A., Morrison, M.L., 2018. Suitability of NDVI and OSAVI as estimators of green biomass and coverage in a semi-arid rangeland. Ecol Indic 94, 16–21. https://doi.org/10.1016/j.ecolind.2018.06.029

Fondo Español de Garantía Agraria, 2021. Visor SigPac (FEGA) [WWW Document]. https://sigpac.mapa.es/fega/visor/.

Friedel, M.H., Foran, B., Stafford Smith, M., 1990. Where the creeks run dry or ten feet high: pastoral management in arid Australia.

Frisch, U. and Parisi, G., 1985. Fully Developed Turbulence and Intermittency, in: Ghil, M., Benzi, R. and Parisi, G. (Ed.), Turbulence and Predictability in Geophysical Fluid Dynamics and Climate Dynamics. New York, pp. 84–88.

Frisch, U., Kolmogorov, A.N., 1995. Turbulence: the legacy of AN Kolmogorov. Cambridge university press.

Frontier, S., 1987. Applications of fractal theory to ecology, in: Develoments in Numerical Ecology. Springer, pp. 335–378.

Gang, W., Congbin, F., 2000. Large scale features of the seasonal phenological responses to the monsoon climate in East China: Multi-year average results. Chinese Journal of Atmosphere Sciences 24, 678–682.

Ghebrezgabher, M.G., Yang, T., Yang, X., Sereke, T.E., 2020. Assessment of NDVI variations in responses to climate change in the Horn of Africa. The Egyptian Journal of Remote Sensing and Space Science. https://doi.org/10.1016/j.ejrs.2020.08.003

Girvetz, E.H., McDonald, R., Heiner, M., Kiesecker, J., Davaa, G., Pague, C., Durnin, M., Oidov, E., 2012. Eastern mongolian grassland steppe, in: Climate and Conservation. Springer, pp. 92–103.

Gross, J.E., McAllister, R.R.J., Abel, N., Smith, D.M.S., Maru, Y., 2006. Australian rangelands as complex adaptive systems: a conceptual model and preliminary results. Environmental modelling & software 21, 1264–1272. https://doi.org/10.1016/j.envsoft.2005.04.024

Guan, Y., Lu, H., Yin, C., Xue, Y., Jiang, Y., Kang, Y., He, L., Heiskanen, J., 2020. Vegetation response to climate zone dynamics and its impacts on surface soil water content and albedo in China. Science of the Total Environment 747. https://doi.org/10.1016/j.scitotenv.2020.141537

Guichard, F., Gouhier, T.C., 2014. Non-equilibrium spatial dynamics of ecosystems. Math Biosci 255, 1–10. https://doi.org/10.1016/j.mbs.2014.06.013

Guo, X., Zhang, H., Yuan, T., Zhao, J., Xue, Z., 2015. Detecting the temporal scaling behavior of the normalized difference vegetation index time series in China using a detrended fluctuation analysis. Remote Sens (Basel) 7, 12942–12960. https://doi.org/10.3390/rs71012942

Halley, J.M., Hartley, S., Kallimanis, A.S., Kunin, W.E., Lennon, J.J., Sgardelis, S.P., 2004. Uses and abuses of fractal methodology in ecology. Ecol Lett 7, 254–271. https://doi.org/10.1111/j.1461-0248.2004.00568.x

Hao, F., Zhang, X., Ouyang, W., Skidmore, A.K., Toxopeus, A.G., 2012. Vegetation NDVI linked to temperature and precipitation in the upper catchments of Yellow River. Environmental Modeling & Assessment 17, 389–398. https://doi.org/10.1007/s10666-011-9297-8

Hao, Z., AghaKouchak, A., 2013. Multivariate standardized drought index: a parametric multi-index model. Adv Water Resour 57, 12–18. https://doi.org/10.1016/j.advwatres.2013.03.009

Hartigan, J.A., Wong, M.A., 1979. Algorithm AS 136: A k-means clustering algorithm. J R Stat Soc Ser C Appl Stat 28, 100–108. https://doi.org/10.2307/2346830

Heady, H.F., Cooper, D.W., Rible, J.M., Hooper, J.F., 1975. Comparative Forage Values of California Oafgrass and Soft Chess. Journal of Range Management 51–54.

He, B., Chen, A., Wang, H., Wang, Q., 2015. Dynamic response of satellite-derived vegetation growth to climate change in the Three North Shelter Forest Region in China. Remote Sens (Basel) 7, 9998–10016. https://doi.org/10.3390/rs70809998

He, J., Yang, X., Li, Z., Zhang, X., Tang, Q., 2016. Spatiotemporal variations of meteorological droughts in China during 1961–2014: An investigation based on multi-threshold identification. International Journal of Disaster Risk Science 7, 63–76. https://doi.org/10.1007/s13753-016-0083-8

Henebry, G.M., 1993. Detecting change in grasslands using measures of spatial dependence with Landsat TM data. Remote Sens Environ 46, 223–234. https://doi.org/10.1016/0034-4257(93)90097-H

Hirschi, M., Mueller, B., Dorigo, W., Seneviratne, S.I., 2014. Using remotely sensed soil moisture for land-atmosphere coupling diagnostics: The role of surface vs. root-zone soil moisture variability. Remote Sens Environ 154, 246–252. https://doi.org/10.1016/j.rse.2014.08.030

Holling, C.S., 1973. Resilience and stability of ecological systems. Annu Rev Ecol Syst 1–23. https://doi.org/10.1146/annurev.es.04.110173.000245

Holzapfel, C., Tielbörger, K., Parag, H.A., Kigel, J., Sternberg, M., 2006. Annual plant–shrub interactions along an aridity gradient. Basic Appl Ecol 7, 268–279.

Hou, W., Feng, G., Yan, P., Li, S., 2018. Multifractal analysis of the drought area in seven large regions of China from 1961 to 2012. Meteorology and Atmospheric Physics 130, 459–471. https://doi.org/10.1007/s00703-017-0530-0

Hubert, L., Arabie, P., 1985. Comparing partitions. J Classif 2, 193–218. https://doi.org/10.1007/BF01908075

Huete, A.R., 1988. A soil-adjusted vegetation index (SAVI). Remote Sens Environ 25, 295–309. https://doi.org/10.1016/0034-4257(88)90106-X

Hughes, L., 2003. Climate change and Australia: trends, projections and impacts. Austral Ecol 28, 423–443.

Hurst, H.E., 1951. Long-term Storage Capacity of Reservoirs. Transactions of the American Society of Civil Engineers 116, 770–799. https://doi.org/10.1061/TACEAT.0006518

Ichii, K., Kawabata, A., Yamaguchi, Y., 2002. Global correlation analysis for NDVI and climatic variables and NDVI trends: 1982-1990. Int J Remote Sens 23, 3873–3878. https://doi.org/10.1080/01431160110119416

Igbawua, T., Zhang, J., Yao, F., Ali, S., 2019. Long Range Correlation in Vegetation Over West Africa From 1982 to 2011. IEEE Access 7, 119151–119165. https://doi.org/10.1109/ACCESS.2019.2933235.

Iglesias, E., Báez, K., Diaz-Ambrona, C.H., 2016. Assessing drought risk in Mediterranean Dehesa grazing lands. Agric Syst 149, 65–74. https://doi.org/10.1016/j.agsy.2016.07.017

Jafari, R., Lewis, M.M., Ostendorf, B., 2007. Evaluation of vegetation indices for assessing vegetation cover in southern arid lands in South Australia, in: Rangeland Journal. pp. 39–49. https://doi.org/10.1071/RJ06033

Janssen, M.A., Walker, B.H., Langridge, J., Abel, N., 2000. An adaptive agent model for analysing co-evolution of management and policies in a complex rangeland system. Ecol Modell 131, 249–268. https://doi.org/10.1016/S0304-3800(00)00256-8

Jensen, M.E., Burman, R.D., Allen, R.G., 1990. Evapotranspiration and irrigation water requirements. ASCE.

Joiner, J., Yoshida, Y., Anderson, M., Holmes, T., Hain, C., Reichle, R., Koster, R., Middleton, E., Zeng, F.-W., 2018. Global relationships among traditional reflectance vegetation indices (NDVI and NDII), evapotranspiration (ET), and soil moisture variability on weekly timescales. Remote Sens Environ 219, 339–352. https://doi.org/10.1016/j.rse.2018.10.020

Jorgensen, S.E., Fath, B., 2014. Encyclopedia of ecology, Elsevier. ed. Newnes.

Kalisa, W., Zhang, J., Igbawua, T., Kayiranga, A., Ujoh, F., Aondoakaa, I.S., Tuyishime, P., Li, S., Simbi, C.H., Nibagwire, D., 2021. Spatial Multi-Criterion Decision Making (SMDM) Drought Assessment and Sustainability over East Africa from 1982 to 2015. Remote Sens (Basel) 13, 5067. https://doi.org/10.3390/rs13245067

Kantelhardt, J.W., Zschiegner, S.A., Koscielny-Bunde, E., Havlin, S., Bunde, A., Stanley, H.E., 2002. Multifractal detrended fluctuation analysis of nonstationary time series. Physica A: Statistical Mechanics and its Applications 316, 87–114. https://doi.org/10.1016/S0378-4371(02)01383-3

Katul, G., Lai, C.T., Schäfer, K., Vidakovic, B., Albertson, J., Ellsworth, D., Oren, R., 2001. Multiscale analysis of vegetation surface fluxes: From seconds to years. Adv Water Resour 24, 1119–1132. https://doi.org/10.1016/S0309-1708(01)00029-X

Kauth, R.J., Lambeck, P.F., Richardson, W., Thomas, G.S., Pentland, A.P., 1979. Feature extraction applied to agricultural crops as seen by Landsat. NASA. Johnson Space Center Proc. of Tech. Sessions, Vol. 1 and 2.

Kendall, M.G., 1975. Rank Correlation Methods. London: Charles Griffin & Co.

Kim, D.-W., Byun, H.-R., Choi, K.-S., 2009. Evaluation, modification, and application of the Effective Drought Index to 200-Year drought climatology of Seoul, Korea. J Hydrol (Amst) 378, 1–12. https://doi.org/10.1016/j.jhydrol.2009.08.021

Klisch, A., Atzberger, C., 2016. Operational drought monitoring in Kenya using MODIS NDVI time series. Remote Sens (Basel) 8, 267. https://doi.org/10.3390/rs8040267

Kogan, F.N., 1995. Application of vegetation index and brightness temperature for drought detection. Advances in space research 15, 91–100.

le Houerou, H.N., 2012. The grazing land ecosystems of the African Sahel. Springer Science & Business Media.

le Houérou, H.N., Bingham, R.L., Skerbek, W., 1988. Relationship between the variability of primary production and the variability of annual precipitation in world arid lands. J Arid Environ 15, 1–18. https://doi.org/10.1016/S0140-1963(18)31001-2

Lempert, R.J., 2002. A new decision sciences for complex systems. Proceedings of the National Academy of Sciences 99, 7309–7313. https://doi.org/10.1073/pnas.082081699

Levin, S.A., 1998. Ecosystems and the biosphere as complex adaptive systems. Ecosystems 1, 431–436. https://doi.org/10.1007/s100219900037

Liang, S., Yi, Q., Liu, J., 2015. Vegetation dynamics and responses to recent climate change in Xinjiang using leaf area index as an indicator. Ecol Indic 58, 64–76. https://doi.org/10.1016/j.ecolind.2015.05.036

Liaw, A., Wiener, M., 2002. Classification and regression by randomForest. R news 2, 18–22.

Liu, H.Q., Huete, A., 2019. A feedback based modification of the NDVI to minimize canopy background and atmospheric noise. IEEE Transactions on Geoscience and Remote Sensing 33, 457–465. https://doi.org/10.1109/tgrs.1995.8746027

Liu, J., Wu, J., Wu, Z., Liu, M., 2013. Response of NDVI dynamics to precipitation in the Beijing–Tianjin sandstorm source region. Int J Remote Sens 34, 5331–5350. https://doi.org/10.1080/01431161.2013.787505

Liu, S., Cheng, F., Dong, S., Zhao, H., Hou, X., Wu, X., 2017. Spatiotemporal dynamics of grassland aboveground biomass on the Qinghai-Tibet Plateau based on validated MODIS NDVI. Sci Rep 7, 1–10. https://doi.org/10.1038/s41598-017-04038-4

Liu, W.T., Kogan, F.N., 1996. Monitoring regional drought using the vegetation condition index. Int J Remote Sens 17, 2761–2782. https://doi.org/10.1080/01431169608949106

Liu, Y., Li, L., Chen, X., Zhang, R., Yang, J., 2018. Temporal-spatial variations and influencing factors of vegetation cover in Xinjiang from 1982 to 2013 based on GIMMS-NDVI3g. Glob Planet Change 169, 145–155. https://doi.org/10.1016/j.gloplacha.2018.06.005

Li, X.-B., Shi, P., 2000. Sensitivity analysis of variation in NDVI, temperature and precipitation in typical vegetation types a across China. Chinese Journal of Plant Ecology 24, 379.

Li, X., Lanorte, A., Lasaponara, R., Lovallo, M., Song, W., Telesca, L., 2017. Fisher–Shannon and detrended fluctuation analysis of MODIS normalized difference vegetation index (NDVI) time series of fire-affected and fire-unaffected pixels. Geomatics, Natural Hazards and Risk 8, 1342–1357. https://doi.org/10.1080/19475705.2017.1337652

Lloyd, S., 1982. Least squares quantization in PCM. IEEE Trans Inf Theory 28, 129–137. https://doi.org/10.1109/TIT.1982.1056489

Lovejoy, S., Pecknold, S., Schertzer, D., 2001. Stratified multifractal magnetization and surface geomagnetic fields—I. Spectral analysis and modelling. Geophys J Int 145, 112–126.

Lovejoy, S., Tarquis, A.M., Gaonac'h, H., Schertzer, D., 2008. Single-and Multiscale Remote Sensing Techniques, Multifractals, and MODIS-Derived Vegetation and Soil Moisture. Vadose Zone Journal 7, 533–546. https://doi.org/10.2136/vzj2007.0173

Ludwig, J.A., Coughenour, M.B., Liedloff, A.C., Dyer, R., 2001. Modelling the resilience of Australian savanna systems to grazing impacts. Environ Int 27, 167–172. https://doi.org/10.1016/S0160-4120(01)00078-2

Ludwig, J.A., Tongway, D.J., 2000. Viewing rangelands as landscape systems, in: Rangeland Desertification. Springer, pp. 39–52. https://doi.org/10.1007/978-94-015-9602-2_4

MacKay, D., 2003. An example inference task: Clustering, in: Information Theory, Inference and Learning Algorithms. Cambridge Univ. Press Cambridge, UK, pp. 284–292.

Mack, R.N., Thompson, J.N., 1982. Evolution in steppe with few large, hooved mammals. Am Nat 119, 757–773.

MacQueen, J., 1967. Some methods for classification and analysis of multivariate observations, in: Proceedings of the Fifth Berkeley Symposium on Mathematical Statistics and Probability. Oakland, CA, USA, pp. 281–297.

Maestre, F.T., Salguero-Gomez, R., Quero, J.L., 2012. It is getting hotter in here: determining and projecting the impacts of global environmental change on drylands. https://doi.org/10.1098/rstb.2011.0323

Mahmoudi, P., Rigi, A., Kamak, M.M., 2019. Evaluating the sensitivity of precipitation-based drought indices to different lengths of record. J Hydrol (Amst) 579, 124181. https://doi.org/10.1016/j.jhydrol.2019.124181

Mahyou, H., Karrou, M., Mimouni, J., Mrabet, R., el Mourid, M., 2010. Drought risk assessment in pasture arid Morocco through remote sensing. Afr J Environ Sci Tech 4, 845–852.

Mali, P., 2015. Multifractal characterization of global temperature anomalies. Theor Appl Climatol 121, 641–648. https://doi.org/10.1007/s00704-014-1268-y

Mandelbrot, B., 1977. Fractals. Freeman San Francisco.

Mandelbrot, B.B., 1983. The fractal geometry of nature/Revised and enlarged edition. whf.

Mann, H.B., 1945. Nonparametric Tests Against Trend. Econometrica 13, 245. https://doi.org/10.2307/1907187

Ma, Q., Li, Y., Liu, F., Feng, H., Biswas, A., Zhang, Q., 2022. SPEI and multi-threshold run theory based drought analysis using multi-source products in China. J Hydrol (Amst) 128737.

Marshak, A., Davis, A., Cahalan, R., Wiscombe, W., 1994. Bounded cascade models as nonstationary multifractals. Phys Rev E 49, 55. https://doi.org/10.1103/PhysRevE.49.55

Martens, S.N., Breshears, D.D., Meyer, C.W., 2000. Spatial distributions of understory light along the grassland/forest continuum: effects of cover, height, and spatial pattern of tree canopies. Ecol Modell 126, 79–93.

Martiny, N., Camberlin, P., Richard, Y., Philippon, N., 2006. Compared regimes of NDVI and rainfall in semi-arid regions of Africa. Int J Remote Sens 27, 5201–5223. https://doi.org/10.1080/01431160600567787

McKee, T.B., Doesken, N.J., Kleist, J., 1993. The relationship of drought frequency and duration to time scales, in: Proceedings of the 8th Conference on Applied Climatology. Boston, pp. 179–183.

Miao, L., Liu, Q., Fraser, R., He, B., Cui, X., 2015. Shifts in vegetation growth in response to multiple factors on the Mongolian Plateau from 1982 to 2011. Physics and Chemistry of the Earth, Parts A/B/C 87, 50–59. https://doi.org/10.1016/j.pce.2015.07.010

Middleton, N., Thomas, D.S.G., 1992. World Atlas of Desertification. First Edition 1992. United Nations Environment Programme (UNEP). Edward Arnold, London.

Milton, S.J., du Plessis, M.A., Siegfried, W.R., 1994. A conceptual model of arid rangeland degradation. Bioscience 44, 70–76. https://doi.org/10.2307/1312204

Ministerio de Agricultura, 2020. SIAR: Sistema de Información Agroclimática para el Regadío. [WWW Document]. URL http://www.mapa.es/siar/Informacion.asp (accessed 2.9.20).

Movahed, M.S., Jafari, G.R., Ghasemi, F., Rahvar, S., Tabar, M.R.R., 2006. Multifractal detrended fluctuation analysis of sunspot time series. Journal of Statistical Mechanics: Theory and Experiment 2006, P02003. https://doi.org/10.1088/1742-5468/2006/02/P02003

Muller, F., 2000. Handbook of ecosystem theories and management. CRC Press.

Naeem, S., Li, S., 1997. Biodiversity enhances ecosystem reliability. Nature 390, 507–509. https://doi.org/10.1038/37348

Nastos, P.T., Politi, N., Kapsomenakis, J., 2013. Spatial and temporal variability of the Aridity Index in Greece. Atmos Res 119, 140–152. https://doi.org/10.1016/j.atmosres.2011.06.017

Ng, A., 2012. Clustering with the k-means algorithm. Mach Learn.

Nyamtseren, M., Feng, Q., Deo, R., 2018. A comparative study of temperature and precipitation-based aridity indices and their trends in Mongolia. Int J Environ Res 12, 887–899. https://doi.org/10.1007/s41742-018-0143-6

Pei, Z., Fang, S., Wang, L., Yang, W., 2020. Comparative analysis of drought indicated by the SPI and SPEI at various timescales in inner Mongolia, China. Water (Basel) 12, 1925. https://doi.org/10.3390/w12071925

Peng, J., Liu, Z., Liu, Y., Wu, J., Han, Y., 2012. Trend analysis of vegetation dynamics in Qinghai–Tibet Plateau using Hurst Exponent. Ecol Indic 14, 28–39. https://doi.org/https://doi.org/10.1016/j.ecolind.2011.08.011

Peng, Y., Wang, Q., Fan, M., 2017. Identification of the key ecological factors influencing vegetation degradation in semi-arid agro-pastoral ecotone considering spatial scales. Acta Oecologica 85, 62–68. https://doi.org/10.1016/j.actao.2017.09.011Get rights and content

Peters, A.J., Walter-Shea, E.A., Ji, L., Vina, A., Hayes, M., Svoboda, M.D., 2002. Drought monitoring with NDVI-based standardized vegetation index. Photogramm Eng Remote Sensing 68, 71–75.

Piao, S., Nan, H., Huntingford, C., Ciais, P., Friedlingstein, P., Sitch, S., Peng, S., Ahlström, A., Canadell, J.G., Cong, N., 2014. Evidence for a weakening relationship between interannual temperature variability and northern vegetation activity. Nat Commun 5, 1–7. https://doi.org/10.1038/ncomms6018

Pickup, G., Bastin, G.N., Chewings, V.H., 1998. Identifying trends in land degradation in non-equilibrium rangelands. Journal of Applied Ecology 35, 365–377. https://doi.org/10.3390/land6020031

Piedallu, C., Chéret, V., Denux, J.-P., Perez, V., Azcona, J.S., Seynave, I., Gégout, J.-C., 2019. Soil and climate differently impact NDVI patterns according to the season and the stand type. Science of The Total Environment 651, 2874–2885. https://doi.org/10.1016/j.scitotenv.2018.10.052

Qi, J., Chehbouni, A., Huete, A.R., Kerr, Y.H., Sorooshian, S., 1994. A Modified Soil Adjusted Vegetation Index. Remote Sensing Environment 48, 119–126. https://doi.org/10.1016/0034-4257(94)90134-1

Rand, D.A., 1994. Measuring and characterizing spatial patterns, dynamics and chaos in spatially extended dynamical systems and ecologies. Philosophical Transactions of the Royal Society of London. Series A: Physical and Engineering Sciences 348, 497–514. https://doi.org/10.1098/rsta.1994.0107

R Core Team, 2021. R: A language and environment for statistical computing.

Richardson, A.J., Everitt, J.H., 1992. Using spectral vegetation indices to estimate rangeland productivity. Geocarto Int 7, 63–69. https://doi.org/10.1080/10106049209354353

Ricklefs, R.E., Schluter, D., 1993. Species diversity in ecological communities: historical and geographical perspectives.

Rouse, J.W., Haas, R.H., Schell, J.A., Deering, D.W., 1973. Monitoring the vernal davancemenet and retrogradation (green wave effect) of natural vegetaton. Greenbelt, Maryland.

Saco, P.M., Moreno-de las Heras, M., Keesstra, S., Baartman, J., Yetemen, O., Rodríguez, J.F., 2018. Vegetation and soil degradation in drylands: non linear feedbacks and early warning signals. Curr Opin Environ Sci Health 5, 67–72. https://doi.org/10.1016/j.coesh.2018.06.001

Sadeghi, M., Babaeian, E., Tuller, M., Jones, S.B., 2017. The optical trapezoid model: A novel approach to remote sensing of soil moisture applied to Sentinel-2 and Landsat-8 observations. Remote Sens Environ 198, 52–68. https://doi.org/10.1016/j.rse.2017.05.041

Sampson, A.W., 1923. Range and pasture management. John Wiley & Sons, Incorporated.

Sanz, E., Saa-Requejo, A., Díaz-Ambrona, C.H., Ruiz-Ramos, M., Rodríguez, A., Iglesias, E., Esteve, P., Soriano, B., Tarquis, A.M., 2021a. Normalized Difference Vegetation Index Temporal Responses to Temperature and Precipitation in Arid Rangelands. Remote Sens (Basel) 13, 840. https://doi.org/10.3390/rs13050840

Sanz, E., Saa-Requejo, A., Díaz-Ambrona, C.H., Ruiz-Ramos, M., Rodríguez, A., Iglesias, E., Esteve, P., Soriano, B., Tarquis, A.M., 2021b. Generalized Structure Functions and Multifractal Detrended Fluctuation Analysis Applied to Vegetation Index Time Series: An Arid Rangeland Study. Entropy 23, 576. https://doi.org/10.3390/e23050576

Sanz, E., Sotoca, J.J.M., Saa-Requejo, A., Díaz-Ambrona, C.H., Ruiz-Ramos, M., Rodríguez, A., Tarquis, A.M., 2022. Clustering Arid Rangelands Based on NDVI Annual Patterns and Their Persistence. Remote Sens (Basel) 14, 4949. https://doi.org/10.3390/rs14194949

Savitzky, A., Golay, M.J.E., 1964. Smoothing and differentiation of data by simplified least squares procedures. Anal Chem 36, 1627–1639. https://doi.org/https://doi.org/10.1021/ac60214a047

Schlesinger, W.H., Reynolds, J.F., Cunningham, G.L., Huenneke, L.F., Jarrell, W.M., Virginia, R.A., Whitford, W.G., 1990. Biological feedbacks in global desertification. Science (1979) 247, 1043–1048. https://doi.org/10.1126/science.247.4946.1043

Schnur, M.T., Xie, H., Wang, X., 2010. Estimating root zone soil moisture at distant sites using MODIS NDVI and EVI in a semi-arid region of southwestern USA. Ecol Inform 5, 400–409. https://doi.org/10.1016/j.ecoinf.2010.05.001

Schreiber, T., Schmitz, A., 2000. Surrogate time series. Physica D 142, 346–382. https://doi.org/10.1016/S0167-2789(00)00043-9

Schreiber, T., Schmitz, A., 1996. Improved surrogate data for nonlinearity tests. Phys Rev Lett 77, 635. https://doi.org/10.1103/PhysRevLett.77.635

Schwinning, S., Parsons, A.J., 1999. The stability of grazing systems revisited: spatial models and the role of heterogeneity. Funct Ecol 13, 737–747.

Scordo, A., Maltese, A., Ciraolo, G., La Loggia, G., 2009. Estimation of the time lag occurring between vegetation indices and aridity indices in a Sicilian semi-arid catchment. Ital. J. Remote Sens 41, 33–46.

Sepehr, A., Hassanli, A.M., Ekhtesasi, M.R., Jamali, J.B., 2007. Quantitative assessment of desertification in south of Iran using MEDALUS method. Environ Monit Assess 134, 243–254. https://doi.org/10.1007/s10661-007-9613-6

Sepulcre-Canto, G., Horion, S., Singleton, A., Carrao, H., Vogt, J., 2012. Development of a Combined Drought Indicator to detect agricultural drought in Europe. Natural Hazards and Earth System Sciences 12, 3519–3531. https://doi.org/10.5194/nhess-12-3519-2012

Sheffield, J., Goteti, G., Wen, F., Wood, E.F., 2004. A simulated soil moisture based drought analysis for the United States. Journal of Geophysical Research: Atmospheres 109. https://doi.org/10.1029/2004JD005182

Shofiyati, R., Takeuchi, W., Pasaribu, S.M., Irawan, Y.R., 2021. Space-based drought analysis to support agricultural insurance facing climate change, in: IOP Conference Series: Earth and Environmental Science. IOP Publishing, p. 012130. https://doi.org/10.1088/1755-1315/648/1/012130

SIAM, 2020. Sistema de Información Agraria de Murcia [WWW Document]. URL http://siam.imida.es/ (accessed 2.9.23).

Sjoholm, H., Reynders, M.I., Ffolliott, P.F., ben Salem, B., 1989. Arid zone forestry; a guide for field technicians. FAO, Roma (Italia).

Skees, J.R., Gober, S., Varangis, P., Lester, R., Kalavakonda, V., 2001. Developing rainfall-based index insurance in Morocco. World Bank Publications.

Stavi, I., Ungar, E.D., Lavee, H., Sarah, P., 2008. Grazing-induced spatial variability of soil bulk density and content of moisture, organic carbon and calcium carbonate in a semi-arid rangeland. Catena (Amst) 75, 288–296. https://doi.org/10.1016/j.catena.2008.07.007

Stefanov, W.L., Netzband, M., 2005. Assessment of ASTER land cover and MODIS NDVI data at multiple scales for ecological characterization of an arid urban center. Remote Sens Environ 99, 31–43.

Stone, L., Ezrati, S., 1996. Chaos, cycles and spatiotemporal dynamics in plant ecology. Journal of Ecology 84, 279–291. https://doi.org/10.2307/2261363

Talbot, W.J., 1961. Land utilization in the arid regions of southern Africa. Part I. South Africa. A history of land use in arid regions. Arid Zones Research 299–338.

Tarnavsky, E., Garrigues, S., Brown, M.E., 2008. Multiscale geostatistical analysis of AVHRR, SPOT-VGT, and MODIS global NDVI products. Remote Sens Environ 112, 535–549. https://doi.org/10.1016/j.rse.2007.05.008

Team, A., 2020. Application for Extracting and Exploring Analysis Ready Samples (AppEEARS). NASA EOSDIS Land Processes Distributed Active Archive Center (LP DAAC), USGS/Earth Resources Observation and Science (EROS) Center: Sioux Falls, SD, USA. Available online: https://lpdaacsvc. cr. usgs. gov/appeears/ (accessed June 2, 2020).

Tietjen, B., Jeltsch, F., 2007. Semi-arid grazing systems and climate change: a survey of present modelling potential and future needs. Journal of Applied Ecology 44, 425–434. https://doi.org/10.1111/j.1365-2664.2007.01280.x

Tilman, D., Reich, P.B., Knops, J., Wedin, D., Mielke, T., Lehman, C., 2001. Diversity and productivity in a long-term grassland experiment. Science (1979) 294, 843–845. https://doi.org/10.1126/science.1060391

Tilman, D., Wedin, D., Knops, J., 1996. Productivity and sustainability influenced by biodiversity in grassland ecosystems. Nature 379, 718–720. https://doi.org/10.1038/379718a0

Tong, S., Zhang, J., Bao, Yuhai, Lai, Q., Lian, X., Li, N., Bao, Yongbin, 2018. Analyzing vegetation dynamic trend on the Mongolian Plateau based on the Hurst exponent and influencing factors from 1982–2013. Journal of Geographical Sciences 28, 595–610. https://doi.org/https://doi.org/10.1007/s11442-018-1493-x

Tongway, D.J., Ludwig, J.A., 1997. The nature of landscape dysfunction in rangelands, in: Landscape Ecology: Function and Mangement: Principles from Australia's Rangelands. CSIRO Publishing, Melbourne, pp. 49–61.

Triscowati, D.W., Sartono, B., Kurnia, A., Domiri, D.D., Wijayanto, A.W., 2019. Multitemporal remote sensing data for classification of food crops plant phase using supervised random forest, in: Sixth Geoinformation Science Symposium. International Society for Optics and Photonics, p. 1131102. https://doi.org/https://doi.org/10.1117/12.2547216

Uehara, T.D.T., Soares, A.R., Quevedo, R.P., Körting, T.S., Fonseca, L.M.G., Adami, M., 2020. Land Cover Classification of an Area Susceptible to Landslides Using Random Forest and NDVI Time Series Data, in: IGARSS 2020 - 2020 IEEE International Geoscience and Remote Sensing Symposium. pp. 1345–1348. https://doi.org/10.1109/IGARSS39084.2020.9324108

Ünal, E., Mermer, A., Yildiz, H., 2014. Assessment of rangeland vegetation condition from time series NDVI data. Journal of Field Crops Central Research Institute 23, 14–21. https://doi.org/https://doi.org/10.21566/tbmaed.41458

UNEP, 1992. World atlas of desertification. Kent, UK.

Vavrek, M.J., 2011. Fossil: palaeoecological and palaeogeographical analysis tools. Palaeontologia electronica 14, 16.

Vetter, S., 2005. Rangelands at equilibrium and non-equilibrium: recent developments in the debate. J Arid Environ 62, 321–341. https://doi.org/10.1016/j.jaridenv.2004.11.015

Vicente-Serrano, S.M., Beguería, S., López-Moreno, J.I., 2010. A multiscalar drought index sensitive to global warming: the standardized precipitation evapotranspiration index. J Clim 23, 1696–1718. https://doi.org/10.1175/2009JCLI2909.1

Vicente-Serrano, S.M., Gouveia, C., Camarero, J.J., Beguería, S., Trigo, R., López-Moreno, J.I., Azorín-Molina, C., Pasho, E., Lorenzo-Lacruz, J., Revuelto, J., 2013. Response of vegetation to drought time-scales across global land biomes. Proceedings of the National Academy of Sciences 110, 52–57. https://doi.org/10.1073/pnas.1207068110

Wabnitz, C.C., Andréfouët, S., Torres-Pulliza, D., Müller-Karger, F.E., Kramer, P.A., 2008. Regional-scale seagrass habitat mapping in the Wider Caribbean region using Landsat sensors: Applications to conservation and ecology. Remote Sens Environ 112, 3455–3467. https://doi.org/10.1016/j.rse.2008.01.020

Wallace, J., Behn, G., Furby, S., 2006. Vegetation condition assessment and monitoring from sequences of satellite imagery. https://doi.org/10.1111/j1442-8903.2006.00289.x

Wang, B., Xu, G., Li, P., Li, Z., Zhang, Y., Cheng, Y., Jia, L., Zhang, J., 2020. Vegetation dynamics and their relationships with climatic factors in the Qinling Mountains of China. Ecol Indic 108, 105719. https://doi.org/10.1016/j.ecolind.2019.105719

Wang, J., Rich, P.M., Price, K.P., 2003. Temporal responses of NDVI to precipitation and temperature in the central Great Plains, USA. Int J Remote Sens 24, 2345–2364. https://doi.org/10.1080/01431160210154812

Wang, L., Qu, J.J., 2009. Satellite remote sensing applications for surface soil moisture monitoring: A review. Frontiers of Earth Science in China 3, 237–247. https://doi.org/10.1007/s11707-009-0023-7

Wang, X., Wang, C., Niu, Z., 2005. Application of R/S method in analyzing NDVI time series. Geography and Geo-Information Science 21, 20–24.

Wang, X., Xie, H., Guan, H., Zhou, X., 2007. Different responses of MODIS-derived NDVI to root-zone soil moisture in semi-arid and humid regions. J Hydrol (Amst) 340, 12–24. https://doi.org/10.1016/j.jhydrol.2007.03.022

Watt, A.S., 1947. Pattern and process in the plant community. Journal of ecology 35, 1–22. https://doi.org/10.2307/2256497

West, N.E., 1993. Biodiversity of rangelands. Rangeland Ecology & Management/Journal of Range Management Archives 46, 2–13.

Wilhite, D., 2006. Drought monitoring and early warning: Concepts, progress and future challenges. World Meteorological Organization, Geneva, Switzerland. WMO 1006.

Wilhite, D.A., Buchanan-Smith, M., 2005. Drought as hazard: understanding the natural and social context. Drought and water crises: Science, technology, and management issues 3, 29.

Willeke, G., Hosking, J.R.M., Wallis, J.R., Guttman, N.B., 1994. The national drought atlas. Institute for water resources report 94.

Wolf, T. de, Holvoet, T., 2004. Emergence versus self-organisation: Different concepts but promising when combined, in: International Workshop on Engineering Self-Organising Applications. Springer, pp. 1–15.

Woodward, F.I., Lomas, M.R., 2004. Vegetation dynamics–simulating responses to climatic change. Biological reviews 79, 643–670. https://doi.org/10.1017/S1464793103006419

Yagci, A.L., Di, L., Deng, M., 2014. The influence of land cover-related changes on the NDVI-based satellite agricultural drought indices, in: 2014 IEEE Geoscience and Remote Sensing Symposium. IEEE, pp. 2054–2057. https://doi.org/10.1109/IGARSS.2014.6946868

Yue, W., Xu, J., Tan, W., Xu, L., 2007. The relationship between land surface temperature and NDVI with remote sensing: application to Shanghai Landsat 7 ETM+ data. Int J Remote Sens 28, 3205–3226. https://doi.org/10.1080/01431160500306906

Zerga, B., 2015. Degradation of Rangelands and Rehabilitation efforts in Ethiopia: The case of Afar rangelands. Journal of Mechanical and Industrial Engineering Research 4, 45.

Zewdie, W., Csaplovics, E., Inostroza, L., 2017. Monitoring ecosystem dynamics in northwestern Ethiopia using NDVI and climate variables to assess long term trends in dryland vegetation variability. Applied geography 79, 167–178. https://doi.org/10.1016/j.apgeog.2016.12.019

Zhang, Y., Wang, X., Li, C., Cai, Y., Yang, Z., Yi, Y., 2018. NDVI dynamics under changing meteorological factors in a shallow lake in future metropolitan, semiarid area in North China. Sci Rep 8, 1–13. https://doi.org/10.1038/s41598-018-33968-w

Zhao, L.-X., Xu, C., Ge, Z.-M., van de Koppel, J., Liu, Q.-X., 2019. The shaping role of self-organization: linking vegetation patterning, plant traits and ecosystem functioning. Proceedings of the Royal Society B 286, 20182859. https://doi.org/10.1098/rspb.2018.2859

Zhao, X., Tan, K., Fang, J.Y., 2011. NDVI-based interannual and seasonal variations of vegetation activity in Xinjiang during the period of 1982–2006. Arid Zone Research 28, 10–16.

Zheng, X., Zhu, J., 2017. A new climatic classification of afforestation in Three-North regions of China with multi-source remote sensing data. Theor Appl Climatol 127, 465–480. https://doi.org/10.1007/s00704-015-1646-0

Zhou, Z., Ding, Y., Shi, H., Cai, H., Fu, Q., Liu, S., Li, T., 2020. Analysis and prediction of vegetation dynamic changes in China: Past, present and future. Ecol Indic 117, 106642. https://doi.org/https://doi.org/10.1016/j.ecolind.2020.106642

9. APPENDICES

9.1. Appendix 1: UTM coordinates for areas used to study the temporal response of NDVI to temperature and precipitation and its scaling properties

Table 9.1. UTM coordinates of each corner of the areas and the coordinates for their respective meteorological station.

Areas	Area 1	Area 2	Area 3	Area 4
Xmin (m)	660,520	635,796	650,064	614,504
Xmax (m)	663,020	638,296	652,564	617,004
Ymin(m)	4,284,420	4,273,396	4,225,985	4,219,731
Ymax (m)	4,286,920	4,275,896	4,228,485	4,222,231
Stations	AL-10 (SIAM)	AL-06 (SIAR)	CI-32 (SIAR)	CR-32 (SIAM)
X station (m)	675,585	630,946	652,564	615,466
Y station (m)	4,289,270	4,276,000	4,228,485	4,218,939

9.2. Appendix 2: Regression analysis used to study temporal response of NDVI to temperature and precipitation

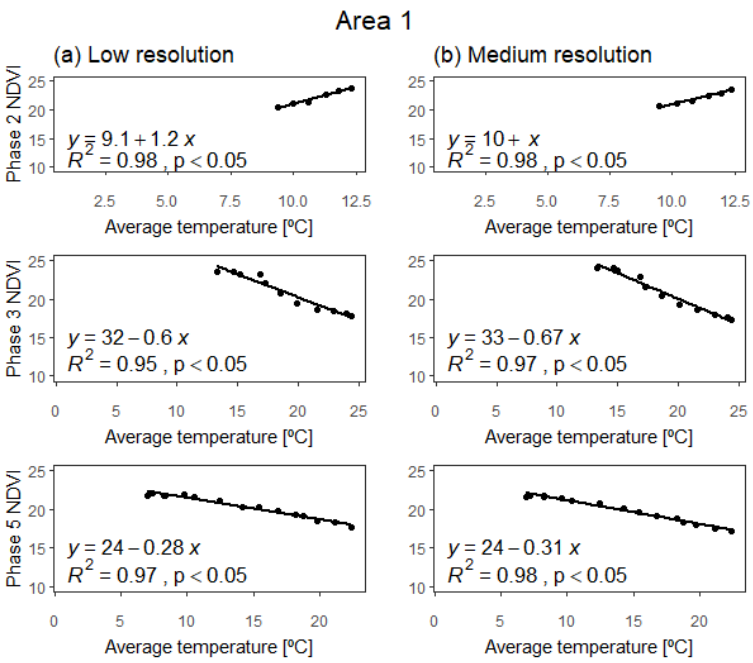

Figure 9.1. Regression analysis of average NDVI and temperature series separated by phases for LR (**a**) and MR (**b**) for A1.

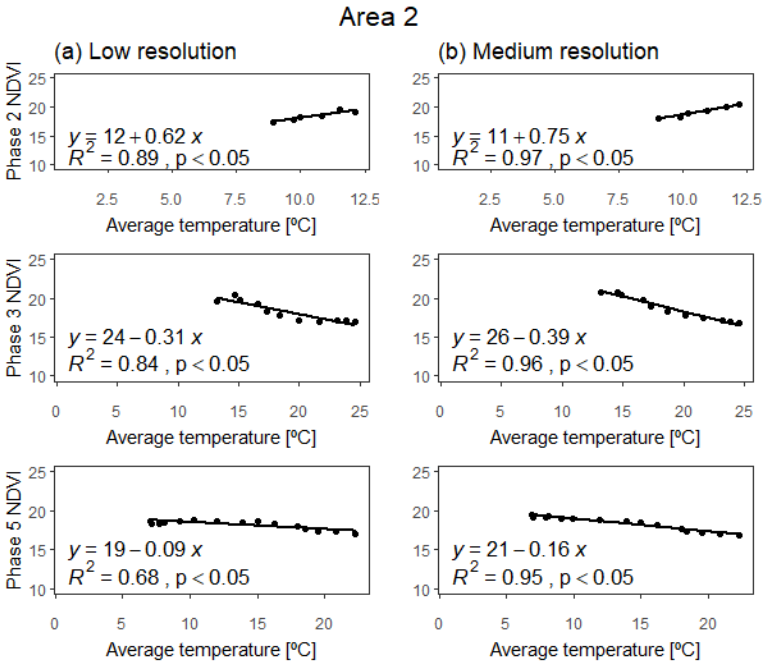

Figure 9.2. Regression analysis of average NDVI and temperature series separated by phases for LR (a) and MR (b) for A2.

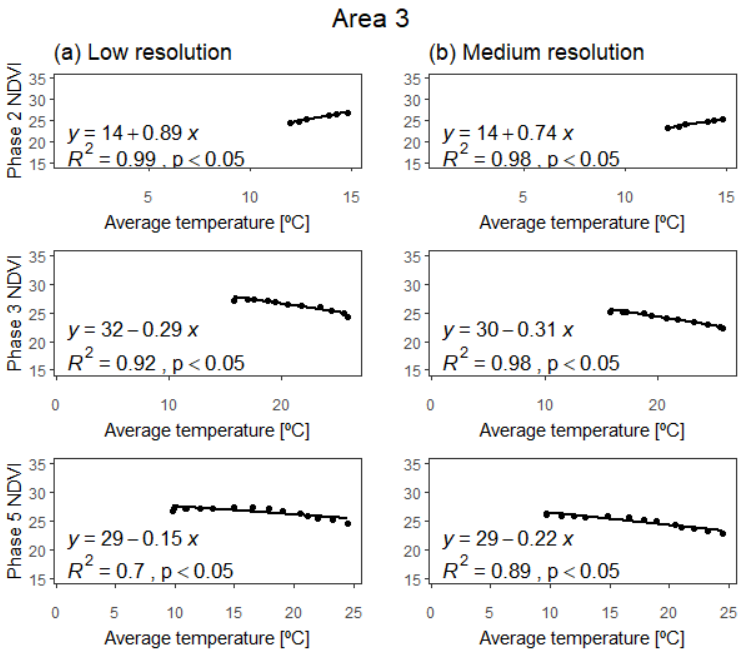

Figure 9.3. Regression analysis of average NDVI and temperature series separated by phases for LR (**a**) and MR (**b**) for A3.

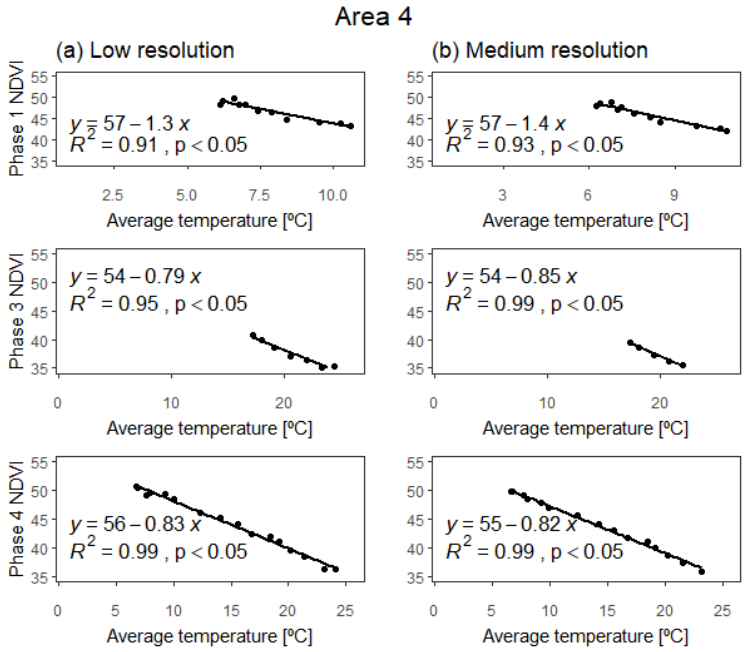

Figure 9.4. Regression analysis of average NDVI and temperature series separated by phases for LR (**a**) and MR (**b**) for A4.

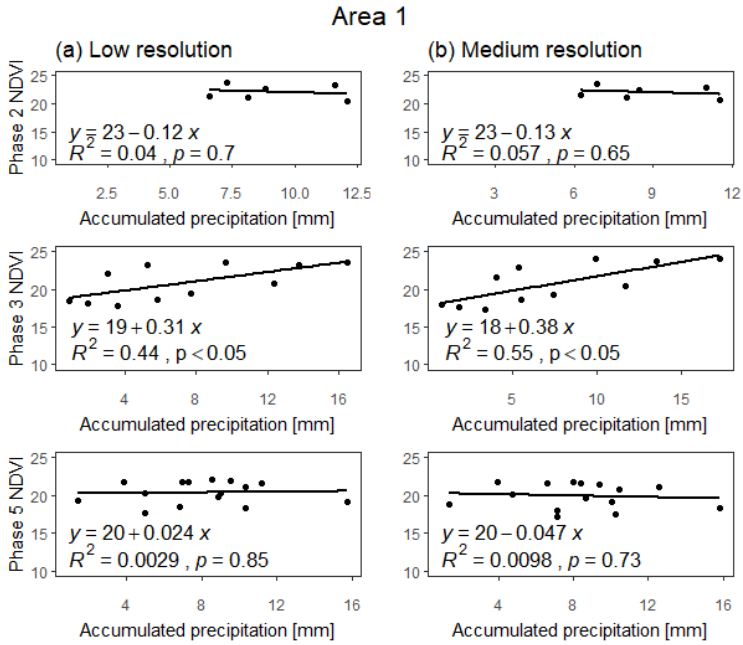

Figure 9.5. Regression analysis of average NDVI and precipitation series separated by phases for LR (**a**) and MR (**b**) for A1.

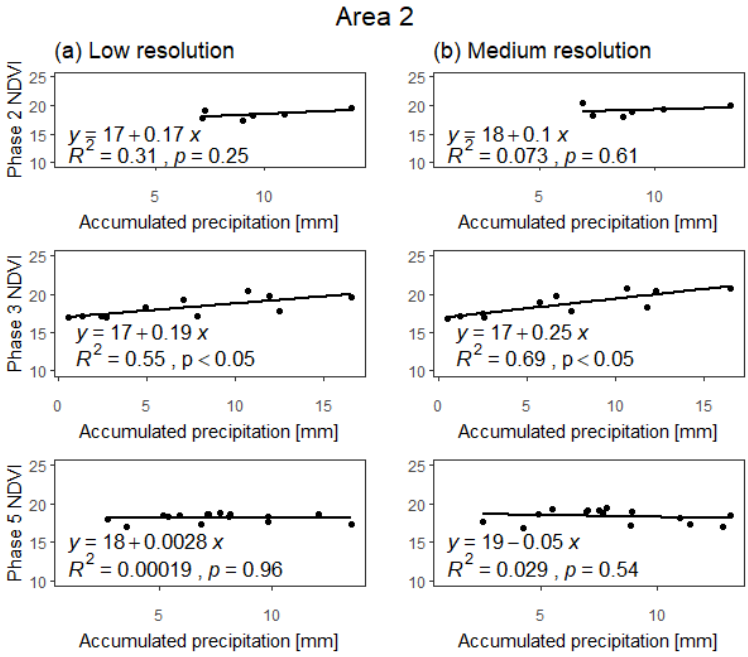

Figure 9.6. Regression analysis of average NDVI and precipitation series separated by phases for LR (a) and MR (b) for A2.

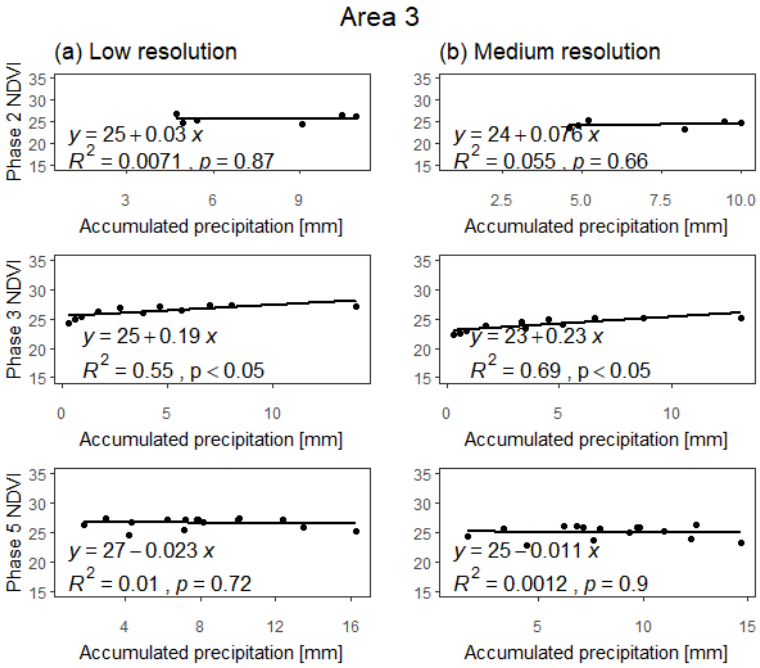

Figure 9.7. Regression analysis of average NDVI and precipitation series separated by phases for LR (a) and MR (b) for A3.

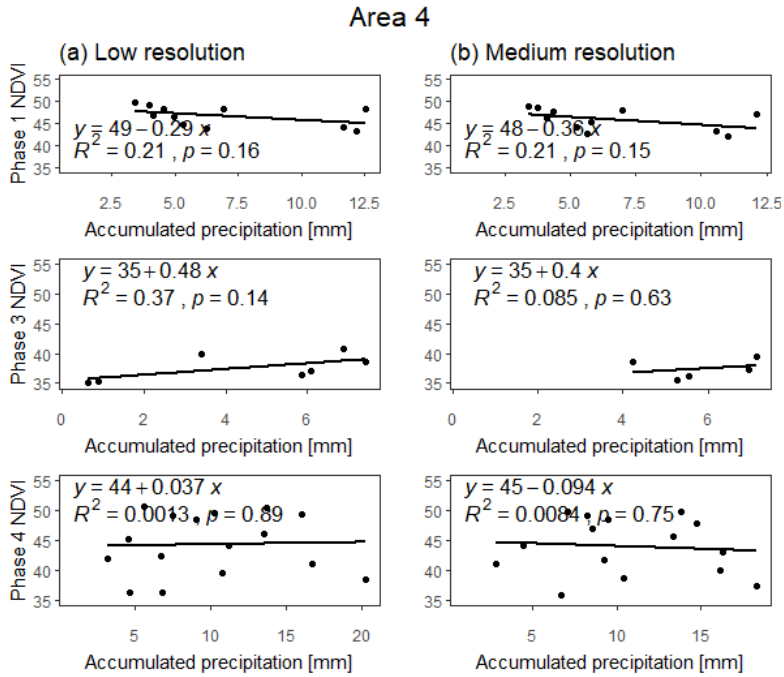

Figure 9.8. Regression analysis of average NDVI and precipitation series separated by phases for LR (**a**) and MR (**b**) for A4.

9.3. Appendix 3 Lagged partial correlation of NDVI and meteorological parameters

Table 9.2 Lagged partial correlations of medium resolution NDVI and meteorological parameters (Meteo) for A1 to A4. Only the phases with an increasing or decreasing NDVI trend are included. For each phase, bold values show the strongest correlations among the different time lags tested.

Area	Meteo	Phase	Lag Time (Days)						
			0	8	16	24	32	40	48
A1	Temp	Phase2	0.28	0.35	**0.37**	0.31	0.32	0.25	0.19
		Phase3	−0.71	−0.71	−0.71	−0.7	**−0.72**	−0.69	−0.65
		Phase5	−0.5	−0.51	**−0.52**	−0.51	−0.5	−0.49	−0.47
	Pp	Phase2	0.19	0.27	**0.32**	0.27	0.31	0.32	0.23
		Phase3	0.13	0.17	0.16	**0.19**	0.01	0.08	0.08
		Phase5	0.08	0.07	0.09	0.08	0.11	0.15	**0.16**
A2	Temp	Phase2	0.21	0.24	**0.27**	0.24	0.3	0.25	0.18
		Phase3	−0.57	−0.57	−0.56	−0.57	**−0.59**	−0.57	−0.53
		Phase5	−0.34	**−0.35**	−0.34	−0.34	−0.32	−0.31	−0.29
	Pp	Phase2	0.16	0.16	0.18	0.19	0.19	**0.2**	0.07
		Phase3	−0.1	−0.04	0	0.03	0.02	**0.06**	0.05
		Phase5	0.13	0.13	0.16	0.17	**0.18**	0.16	0.19
A3	Temp	Phase2	0.11	0.18	0.24	**0.32**	0.32	0.28	0.22
		Phase3	−0.48	−0.48	−0.49	**−0.5**	−0.48	−0.47	−0.43

		Phase5	−0.34	**−0.34**	−0.33	−0.32	−0.3	−0.28	−0.24
	Pp	Phase2	**0.32**	0.31	0.27	0.18	0.18	0.24	0.15
		Phase3	−0.09	−0.04	0.05	0.11	0.1	0.14	**0.14**
		Phase5	0.13	0.12	0.14	0.14	**0.15**	0.2	0.21
A4	Temp	Phase1	**−0.14**	−0.11	−0.06	0	−0.05	0.02	0.07
		Phase3	−0.69	−0.7	**−0.71**	−0.7	−0.71	−0.69	−0.67
		Phase4	**−0.23**	−0.15	−0.17	−0.07	−0.03	0.03	0.04
	Pp	Phase1	−0.01	0.01	0.09	0.08	**0.12**	0.1	0.09
		Phase3	−0.08	−0.02	0	0.02	0.01	0.04	**0.05**
		Phase4	0.26	**0.3**	0.26	−0.06	−0.02	0.06	0.04

Table 9.3 Lagged partial correlations of low resolution NDVI and meteorological parameters (Meteo) for A1 to A4. Only the phases with an increasing or decreasing NDVI trend are included. For each phase, bold values show the strongest correlations among the different time lags tested.

Area	**Meteo**	**Phase**	**Lag Time (Days)**						
			0	**8**	**16**	**24**	**32**	**40**	**48**
A1	Temp	Phase2	0.24	0.30	0.34	0.31	**0.37**	0.31	0.24
		Phase3	**−0.07**	−0.03	−0.01	−0.04	−0.01	−0.05	−0.04
		Phase5	−0.45	−0.46	**−0.46**	−0.45	−0.45	−0.43	−0.40
	Pp	Phase2	0.23	0.27	**0.30**	0.24	0.27	0.32	0.24
		Phase3	0.12	0.18	0.23	**0.28**	0.06	0.11	0.10
		Phase5	0.11	0.09	0.11	0.10	0.12	0.17	**0.18**
A2	Temp	Phase2	0.20	0.20	0.26	0.25	**0.33**	0.29	0.24
		Phase3	−0.06	−0.01	−0.12	**−0.13**	−0.11	−0.09	−0.06
		Phase5	−0.20	**−0.21**	−0.20	−0.19	−0.17	−0.15	−0.13
	Pp	Phase2	0.17	0.16	0.19	**0.19**	0.18	0.17	0.04
		Phase3	0.05	0.02	0.05	0.10	0.02	**0.15**	0.13
		Phase5	0.14	0.15	0.18	0.18	**0.20**	0.18	0.20
A3	Temp	Phase2	0.11	0.18	0.25	0.34	**0.36**	0.30	0.23
		Phase3	**−0.15**	−0.11	−0.06	−0.04	−0.06	−0.05	−0.03
		Phase5	−0.28	**−0.28**	−0.27	−0.26	−0.24	−0.20	−0.17
	Pp	Phase2	**0.31**	0.30	0.27	0.18	0.15	0.22	0.14
		Phase3	0.20	**0.23**	0.19	−0.06	0.00	−0.04	−0.07
		Phase5	0.16	0.14	**0.16**	0.15	0.15	0.21	0.19
A4	Temp	Phase1	**−0.14**	−0.08	−0.01	0.03	−0.05	−0.01	0.04
		Phase3	−0.68	−0.69	−0.70	**−0.70**	−0.70	−0.68	−0.66
		Phase4	**−0.20**	−0.14	−0.15	−0.05	−0.02	0.02	0.03
	Pp	Phase1	0.01	0.02	0.09	0.08	**0.15**	0.12	0.08
		Phase3	−0.06	0.00	0.01	0.03	0.01	0.04	**0.05**
		Phase4	0.30	**0.31**	0.27	−0.07	−0.01	0.07	0.04

9.4. Appendix 4: Silhouette indices calculated for all URF changing mtry and number of trees for three clusters.

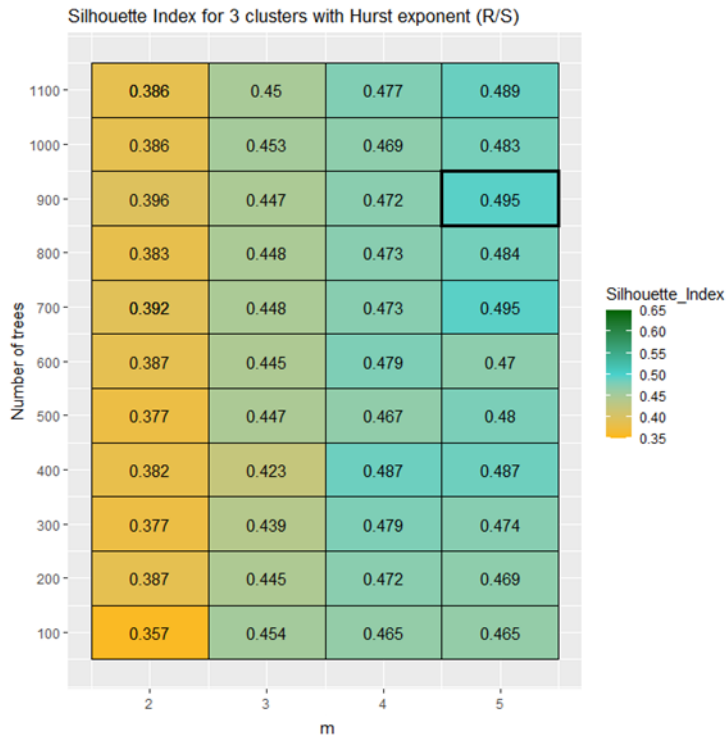

Figure 9.9. Silhouette indices for three clusters for URF using Hurst exponent calculated with Rescaled Range method. "m" represents the number of predictors tested on each node.

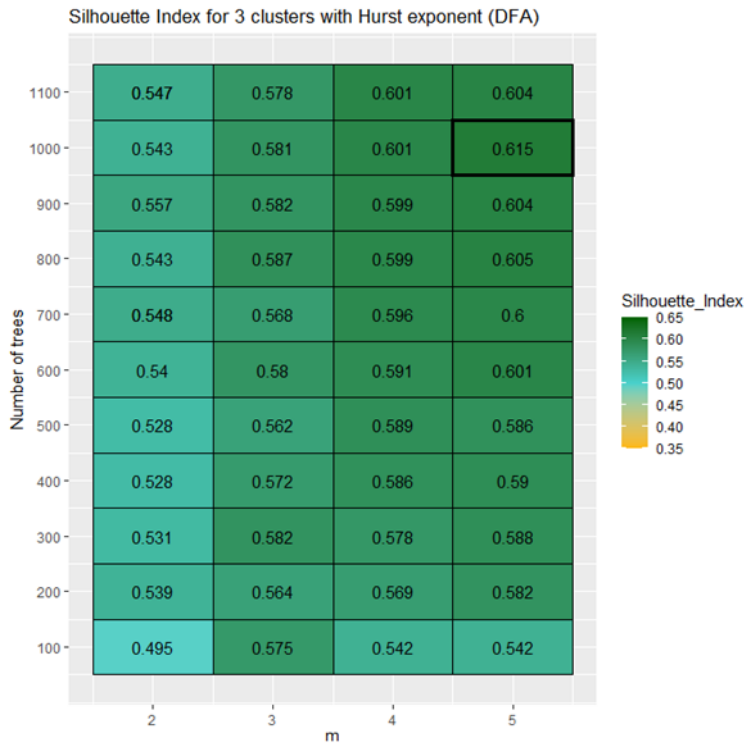

Figure 9.10. Silhouette indices for three clusters for URF using Hurst exponent calculated with Detrended fluctuation analysis. "m" represents the number of predictors tested on each node.

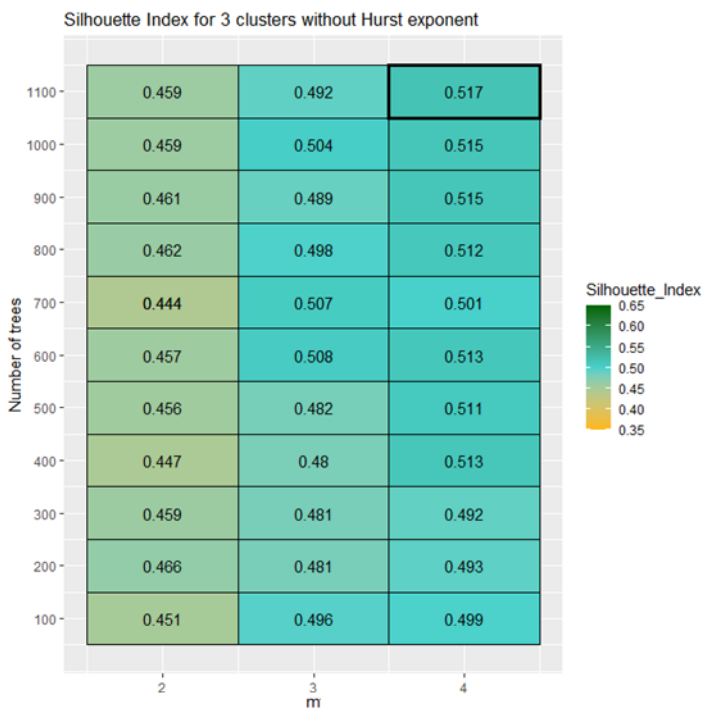

Figure 9.11. Silhouette indices for three clusters for URF not using any Hurst exponent. "m" represents the number of predictors tested on each node.

9.5. Appendix 5: Maps of the clusters using URF with HI and H2 for the three study provinces.

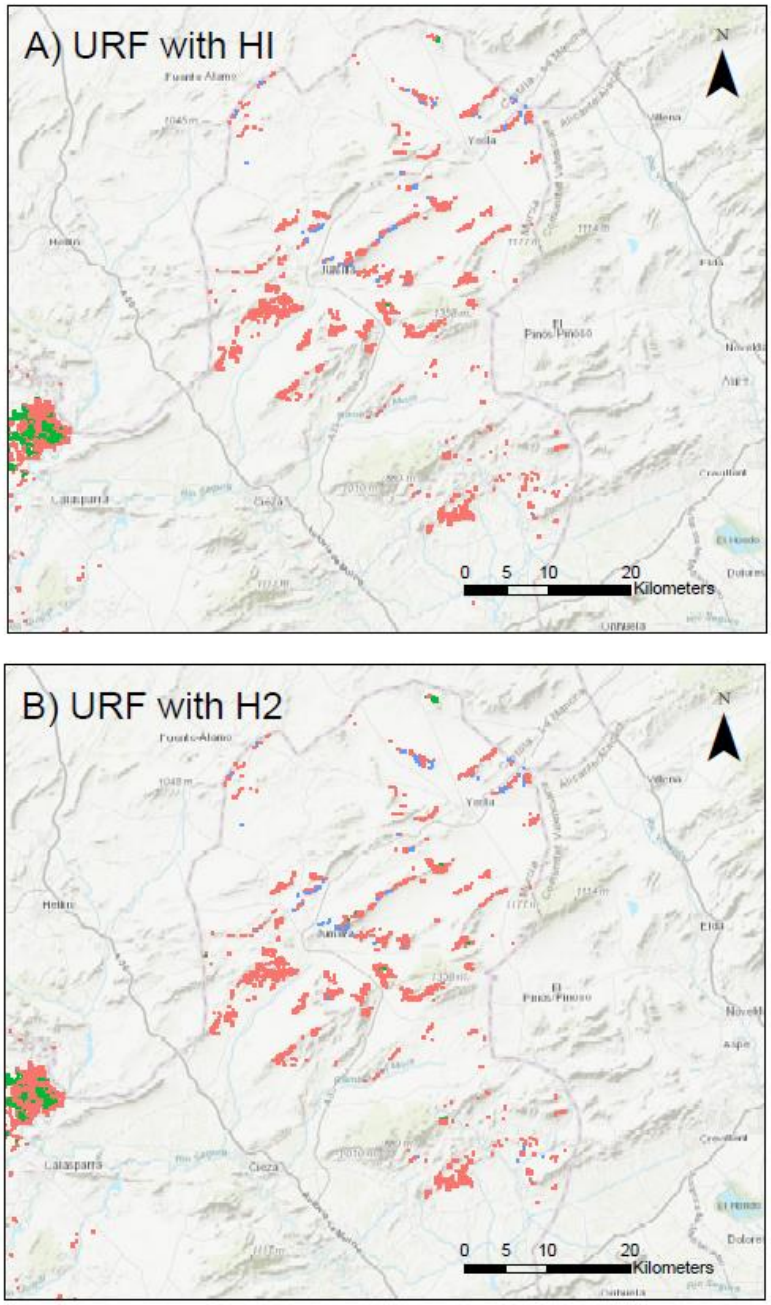

Figure 9.12. Comparison of the clustering results of URF using HI (a) and H2 (b) in the agricultural region of Murcia-NE. Cluster 1 is pink, cluster 2 is green, and cluster 3 is blue.

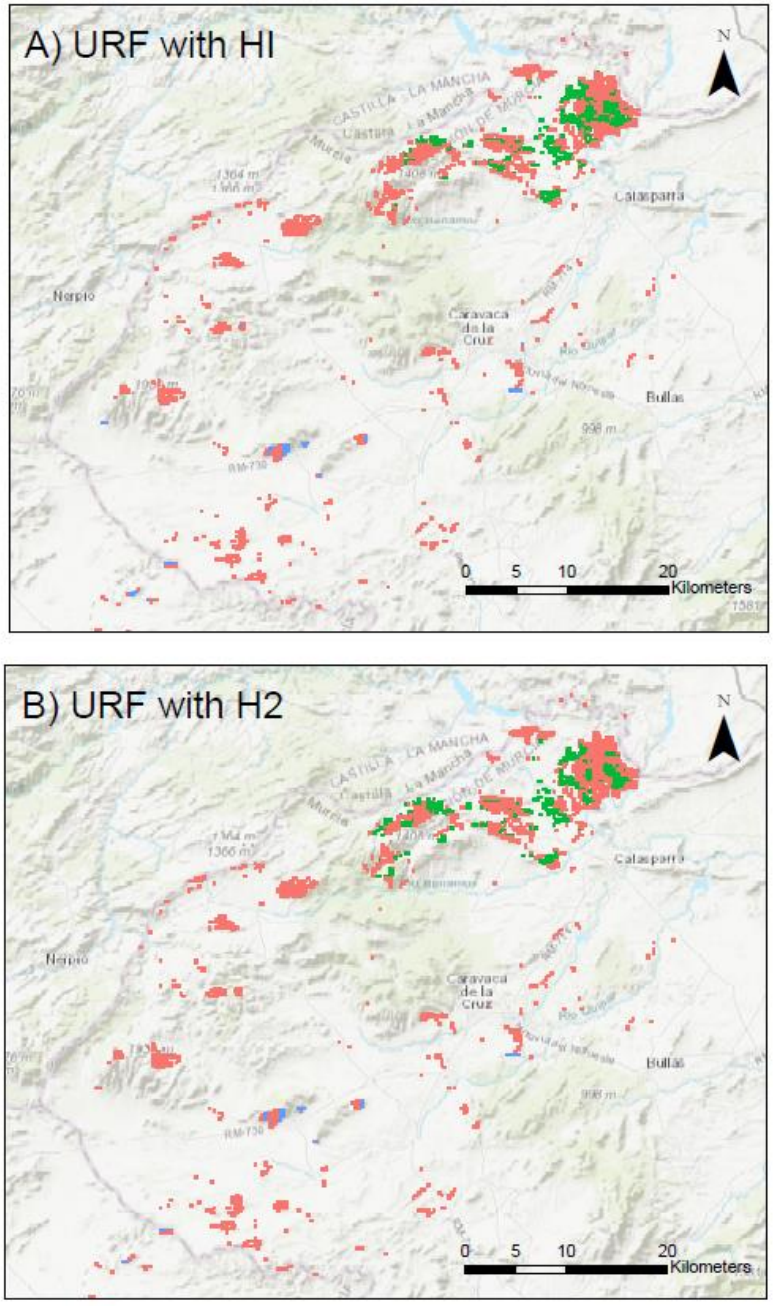

Figure 9.13. Comparison of the clustering results of URF using HI (a) and H2 (b) in the agricultural region of Murcia-NW. Cluster 1 is pink, cluster 2 is green, and cluster 3 is blue.

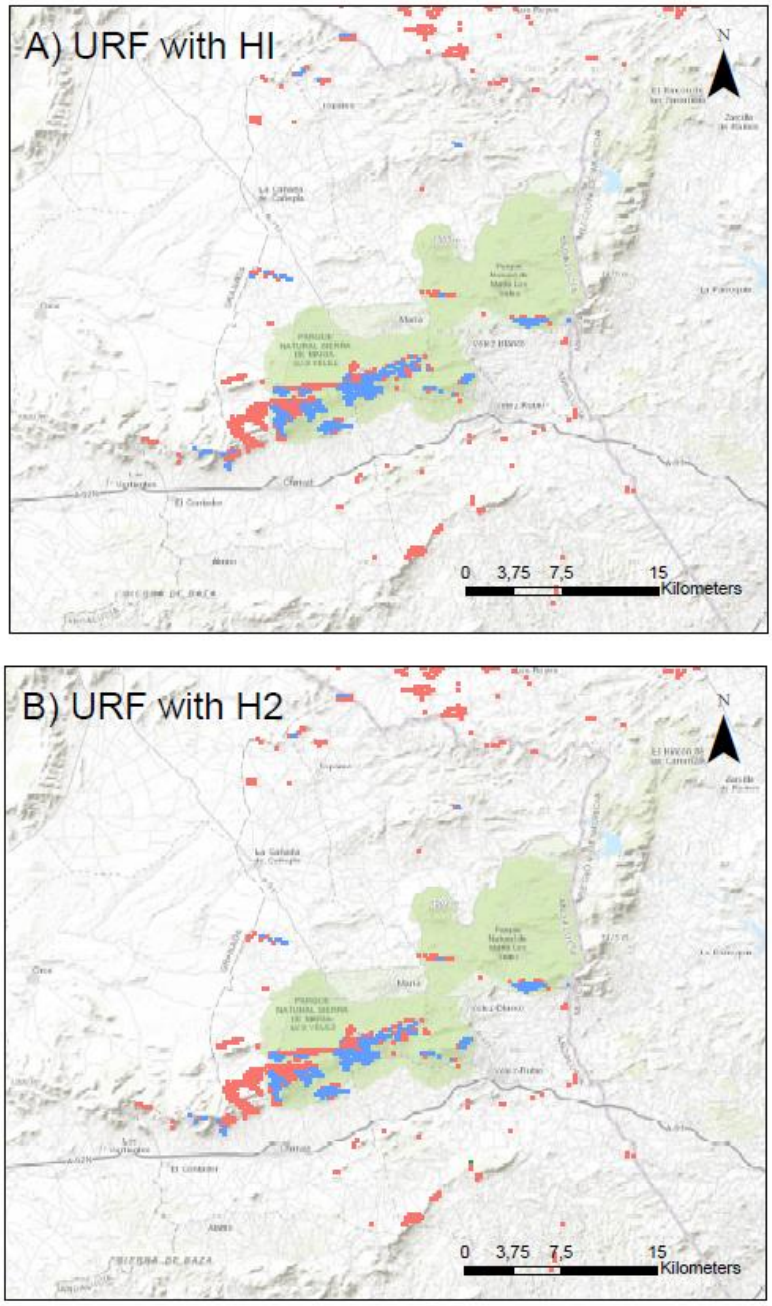

Figure 9.14. Comparison of the clustering results of URF using HI (a) and H2 (b) in the agricultural region of Los Velez (Almeria). Cluster 1 is pink, cluster 2 is green, and cluster 3 is blue.